Myeloid cells in the CNS counteract neuroinflammation via cellular responses to T cell infiltration

Dissertation

zur Erlangung des Grades

„Doktor der Naturwissenschaften“

im Promotionsfach Chemie

am Fachbereich Chemie, Pharmazie und Geowissenschaften

der Johannes Gutenberg-Universität Mainz

Beatrice Waßer

geb. in Mönchengladbach-Neuwerk

Mainz, 2017

Dekan:

1. Berichterstatter:

2. Berichterstatter:

Tag der mündlichen Prüfung: 23.04.2018

Hiermit versichere ich gemäß §10 Abs. 3d der Promotionsordnung vom 24.07.2007, dass ich die als Dissertation vorgelegte Arbeit selbst angefertigt und alle benutzten Hilfsmittel (Literatur, Geräte, Materialien) in der Arbeit angegeben habe.
Die als Dissertation vorgelegte Arbeit wurde in der Zeit von November 2013 bis November 2017 am Institut für Neurologie an der Universitätsmedizin der Johannes Gutenberg Universität Mainz in der Arbeitsgruppe von Frau Prof. Dr. Frauke Zipp durchgeführt.

Contents

Publication List

(1) "Increase of Alternatively Activated Antigen Presenting Cells in Active Experimental Autoimmune Encephalomyelitis"

Beatrice Wasser, Gautam Pramanik, Moritz Hess, Matthias Klein, Felix Luessi, Klaus Dornmair, Tobias Bopp, Frauke Zipp, Esther Witsch

J Neuroimmune Pharmacol (2016) (Wasser et al., 2016)

---

(2) "Protein kinase CK2 governs the molecular decision between encephalitogenic TH17 cell and Treg cell development"

Alexander Ulges*, Esther Witsch*, Gautam Pramanik, Matthias Klein, Katharina Birkner, Ulrike Bühler, **Beatrice Wasser**, Felix Luessi, Natascha Stergiou, Sarah Dietzen, Till-Julius Brühl, Toszka Bohn, Georg Bündgen, Horst Kunz, Ari Waisman, Hansjörg Schild, Edgar Schmitt, Frauke Zipp*, Tobias Bopp*

*equally contributing

Proc Natl Acad Sci U S A. (2016) (Ulges et al., 2016)

---

(3) "The role of ERK signaling in experimental autoimmune encephalomyelitis"

Katharina Birkner, **Beatrice Wasser**, Julia Loos, Alexander Plotnikov, Rony Seger, Frauke Zipp, Esther Witsch*, Stefan Bittner*

*equally contributing

Int. J. Mol. Sci. (2017) (Birkner et al., 2017)

---

(4) "Microglia remove living CNS-invading T cells during neuroinflammation"

Beatrice Wasser*, Dirk Luchtman*, Julian Löffel, Katharina Birkner, Kerstin Robohm, Albrecht Stroh, Christina Francisca Vogelaar, Frauke Zipp*, Stefan Bittner*

*equally contributing

Submitted

---

(5) "A novel β1-integrin/K_V1.3-controlled vesicular glutamate release pathway in Th17 cells causing neuronal hyperexcitability upon VCAM-1 binding"

Katharina Birkner, **Beatrice Wasser**, Carine Thalman, Tobias Ruck, Lynn Bitar, Carlos Maldet, Samantha Schmaul, Albrecht Stroh, Sven G. Meuth, Frauke Zipp and Stefan Bittner

Submitted

---

(6) "Th17 lymphocytes are capable to interact straightly with oligodendrocytes in the CNS of EAE-diseased mice and MS patients: Two-Photon *in vivo* visualization"

Catherine Larochelle *, **Beatrice Wasser***, Julian Löffel, Nicole Büss, Dirk Luchtman, Christin Liefländer, Jérôme Birkenstock, Katharina Birkner, Volker Siffrin, Albrecht Stroh, Stefan Bittner *, Frauke Zipp*

*equally contributing

In preparation

---

(7) "The form-function connection of M1/M2 microglia revisited"

Dirk Luchtman*, **Beatrice Wasser***, Kerstin Robohm, Frauke Zipp* and Stefan Bittner*

*equally contributing

In preparation

---

(8) "The lysosomal K^+ channel KCNK6 correlates with upregulated T cell autophagy in MS patients"

Falk Steffen, Tobias Ruck, Majella Hofmann, Li-Ming Lee, **Beatrice Wasser**, Frauke Zipp, Sven G. Meuth, Stefan Bittner

In preparation

Myeloid cells in the CNS counteract neuroinflammation via cellular responses to T cell infiltration

Beatrice Waßer, Dipl. Chem

Thesis advisors: xxx and xxx.

ABSTRACT

Multiple Sclerosis (MS) is an inflammatory disabling disease of the central nervous system (CNS) and is one of the most frequent causes of irreversible disability in young people. Both adaptive and innate immune cells infiltrate the CNS during MS and in its animal model experimental autoimmune encephalomyelitis (EAE). This thesis focuses on the impact of CNS-infiltrating and CNS-resident myeloid cells during neuroinflammation. Using deep mRNA sequencing (RNA-Seq), three distinct markers of alternatively activated myeloid cells (aaMC), namely Ms4a8a, Ym1 and Arginase1, were here identified to be more highly expressed in the CNS during exacerbation of the disease compared to all other considered time points of disease development. This upregulation was detected in two different mouse strains despite strong genetic differences. aaMC exhibit beneficial properties during the disease and the upregulation of aaMC markers during the active state of the disease suggests the attempt of myeloid cells in the CNS to counteract disease progression. Among myeloid cells, microglia are CNS-resident and therefore particularly relevant regarding CNS inflammation. In the here presented work it was shown that microglia attempt to remove invading pathogenic T cells from the CNS tissue during the disease. Intravital two-photon imaging revealed that microglia intensely contacted pathogenic Th17 cells in inflammatory lesions. Strikingly, microglia were able to respond to CNS inflammation by engulfing invading T cells. This as of yet undefined engulfment process targeted fully viable T cells and was dependent on the strength of both T cell and microglial activation. While microglial activation significantly increased engulfment processes, inhibition of T cell activity decreased the engulfment of T cells, altogether clearly emphasizing the importance of engulfment processes in inflammation. The engulfment of living T cells in the CNS may therefore reflect a general defense mechanism of the CNS towards invading activated cells. In sum, both the upregulation of aaMC markers during the exacerbation of the disease as well as the engulfment of CNS-invading Th17 cells could serve as myeloid cell-mediated mechanisms to counteract neuroinflammation.

Myeloide Zellen im ZNS wirken einer Neuroinflammation durch zelluläre Reaktionen auf die T-Zell-Infiltration entgegen

Beatrice Waßer, Dipl. Chem

Betreuer: xxx und xxx.

ZUSAMMENFASSUNG

Multiple Sklerose (MS) ist eine inflammatorische Erkrankung des zentralen Nervensystems (ZNS) und gehört zu den häufigsten Ursachen irreversibler Behinderungen im jungen Erwachsenenalter. Sowohl Immunzellen der angeborenen als auch Immunzellen der adaptiven Immunantwort infiltrieren das ZNS während der MS und ebenso in deren Tiermodell, der experimentellen autoimmunen Enzephallomyelitis (EAE). In dieser Arbeit steht die Bedeutung von ZNS-infiltrierenden und ZNS-residenten myeloiden Zellen während der Neuro-Inflammation im Fokus. Mittels RNA-Sequenzierung wurden dabei drei Gene identifiziert, die während eines verschärften Symptom-Auftretens höher exprimiert waren, als zu allen anderen betrachteten Zeitpunkten der Erkrankung. Die Expression dieser drei Gene, namentlich Ms4a8a, YM1 und Arginase1, sind kennzeichnend für sogenannte alternativ-aktivierte myleoide Zellen, welche den Krankheitsverlauf begünstigen können. Die erhöhte Expression dieser drei Gene während der aktiven Phase der Erkrankung verdeutlichte die Intention myeloider Zellen des ZNS, dem Fortschreiten der Erkrankung entgegenzuwirken. Mikroglia sind die ZNS-residenten myeloiden Zellen und sind daher von besonderer Bedeutung während der ZNS-Inflammation. In dieser Arbeit konnte gezeigt werden, dass Mikroglia während der EAE versuchten, pathogene, infiltrierende T-Zellen aus dem ZNS-Gewebe zu entfernen. Intravitale zwei-Photonen-Mikroskopie zeigte, dass Mikroglia in inflammatorischen Läsionen intensive Kontakte mit Th17-Zellen eingingen. Mikroglia zeigten dabei die bemerkenswerte Fähigkeit auf die Inflammation zu reagieren, indem sie sich einwandernde T-Zellen einverleibten. Dieser bisher unbekannte Prozess des Einverleibens zielte auch auf vitale T-Zellen ab und war dabei sowohl abhängig von der T-Zell-Aktivität, als auch von der Mikroglia-Aktivität. Während die Aktivierung der Mikroglia-Zellen zu einem signifikanten Anstieg des Einverleibungs-Prozesses führte, erniedrigte eine Inhibierung der T-Zell-Aktivität selbigen Prozess. Das Einverleiben von T-Zellen spiegelt daher einen möglicherweise generellen Abwehr-Mechanismus des ZNS gegenüber aktivierten, einwandernden Zellen wider.

1) Introduction

1.1) Multiple Sclerosis and Experimental autoimmune Encephalomyelitis

Multiple Sclerosis (MS) is an inflammatory disabling disease of the central nervous system (CNS), mainly manifesting in young adults and thereby one of the most frequent causes of irreversible disability in young people (Compston and Coles, 2008; Larochelle et al., 2016).

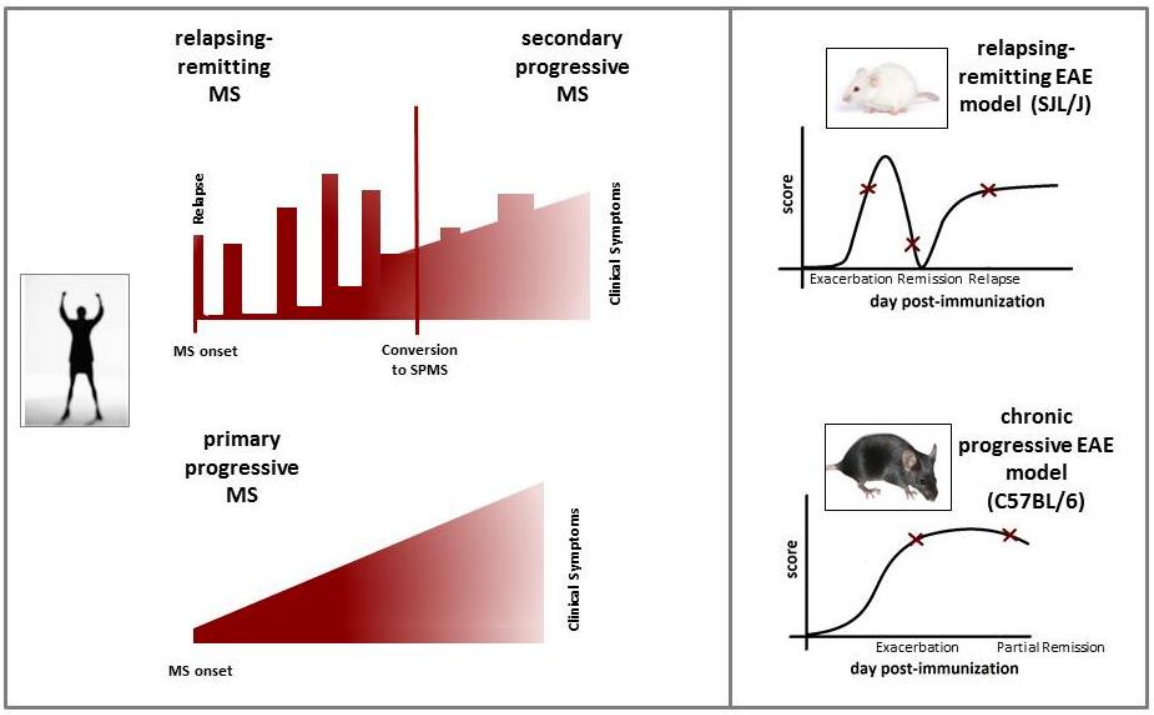

Figure 1: Schematic disease progression in MS and EAE. The time-dependent progression of clinical MS-symptoms (disability) is shown during relapsing-remitting MS, secondary progressive MS and primary progressive MS in human (left). Similarly, the time-dependent progression of EAE symptoms (score) is shown during relapsing remitting EAE in SJL/J mice (right, upper part) and during chronic progressive EAE in C57BL/6 mice (right, lower part).

Characteristic symptoms of MS include, but are not restricted to, loss of vision, motor impairments, pain, cognitive deficits and fatigue (Compston and Coles, 2008). Although the disease progression in individual patients is highly variable, the disease starts most commonly in a relapsing-remitting manner (relapsing-remitting MS, RRMS), in which acute exacerbations alternate with time periods with no or only marginal clinical symptoms (Compston and Coles, 2008; Lublin and Reingold, 1996; Siffrin et al., 2010b). 65 % of MS patients subsequently develop secondary progressive MS (SPMS), characterized by the continuous increase of disease severity leading to chronic disease activity. Only low

percentages of patients (≈20 %) suffer from primary progressive MS (PPMS), in which the illness is progressive from the onset of the disease (Compston and Coles, 2008; Larochelle et al., 2016) (**Figure 1**).

To investigate the pathophysiological mechanisms during the disease, the animal model of MS, experimental autoimmune encephalomyelitis (EAE) is widely used (Croxford et al., 2011). Active EAE is induced in mice by the subcutaneous (s.c.) injection of a CNS resident peptide (e.g., myelin oligodendrocyte glycoprotein (MOG) or myelin proteolipid protein (PLP)), which stimulates the active generation of endogenous autoreactive immune cells (’t Hart et al., 2011). Analogous to MS patients, EAE-diseased mice exhibit different disease courses. Notably, the s.c. injection of $PLP_{139-151}$ usually induces a relapsing-remitting EAE in SJL/J mice (McRae et al., 1992), while the s.c. injection of MOG_{35-55} usually induces a chronic progressive disease in C57BL/6 mice (Mendel et al., 1995; Thakker et al., 2007) (**Figure 1**). The adoptive transfer of pathogenic T helper (Th)17 cells into SJL/J or C57BL/6 recipient mice similarly causes a chronic progressive disease course (Aktas et al., 2005; Flügel et al., 2001; Siffrin et al., 2010a).

Disease pathology and the mechanisms responsible for the different disease courses are still poorly understood in humans and in mice. However, it is well known that immune cells infiltrate the CNS both during MS and EAE (Dendrou et al., 2015; Friese et al., 2014; Goverman, 2009) and the available therapeutics approved for the treatment of MS target inflammation (Haghikia et al., 2013; Wiendl et al., 2008). Although these therapeutics are successful in diminishing MS exacerbations in RRMS, they are often accompanied by side effects and especially the treatment strategies of SPMS and PPMS remain unsatisfying, demanding new insights into disease pathology.

1.2) Disease pathogenesis and therapeutic treatment of MS

The infiltration of active peripheral immune cells into the CNS is well defined during both MS and EAE (Dendrou et al., 2015; Friese et al., 2014; Goverman, 2009), and it was clearly shown in EAE that pathology is driven by myelin-specific T cells which need to be restimulated in the CNS to drive the disease (Kawakami et al., 2004; McMahon et al., 2005; Tompkins et al., 2002). However, the reasons for the presence of active autoreactive adaptive immune cells causing MS in patients remain unknown. The activation of these autoreactive cells in the

lymph nodes is discussed to be based on molecular mimicry, the release of CNS antigen and bystander activation (Chastain and Miller, 2012; Fujinami et al., 2006; Guo and Janigro, 2013). Of note, genetic and environmental factors can increase the MS risk (Belbasis et al., 2015; Lill et al., 2015).

Once activated, peripheral immune cells can cross the blood-brain barrier (BBB), which gets disrupted during the early phase of the disease, allowing infiltration into the immune privileged CNS. During the first wave of the disease, predominantly macrophages, B cells and $CD8^+$ T cells as well as differentiated $CD4^+$ Th1 and Th17 cells enter the CNS to cause inflammation and subsequently damage to oligodendrocytes and neurons (Dendrou et al., 2015). While in the past Th1 cells were believed to be the main drivers of the disease, an additional pivotal role of Th17 became evident in the last decades (Lovett-Racke et al., 2011). The skewing of T cell differentiation away from Th1 and Th17 towards a Th2 phenotype is part of the effector mechanism of therapies making use of interferon (IFN)-β (Kozovska et al., 1999), glatiramer acetate (Miller et al., 1998) and dimethyl fumarate (Gross et al., 2015). Beyond their impact on T cell differentiation, both CNS-infiltrating myeloid cells such as dendritic cells and macrophages, and microglia as the CNS-resident myeloid cells are discussed to cause re-activation of infiltrated T cells in the CNS, thus being vigorously involved in disease progression. The beneficial and detrimental properties of peripheral and CNS-resident myeloid cells in EAE and MS are presented in detail in the following sections.

1.2.1) Myeloid cells during EAE and MS

Myeloid cells are defined as cells which originate from a common myeloid progenitor cell, and thus include granulocytes and monocytes as well as dendritic cells, macrophages and microglia (Kawamoto and Minato, 2004; Ransohoff and Cardona, 2010) (**Figure 2a**). Interestingly, dendritic cells, macrophages and microglia do not only show common characteristics in the expression of surface molecules (Goldmann et al., 2013; Ponomarev et al., 2005), but in addition exhibit common functions like phagocytosis, antigen presentation and the secretion of pro- and anti-inflammatory mediators such as chemokines, cytokines and both neurotoxic and neurotrophic factors (s. 1.2.1.1-1.2.1.3 and **Figure 2b**). Although dendritic cells and macrophages are barely present in the healthy CNS, they are able to infiltrate the CNS parenchyma during MS and EAE after the disruption of the BBB (Bailey et al., 2007; Jiang et al., 2014; Lüssi et al., 2016). Thus, all these three distinct myeloid cell

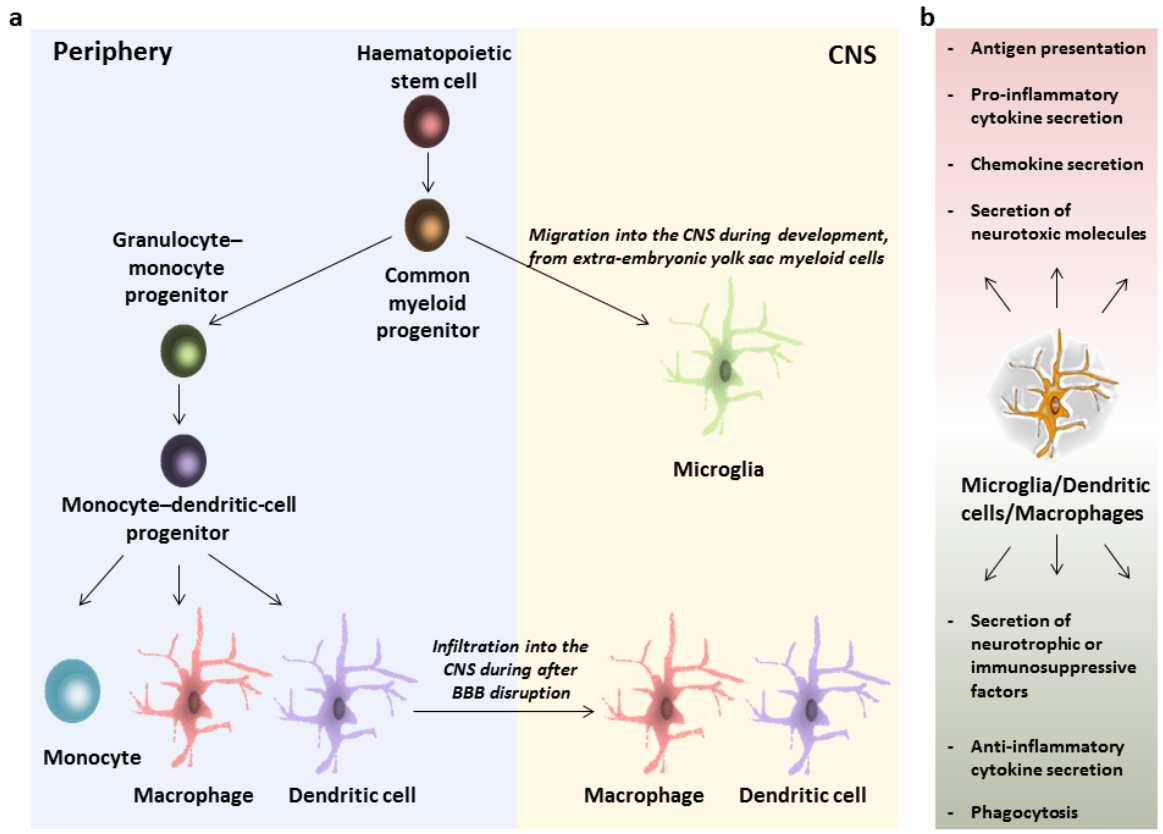

Figure 2: Schematic overview of the development and function of macrophages, dendritic cells and microglia. (a) Myeloid cells as macrophages, dendritic cells and microglia originate from a common myeloid progenitor cell. While microglia infiltrate the CNS only during development, macrophages and dendritic cells enter the CNS in adults if the blood-brain barrier (BBB) is disrupted. **(b)** Microglia, dendritic cells and macrophages show common functions, which could mediate detrimental (upper panel) and beneficial

subsets are able to impact the inflammatory milieu in the CNS during EAE and MS. In order to capture their beneficial and detrimental impacts on EAE disease, the entirety of dendritic cells, macrophages and microglia were further investigated in this study.

1.2.1.1) Dendritic cells during EAE and MS

In the steady state, dendritic cells predominantly reside in the periphery and only low numbers of dendritic cells are detectable in the CNS, where they are mainly located in vessel-rich areas both in humans and in mice (Lüssi et al., 2016; Prodinger et al., 2011). In the absence of inflammation, dendritic cells usually display an immature phenotype, characterized by low surface expressions of MHC-proteins and co-stimulatory molecules and by a high endocytic capacity, which quickly turns into an activated phenotype able to activate naïve T cells, upon interaction with microbial ligands or pro-inflammatory cytokines (Rescigno et al., 1998). Dendritic cells are commonly termed professional antigen presenting

cells (APC), due to their high capacity in stimulating and re-stimulating T cells (Sprent, 1995). After the phagocytic uptake of antigens, APC process the antigen proteins to small peptides, which are in the murine organism either presented on MHC-II molecules to stimulate $CD4^+$ T cell activation, proliferation and differentiation, or on MHC-I molecules to stimulate $CD8^+$ T cells (Germain and Margulies, 1993; Pennock et al., 2013). To prevent T cell anergy, the further upregulation of costimulatory molecules on APC is necessary (Harding et al., 1992). In EAE, CNS inflammation is associated with the recruitment of dendritic cells into the CNS (Bailey et al., 2007; Serafini et al., 2000). Comparably, dendritic cell accumulation has been reported in MS lesions (Serafini et al., 2006). Due to their high efficiency in antigen presentation and co-stimulation, dendritic cells were discussed to be pivotal during EAE and MS to (re-)stimulate pathogenic Th17 cells peripherally in the lymph nodes (de Vos et al., 2002), but also in the target organ, the CNS (Bailey et al., 2007; Karman et al., 2006; Tompkins et al., 2002). In the animal model, it has been shown *in vivo* that $CD11c^+$ dendritic cells were sufficient alone without the requirement of other MHC-II^+ APC to present antigen in order to induce CNS inflammation (Greter et al., 2005). T cell (re-)stimulation and differentiation has been shown to be dependent on the cytokine profile secreted by dendritic cells (de Jong et al., 2005; Diebold, 2008; Fletcher et al., 2010). In this context, it has been shown that untreated MS patients harbor higher levels of dendritic cells that secrete pro-inflammatory cytokines such as IFN-γ, tumor necrosis factor (TNF)-α and interleukin (IL)-23 compared to healthy controls (Huang et al., 1999; Vaknin-Dembinsky et al., 2006). Notably, the secretion of cytokines by dendritic cells varies not only between MS patients and healthy controls, but also between MS patients exhibiting different disease progressions. Whereas dendritic cells from RRMS patients could be described to induce both higher levels of Th1 cells and higher levels of Th2 cells compared to healthy controls, dendritic cells from SPMS patients only induced a polarized Th1 response, which was even elevated compared to the Th1 response in RRMS patients (Karni et al., 2006). Similarly, differences in the activation state of dendritic cells could be described comparing RRMS patients, SPMS patients and healthy controls, demonstrated by an altered expression of activation markers (Karni et al., 2006). These results indicate different roles of dendritic cells during different disease states.

Recently, the relevance of dendritic cells in the mediation of CNS autoimmunity was further demonstrated, as they were found to strongly express the inflammatory chemokines Ccl5,

Cxcl9, and Cxcl10 and to function as gatekeepers in the CNS (Archambault et al., 2005; Paterka et al., 2016). In contrast, dendritic cells were also shown to be capable of promoting self-tolerance, which is predominantly mediated by the provision of central tolerance due to the thymic negative selection of autoreactive T cells (Brocker et al., 1997; Matzinger and Guerder, 1989) and by the stimulation of regulatory T cells, providing peripheral tolerance (Darrasse-Jèze et al., 2009; Steinman and Nussenzweig, 2002; Yogev et al., 2012). Consequently, the transfer of dendritic cells has been shown to mediate regulatory functions in EAE-diseased mice (Duraes et al., 2016; Legge et al., 2002; Li et al., 2008; Menges et al., 2002), whereas the ablation of dendritic cells led to an increased disease course (Paterka et al., 2017). On the other hand, other studies could show that augmentation of dendritic cell numbers during EAE mediated an increase in EAE severity, and conversely, the depletion of dendritic cells was effective to decrease severity in adoptive transfer EAE (Greter et al., 2005; Paterka et al., 2016). In summary, dendritic cells within the CNS and peripheral dendritic cells are pivotal for controlling the balance of encephalitogenic and regulatory T cells. Different dendritic cell subsets as well as the particular disease state seem to play a decisive role in the fate of these myeloid cells during the disease, but the gene expression profile which could be primarily responsible for the different dendritic cell fates remains elusive and was investigated in this work.

1.2.1.2) Macrophages during EAE and MS

Similar to dendritic cells, only few macrophages infiltrate the CNS under physiological conditions, while a massive infiltration of macrophages is detectable during EAE (Jiang et al., 2014; Ousman and Kubes, 2012). A major function of macrophages includes the phagocytosis of apoptotic cells and pathogens (Martin et al., 2014). Their phagocytic activity can contribute to the clearance of apoptotic cells and myelin debris, which has been reported to be crucial to allow tissue regeneration during EAE (Bogie et al., 2011; Bruck et al., 1992; Neumann et al., 2009). Beside their phagocytic capacities, macrophages are able to contribute to disease progression by their release of pro- and anti-inflammatory mediators. On the one hand, they were shown to secret pro-inflammatory cytokines such as TNF-α, IL-12, IL-6 (Hendriks et al., 2005; Liu et al., 2013) and neurotoxic molecules such as reactive oxidative metabolites (Ding et al., 1988; Kigerl et al., 2009), on the other hand they are able to exert beneficial properties by the release of anti-inflammatory cytokines such as IL-10 (Liu

et al., 2013). In addition, similar to dendritic cells, macrophages are able to function as APC (Park et al., 2005), thus they are possibly contributing to T cell re-stimulation during EAE. Interestingly, neutralization of CCL22 activity has been shown to decrease macrophage accumulation in the CNS and was accompanied by a milder EAE course (Dogan et al., 2011), thus emphasizing the detrimental effects of macrophages during the disease. In the same sense it has been reported that the miRNA-mediated decrease in macrophage-activity inhibited EAE severity (Ponomarev et al., 2011). Cl2MDP-mnL treatment, which was described to transiently eliminate phagocytic macrophages from spleen, bone marrow and liver, but not dendritic cells, decreased clinical signs of EAE (Tran et al., 1998). By contrast, the injection of macrophages which were *in vitro* activated in the presence of opsonized sheep red blood cells prior to EAE induction, markedly protected mice from EAE development, thus highlighting their beneficial capacities (Tierney et al., 2009). The terms "M1" and "M2" macrophages are used in the literature to distinguish classically activated macrophages which exert pro-inflammatory functions and alternatively activated macrophages which exhibit anti-inflammatory properties, respectively (Franco and Fernández-Suárez, 2015; Jiang et al., 2014).

1.2.1.3) Microglia during EAE and MS

Microglia are the brain endogenous macrophages and are abundant both in the healthy and in the EAE- or MS-diseased CNS (Jiang et al., 2014; Ransohoff and Brown, 2012; Ransohoff and Perry, 2009). They are of myeloid origin and invade the CNS from the yolk sac during development, which has been demonstrated in mice (Ginhoux et al., 2010). These yolk sac-derived microglia are maintained by self-renewal throughout the adult animal's lifespan (Ajami et al., 2007; Hashimoto et al., 2013; Ransohoff, 2007).

In the resting state, microglia continuously scan the brain parenchyma by prolonging and retracting their highly motile processes, allowing the screening of the whole CNS parenchyma within a few hours (Nimmerjahn et al., 2005). After acute damage, microglia polarize their motile processes in the direction of the damage origin, where they are able to respond to harmful intruders via the release of pro-inflammatory and other toxic agents, potentially resulting in detrimental effects (Lehnardt, 2010; Ransohoff and Brown, 2012). Besides astrocytes, microglia are the main source of neurotoxic inflammatory mediators such as cytokines, chemokines and reactive oxygen species that promote neurodegeneration (Hanisch, 2002; Heneka et al., 2014). However, microglia as the CNS-resident immune cells,

are not only required to form the first line of defense against invading pathogens, but also to maintain brain homeostasis. In addition to their expression of inflammatory mediators, they also express neurotrophic and immunosuppressive factors, favoring tissue regeneration (Heneka et al., 2014; Kabba et al., 2017). The regeneration favoring state of microglia was discussed recently to be classified as an M2 phenotype, comparable to anti-inflammatory M2 macrophages in the periphery (Franco and Fernández-Suárez, 2015). Although this nomination is controversially discussed, the capacity of microglia to promote tissue repair is well accepted (Ransohoff, 2016). Microglial displacement of inhibitory synapses has been shown to provide neuroprotection in the adult brain (Chen et al., 2014). Analogous to macrophages in the periphery, microglia also act as professional phagocytes in the CNS, thereby enabling the clearance of dead material (Sierra et al., 2013).

During neuroinflammatory diseases, such as EAE and MS, microglia are likely involved in the re-stimulation and thus the activation of infiltrating pathogenic T cells, mediated by the microglial ability to act as APC (Aloisi et al., 1999; Carson, 2002). Antigen presentation by microglia via MHC-I has been clearly demonstrated, while antigen presentation via MHC-II *in vivo* is still a matter of debate (Korn and Kallies, 2017). In addition to their function in antigen presentation, detrimental microglial effects can be mediated via the creation of a cytotoxic inflammatory milieu that induces bystander damage contributing to lesion pathogenesis (Merson et al., 2010). The microglial activation can thereby result among other activators from oligodendrocyte-damage, myelin-damage or axonal damage (Merson et al., 2010). Inflammation-associated oxidative burst in activated microglia and macrophages is important during demyelination and during free radical-mediated tissue injury in the pathogenesis of MS (Fischer et al., 2012; Takeuchi et al., 2006). The decisive role of microglial activation in the disease becomes evident as it has been described to be a hallmark of demyelinating lesions in EAE (Ponomarev et al., 2005) and microglial activity in the cortical grey matter of living MS-diseased individuals corresponded with progression of disability (Politis et al., 2012). Furthermore, another study showed that cortical demyelination and diffuse axonal injury in normal-appearing white matter was associated with profound microglial activation (Kutzelnigg, 2005). Markers of both classically (M1) and alternatively (M2) activated macrophages could be identified among microglia present in microglia nodules in the CNS of MS patients (Singh et al., 2013).

The relevance of microglia is further emphasized by targeting them during the disease. The microglia-specific depletion of the kinase TAK1 was efficient to drastically decrease EAE (Goldmann et al., 2013), pointing to the essential ability of these cells to drive the disease. Of note, microglia were very specifically targeted in this model using a tamoxifen-inducible CX3CR1CreER system and thereby excluding the effect of other myeloid cells from contributing to the decreased disease course after TAK1 depletion. Other studies confirmed the indispensable role of microglia during EAE, reflected by an attenuated disease course after microglia paralysis (Heppner et al., 2005). Pharmacological treatment with macrophage inhibitory factor or minocycline, which target microglia, drastically decreased EAE severity, pointing to the essential impact of these cells on the development of the disease (Bhasin et al., 2007; Popovic et al., 2002).

Interestingly, analogously to the ambivalent effects of dendritic cells and macrophages during the disease, beneficial roles of microglia were described in addition to their detrimental properties during EAE and MS (Kerschensteiner et al., 2003). Microglia are able to secret anti-inflammatory cytokines such as IL-10 and IL-4 (Lobo-Silva et al., 2017; Ponomarev et al., 2007), which are beneficial for the disease outcome. IL-4 has been described to favor the protective potential of microglial cells during MS (Napoli and Neumann, 2010). Both IL-4- and IL-10-deficiency in mice yielded aggravated EAE courses (Bettelli et al., 1998; Falcone et al., 1998). Thereby, CNS-derived IL-4 seems to play a major role compared to peripheral IL-4 in order to mediate beneficial effects (Ponomarev et al., 2007). Beyond cytokine secretion, the beneficial effect of microglia is mediated by their phagocytic capacity, which has not only been found to be important in the resting state, but also to be beneficial in EAE, where significant clearance of cell debris and dead or apoptotic cells promotes the regeneration process in the CNS and reduces inflammation (Kotter, 2006; Lampron et al., 2015; Neumann et al., 2009; Olah et al., 2012; Sierra et al., 2013; Yamasaki et al., 2014). The triggering receptor expressed on myeloid cells 2 (TREM2) is expressed on microglia and its overexpression on myeloid cells has been shown to ameliorate EAE disease severity via the promotion of phagocytosis (Takahashi et al., 2007).

In summary, similarly to dendritic cells and macrophages, both beneficial and detrimental roles of microglia have been described during EAE and MS and inhibition of neurotoxic properties of microglia is likely to be a useful therapeutic strategy in MS.

1.2.2 Therapeutics targeting myeloid cells in MS

In addition to therapeutic treatment strategies which target the infiltration and activation of lymphocytes, many therapeutic treatments of MS directly target myeloid cells, further emphasizing their essential role during the disease (**Figure 3**). As mentioned above, the skewing of T cell differentiation away from Th1 and Th17 towards a Th2 phenotype is part of the effect mechanism of therapies making use of IFN-β (Kozovska et al., 1999), glatiramer acetate (Miller et al., 1998) and dimethyl fumarate (Gross et al., 2015). The IFN-β-dependent skewing away from a Th17 phenotype is likely to be mediated by a direct effect on APC. In this sense, IFN-β has been shown to alter the expression of cytokines and co-stimulatory molecules in myeloid cells isolated from MS patients and healthy controls (Huang et al., 1999; Marckmann et al., 2004; Ramgolam et al., 2009). Glatiramer acetate also directly affects myeloid cells, inducing a regulatory phenotype of these cells (Kim et al., 2004). Comparably, fingolimod and fumarate therapies improve MS by inducing an anti-inflammatory cell phenotype (Ghoreschi et al., 2011; Hughes et al., 2008). Strikingly, dimethyl fumarate showed the capacity to inhibit the production of nitric oxide and pro-inflammatory cytokines in microglial cells (Wilms et al., 2010). In this context, Laquinimod has been shown to exhibit a regulatory effect, which is mediated by the NF-kB pathway on

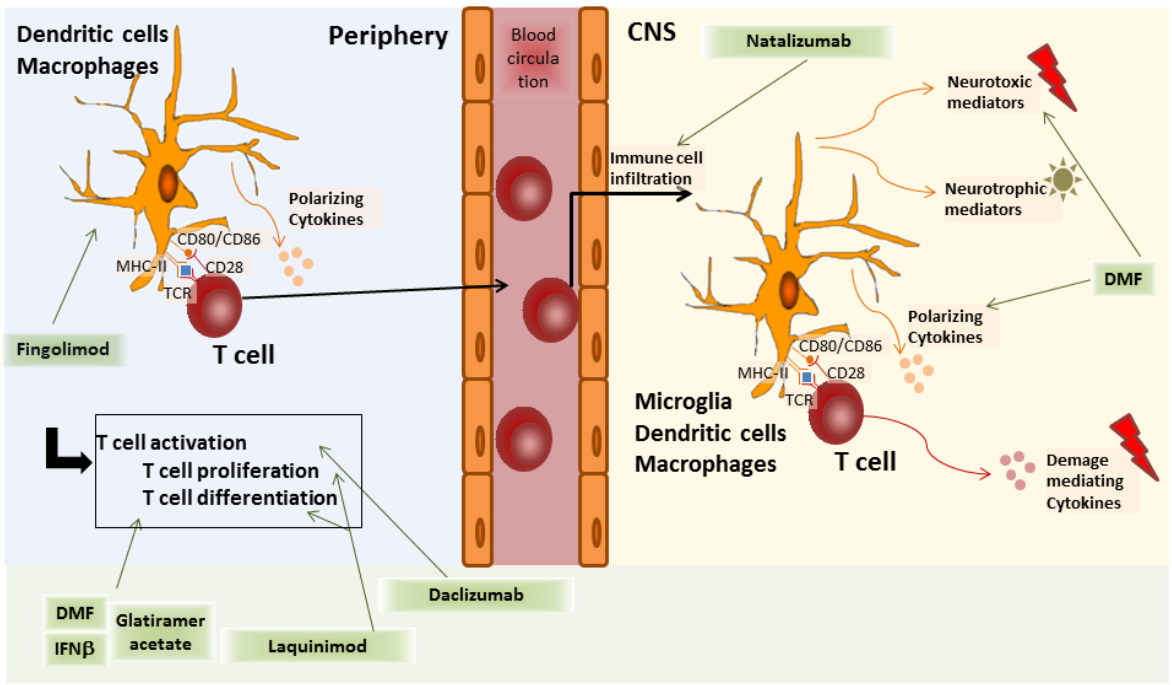

Figure 3: Targets of therapeutics effecting myeloid cells. The role of dendritic cells, macrophages and microglia in the pathogenesis of EAE and MS is shown. The therapeutics which affect these myeloid cells and myeloid cell functions are highlighted in green.

murine and human myeloid cells and impacts the cytokine and chemokine pattern of these cells (Jolivel et al., 2013). Daclizumab has been also described to target myeloid APC, as it is not only able to bind CD25 on T cells, but also to potently inhibit IL-2 trans-presentation during APC-mediated T cell activation (Wuest et al., 2011). Altogether, myeloid cells seem to be substantially involved in EAE and MS. Although the mentioned available therapeutics partly target myeloid cells, their effect mechanisms are rather broad and often accompanied by side effects. Thus, it would be preferable to identify mechanisms which are responsible for the different effects of myeloid cells during the disease and which could reveal more specific targets for new therapeutics.

1.3) Aims and strategies

As described above, myeloid cells fulfill various roles during EAE and MS, among them both beneficial and detrimental effects. To gain deeper insight into the functional roles of myeloid cells in disease exacerbation and regeneration processes and to determine which specific molecular mediators are responsible for these distinct roles of the myeloid cells, two major strategies were followed in this thesis.

First, highly pure $CD11c^+$ myeloid cells were isolated during distinct disease states using fluorescence activated cell sorting (FACS). The surface molecule CD11c was chosen for positive selection to include dendritic cells, but also activated microglia and macrophages, which upregulate the expression of the dendritic cell marker CD11c upon activation (Ponomarev et al., 2005) for further analysis. The isolated $CD11c^+$ myeloid cells were used for deep RNA sequencing to determine differentially expressed genes over the disease course. The up- or downregulation of gene expression in decisive disease stages would indicate a crucial role of the regulated genes during the corresponding disease stage, uncovering their impact on the disease progression and thus potentially revealing a new therapeutic target molecule in EAE and MS.

In addition to genetic approaches, direct interactions between pathogenic T cells and microglia, the most abundant myeloid cell population in the CNS, were evaluated in living EAE-diseased mice during the disease as well as in organotypic hippocampal slices using two-photon microscopy, in order to directly investigate the role of microglia upon Th17 attack. Even though the understanding of the complex balance between detrimental and beneficial

roles of microglia during EAE and MS is essential, live interaction between microglial cells and other immune cells such as T cells in the CNS *in vivo* has not been demonstrated in detail yet.

2) Materials and Methods

2.1) Materials

2.1.1) Instruments

Instrument	Company
Autoclave Heraeus	Thermo Fisher Scientific, Waltham (USA)
Analog Vortex Mixer	VWR International GmbH, Darmstadt (Germany)
BD FACS Canto II	BD Bioscience, Franklin Lakes (USA)
BD FACS Aria II	BD Bioscience, Franklin Lakes (USA)
Bioanalyzer 2100	Agilent, Santa Clara (USA)
Bioanlayzer Chip Vortexer (IKA MS 3)	Agilent, Santa Clara (USA)
Cell Counting Chamber Neubauer improved	Brand , Wertheim (Germany)
Cell Culture Incubator	Binder GmbH, Tuttlingen (Germany)
Cell Culture Microscope, bright field	Hund, Wetzlar (Germany)
Centrifuge Heraeus Fresco 21	Thermo Fisher Scientific, Waltham (USA)
Centrifuge Multifuge Heraeus XIR	Thermo Fisher Scientific, Waltham (USA)
CFX Connect™ Real Time Detection System	Bio-Rad Laboratories, München (Germany)
Confocal Laser Scanning System SP8	Leica GmbH, Wetzlar (Germany)
Eppendorf Research Adjustable-volume Pipettes	Eppendorf GmbH, Wesseling-Berzdorf (Germany)
Fridges and Freezers	Liebherr, Bulle (Switzerland)
Freezer (Sanyo)	EWALD Innovationstechnik GmbH, Rodenberg (Germany)
Gamma irradiator Gammacell 2000	Mølsgaard Medical, Risø (Denmark)
Horizontal Laminar Flow Hood Heraguard	Thermo Fisher Scientific, Waltham (USA)
Magnetic Stand Ambion	Thermo Fisher Scientific, Waltham (USA)
McILWAIN tissue chopper	Campden Instruments LTD, Loughborough (England)
MidiMACS and QuadroMACS Separators	Miltenyi Biotec GmbH, Bergisch Gladbach (Germany)
MiSeq System	Ilumina, San Diego (USA)
NanoDrop 2000c	Thermo Fisher Scientific, Waltham (USA)
Pipetus	Hirschmann Laborgeräte GmbH & Co.KG, Eberstadt (Germany)
Platform Shaker	Edmund Bühler GmbH, Hechingen (Germany)
Qubit® 2.0 Fluorometer	Thermo Fisher Scientific, Waltham (USA)
Surgery Instruments	Fine Science Tools Inc., Heidelberg (Germany)
TC10™ automated cell counter	Bio-Rad Laboratories GmbH, München (Germany)
Thermal Cycler	Peqlab GmbH, Erlangen (Germany)
Vertical Laminar Flow Hood SAFE 2020	Thermo Fisher Scientific, Waltham (USA)
Vibratome Microm HM650V	Thermo Fisher Scientific, Waltham (USA)
Water bath Aqualine AL18	Lauda GmbH & CO. KG, Lauda-Königshofen (Germany)

2.1.1.1) Two-photon Laser Scanning Microscopy (TPLSM) System

Instrument	Company
Bold-Line series of stage top incubators	Okolab, Pozzuoli (Italy)
Leica HCX IRAPO L 25x/0.95 W objective	Leica GmbH, Wetzlar (Germany)
Leica TCS-MP5 multi-photon system	Leica GmbH, Wetzlar (Germany)
MaiTai Laser (Ti:Sa)	Spectra Physics, Irvine (USA)
Olympus BX51 WI upright microscope fitted with an Olympus XLUMPlanFI 20x/0.95 W objective	Olympus Soft Imaging Solutions GmbH, Münster (Germany)
Optical Parametric Oscillator (OPO)	APE, Berlin (Germany)
TriMScope I 2-photon microscope	La Vision BioTec GmbH, Bielefeld (Germany)

2.1.2) Laboratory Supplies, Plastics and Glassware

Product	Company
Cell Counting Slides for TC10™/TC20™ Cell Counter, Dual-Chamber	Bio-Rad Laboratories GmbH, München (Germany)
Cell Culture Dish, polystyrene, Ø 60 mm + 100 mm	Greiner Bio-One GmbH, Frickenhausen (Germany)
Cell Culture Flask, 75 cm^2	Greiner Bio-One GmbH, Frickenhausen (Germany)
Cell strainer, nylon mesh, 100 µm	BD Bioscience, Franklin Lakes (USA)
Centrifuge Tubes, polypropylene (PP), 15 mL + 50 mL	Greiner Bio-One GmbH, Frickenhausen (Germany)
Cling film	Carl Roth GmbH, Karlsruhe (Germany)
Eppendorf Tubes 1.5 mL + 2 mL	Eppendorf GmbH, Wesseling-Berzdorf (Germany)
Hypodermic Needle 20G + 27G	BD Microlance, Gateshead (UK)
MACS LS Columns	Miltenyi Biotec GmbH, Bergisch Gladbach (Germany)
Microscope glass slides	Thermo Fisher Scientific Inc., Waltham (USA)
Millicell cell culture insert, 30 mm, 0,4 µm	Merck Millipore, Darmstadt (Germany)
Multiplate PCR Plates, 96 Wells, clear	Bio-Rad Laboratories GmbH, München (Germany)
Multiwell Plate, tissue-culture treated polystyrene, 24-well, 48-well, 96-well	BD Bioscience, Franklin Lakes (USA)
Netwell insert, 15 mm, mesh size 74 µm	Sigma-Aldrich Corp., St Louis (USA)
Pipette tips 10 µL, 200 µL, 1000 µL	VWR International GmbH, Darmstadt (Germany)
Filter pipette tips 10 µL, 200 µL, 1000 µL	Starlab, Hamburg (Germany)
Polystyrene Round Bottom Test Tubes 5 mL (FACS tubes)	BD Bioscience, Franklin Lakes (USA)
Qubit™ Assay Tubes	Thermo Fisher Scientific, Waltham (USA)
Pre-Separation Filters, 30 µm	Miltenyi Biotec GmbH, Bergisch Gladbach (Germany)
Scalpels	B. Braun AG, Melsungen (Deutschland)
Serological Pipettes, polystyrene, 5 mL + 10 mL + 25 mL	Greiner Bio-One GmbH, Frickenhausen (Germany)
Syringe, 1 mL + 2 mL + 30 mL	B. Braun AG, Melsungen (Deutschland)

2.1.3) Chemicals and Reagents

Compound	Company
Albumin bovine, cell culture grade (BSA)	Serva Electrophoresis, Heidelberg (Germany)
Ammonium chloride (NH_4Cl)	Sigma-Aldrich Corp., St Louis (USA)
Ampure XP beads	Beckman Coulter, Krefeld (Germany)
Annexin V	Biolegend, San Diego (USA)
Aqua bi. dest. Sterile	B. Braun AG, Melsungen (Germany)
Basal Medium Eagle (BME)	Thermo Fisher Scientific, Waltham (USA)
Betaine	Sigma-Aldrich Corp., St Louis (USA)
Brefeldin A	Sigma-Aldrich Corp., St Louis (USA)
Collagenase	R&D Systems, Inc., Minneapolis (USA)
Dexamethasone	Sigma-Aldrich Corp., St Louis (USA)
4,6-diamidino-2phenylindole, dihydrochloride (DAPI)	Thermo Fisher Scientific, Waltham (USA)
D-Glucose	Carl Roth GmbH, Karlsruhe (Germany)
Dispase	R&D Systems, Inc., Minneapolis (USA)
DNase I	F. Hoffmann-La Roche AG, Basel
dNTP mix (10 mM each)	Thermo Fisher Scientific, Waltham (USA)
Dulbeccos PBS with Ca^{2+} & Mg^{2+}	Gentaur, Kampenhout (Belgium)
EB solution	Qiagen, Hilden (Germany)
Ethanol 100 % (v/v) (EtOH)	AppliChem GmbH, Darmstadt (Germany)
Ethanol 70 % (v/v) (EtOH)	AppliChem GmbH, Darmstadt (Germany)
Ethylenediaminetetraacetic acid (EDTA)	Carl Roth GmbH, Karlsruhe (Germany)
EDTA disodium salt dehydrate (Na_2EDTA) solution (0.5 M)	Sigma-Aldrich Corp., St Louis (USA)
Fetal Bovine Serum, heat inactivated (FBS)(FCS)	Biochrom AG, Berlin (Germany)
HEPES	Life Technologies Corp., Grand Island (USA)
Horse Serum, heat inactivated	Thermo Fisher Scientific, Waltham (USA)
IMDM	Life Technologies Corp., Grand Island (USA)
Isoflurane	Abbot, Wiesbaden (Germany)
IS PCR oligo (5'-AAGCAGTGGTATCAACGCAGAGT-3')	biomers.net GmbH, Ulm (Germany)
iQ™ SYBR® Green Supermix	Bio-Rad Laboratories, München (Germany)
KAPA HiFi HotStart ReadyMix (2×)	KAPA Biosystems, Wilmington (USA)
Ketamine	Hameln Pharma Plus GmbH, Hameln (Germany)
L-Glutamine (200 mM)	Sigma-Aldrich Corp., St Louis (USA)
Lipopolysaccharide (LPS)	Enzo Life Sciences GmbH, Lörrach (Germany)
Magnesium chloride ($MgCl_2$)	Sigma-Aldrich Corp., St Louis (USA)
M-CSF	Peprotech, Rocky Hill (USA)
Minimum Essential Medium (MEM)	Thermo Fisher Scientific, Waltham (USA)
NaCl solution 0.9 %	B. Braun AG, Melsungen (Germany)
N-Acetyl-D-Glucosamine (GlcNAc)	Sigma-Aldrich Corp., St Louis (USA)
Normal goat serum (NGS)	Vector Laboratories, Burlingame (USA)
Oligo-dT Primer (5'–AAGCAGTGGTATCAACGCAGAGTACT30VN-3', where 'N' is any base and 'V' is either A, C or G)	biomers.net GmbH, Ulm (Germany)
Paraformaldehyde (PFA)	Carl Roth GmbH, Karlsruhe (Germany)
Penicillin / Streptomycin (P/S) (10,000 units penicillin and 10 mg streptomycin per mL)	Sigma-Aldrich Corp., St Louis (USA)
Percoll	Sigma-Aldrich Corp., St Louis (USA)
Potassium bicarbonate	Sigma-Aldrich Corp., St Louis (USA)
ProLong Gold Antifade Mountant	Thermo Fisher Scientific, Waltham (USA)

Propidium iodide (PI)	Sigma-Aldrich Corp., St Louis (USA)
RNAse inhibitor	Clontech, Mountain View (USA)
Rompun 2 % injection solution (Xylazin)	Bayer Health Care, Leverkusen (Germany)
RPMI 1640	Life Technologies Corp., Grand Island (USA)
Saponine	Carl Roth GmbH & Co. KG, Karlsruhe (Germany)
Sodium bicarbonate ($NaHCO_3$)	Carl Roth GmbH & Co. KG, Karlsruhe (Germany)
Triton X-100	Sigma-Aldrich Corp., St Louis (USA)
Trypan blue	Sigma-Aldrich Corp., St Louis (USA)
TSO (5'-AAGCAGTGGTATCAACGCAGAGTACATrGrG+G-3')	Exiqon, Vedbaek (Denmark)
Wortmannin	Sigma-Aldrich Corp., St Louis (USA)
β-Mercaptoethanol	Sigma-Aldrich Corp., St Louis (USA)

2.1.4) Kits

Kit	Company
CD4 T Cell Isolation Kit	Miltenyi Biotec GmbH, Bergisch Gladbach (Germany)
DNase I recombinant, RNase free with 10x Incubation buffer	F. Hoffmann-La Roche AG, Basel
Hooke Kit™ MOG_{35-55}/CFA Emulsion + PTX	Hooke Laboratories, Inc. Lawrence (USA)
Hooke Kit™ $PLP_{139-151}$/CFA Emulsion + PTX	Hooke Laboratories, Inc. Lawrence (USA)
High Sensitivity DNA kit	Agilent, Santa Clara (USA)
Image-iT® LIVE Red Caspase-3 and -7 detection kit	Thermo Fisher Scientific, Waltham (USA)
MiSeq Reagent Kit v3	Ilumina, San Diego (USA)
Nextera xt DNA library preparation kit	Ilumina, San Diego (USA)
RNA 6000 Pico kit	Agilent, Santa Clara (USA)
RNeasy® Micro Kit	Qiagen, Hilden (Germany)
RNeasy® Mini Kit	Qiagen, Hilden (Germany)
Superscript II reverse transcriptase + Superscript II First strand buffer + DTT	Thermo Fisher Scientific, Waltham (USA)
Superscript III First Strand Synthesis System	Thermo Fisher Scientific, Waltham (USA)
Qubit RNA assay kit	Thermo Fisher Scientific, Waltham (USA)
Qubit dsDNA HS assay kit	Thermo Fisher Scientific, Waltham (USA)

2.1.5) Microbeads

Kit	Isotype	Company
CD8a (Ly-2) MicroBeads	mouse-α-mouse monoclonal IgG2a	Miltenyi Biotec GmbH, Bergisch Gladbach (Germany)
CD11c MicroBeads	hamster-α-mouse monoclonal antimouse IgG	Miltenyi Biotec GmbH, Bergisch Gladbach (Germany)
CD62L MicroBeads	rat-α-mouse monoclonal IgG2a	Miltenyi Biotec GmbH, Bergisch Gladbach (Germany)
CD90.2 MicroBeads	rat-α-mouse monoclonal IgG2b	Miltenyi Biotec GmbH, Bergisch Gladbach (Germany)

2.1.6) Cytokines

Cytokines	Company
huTGF-β	R&D Systems, Inc., Minneapolis (USA)
IL-2	R&D Systems, Inc., Minneapolis (USA)
IL-23	R&D Systems, Inc., Minneapolis (USA)
IL-4	R&D Systems, Inc., Minneapolis (USA)
IL-6	R&D Systems, Inc., Minneapolis (USA)

2.1.7) Custom Buffers, Solutions and Media

Buffer/Solution	Ingredients
Anesthesia solution	20 mL 50 mg/mL Ketamine 2.5 mL 2% Rompun in 77.5 mL 0.9 % NaCl solution
FACS Buffer	0.5 % BSA in PBS
Lysis Buffer	8.29 g/L NH_4Cl 1 g/L $KHCO_3$ 37.2 mg/L NA_2EDTA in dH_2O
MACS Buffer	0.5 % BSA 0.5 M EDTA in PBS
MEM (2x)	160.93 g MEM + 0.35 g $NaHCO_3$ + 5 L Aqua dest.
Paraformaldehyde (PFA) buffer 4 %	40 g Paraformaldehyde + 1000 mL 0.1 M PBS buffer, pH 7.0 – 7.4
Phosphate buffer (PB)	810 mL of 35.6 g/L di-Sodium hydrogenpohphate dihydrate +190 mL of 31.2g/L Sodium dihydrogenphosphate dihydrate + 1L H2O pH 7.35-7.4
Saponine Buffer	0.5 % Saponine 0.5 % BSA in PBS

Media	Ingredients
Mouse Medium (MM)	10 % FCS 1 % P/S 1 % L-Glutamine 0.1 % β-Mercaptoethanol 1 % HEPES in RPMI
Wash Medium (WM)	5 % FCS 1 % P/S 1 % HEPES in RPMI

Slice culture Medium	50 mL 2x MEM + 41.8 mL Aqua dest. Sterile + 50 mL BME + 50 mL heat inactivated horse serum + 2 mL 200 mM L-Glutamine + 6.25 mL 20 % Glucose pH 7.2
Slice preparation medium	100 mL 2x MEM + 98 mL Aqua dest. Sterile + 1 mL 200 mM L-Glutamine pH 7.35

2.1.8) Antibodies

Antibody	Clone	Isotype	Concentration	Company
αCD11c-APC	HL3	hamster-α-mouse monoclonal IgG1, λ2	0.2 mg/mL	BD Bioscience, Franklin Lakes (USA)
αCD16/ αCD32 (FC-block)	2.4G2	rat-α-mouse monoclonal IgG2b, κ	0.5 mg/mL	BD Bioscience, Franklin Lakes (USA)
αCD206-BV421	CO68C2	rat-α-mouse monoclonal IgG2a, κ	0.12 mg/mL	Biolegend, San Diego (USA)
αCD25-APC	PC61	rat-α-mouse monoclonal IgG1, λ	0.2 mg/mL	BD Bioscience, Franklin Lakes (USA)
αCD28	H57-597	hamster-α-mouse monoclonal IgG2, λ1	0.5 mg/mL	BD Bioscience, Franklin Lakes (USA)
αCD3-APC	1452-C11	hamster-α-mouse monoclonal IgG1, κ	0.2 mg/mL	BD Bioscience, Franklin Lakes (USA)
αCD3e	1452-C11	hamster-α-mouse monoclonal IgG1, κ	0.5 mg/mL	BD Bioscience, Franklin Lakes (USA)
αCD45-eFluor605	30-F11	rat-α-mouse polyclonal IgG	0.5 mg/mL	BD Bioscience, Franklin Lakes (USA)
αCD45-FITC	30-F11	rat-α-mouse polyclonal IgG2b κ	0.5 mg/mL	Thermo Fisher Scientific, Waltham (USA)
αCD45.1-PE	A20	mouse-α-mouse monoclonal IgG2a, κ	0.2 mg/mL	Biolegend, San Diego (USA)
αCD4-AF647	RM4-5	rat-α-mouse monoclonal IgG2a	0.1 mg/mL	Life Technologies Corp., Grand Island (USA)
αCD4-Horizon (V450)	RM4-5	rat-α-mouse monoclonal IgG2a, κ	0.2 mg/mL	BD Bioscience, Franklin Lakes (USA)
αCD4-PECy7	RM4-5	rat-α-mouse polyclonal IgG	0.2 mg/mL	BD Bioscience, Franklin Lakes (USA)
αCD44-AF700	IM7	rat-α-mouse monoclonal IgG2b, κ	0.2 mg/mL	Thermo Fisher Scientific, Waltham (USA)
αCD62L-APC	MEL-14	rat-α-mouse monoclonal IgG2a, κ	0.2 mg/mL	BD Bioscience, Franklin Lakes (USA)
αCD90.2-Pacific	53-2.1	rat-α-mouse	0.5 mg/mL	Biolegend, San Diego

Blue		monoclonal IgG2a, κ		(USA)
αGFP	polyclonal	rabbit polyclonal IgG	5 mg/mL	Abcam, Cambridge (UK)
αI-A[b]-PE	AF6-120.1	mouse-α-mouse monoclonal IgG2a, κ	0.2 mg/mL	BD Bioscience, Franklin Lakes (USA)
αI-A[K]-FITC	10-3.6	mouse-α-mouse monoclonal IgG2a, κ	0.5 mg/mL	BD Bioscience, Franklin Lakes (USA)
αIFN-γ	XMG1.2	rat-α-mouse monoclonal IgG1	8.25 mg/mL	BioXCell, West Lebanon (USA)
αIFN-γ-Horizon (V450)	XMG1.2	rat-α-mouse monoclonal IgG1, κ	0.2 mg/mL	BD Bioscience, Franklin Lakes (USA)
αIL-10-APC	JES5-16E3	rat-α-mouse monoclonal IgG	0.2 mg/mL	BD Bioscience, Franklin Lakes (USA)
αIL-12	C17.8	rat-α-mouse monoclonal IgG2a	7.48 mg/mL	BioXCell, West Lebanon (USA)
αIL-17A-APC	eBio17B7	rat-α-mouse monoclonal IgG2a, κ	0.2 mg/mL	Thermo Fisher Scientific, Waltham (USA)
α-rabbit-AF488	polyclonal	goat-α-rabbit polyclonal IgG	2 mg/mL	Thermo Fisher Scientific, Waltham (USA)
αTNF-α-AF700	MP6-XT22	rat-α-mouse monoclonal IgG1, κ	0.2 mg/mL	BD Bioscience, Franklin Lakes (USA)
αVβ11-FITC	RR3-15	rat-α-mouse monoclonal IgG2b, κ	0.5 mg/mL	BD Bioscience, Franklin Lakes (USA)

2.1.9) qRT-PCR Primers

Gene	Fw Sequence	Rev Sequence	Concentration	Tm [°C]
murine ß-actin	AATCTTCCGCCTTAATACT	AGCCTTCATACATCAAGT	100 nM	59
murine Arginase-1	AAGGTCTCTACATCACAGAA	GAAGCAAGCCAAGGTTAA	200 nM	60
murine Ms4a8a	AGATAAGTGAACCTGAAGATT	GTGAGTTGAAGCAAGAGT	400 nM	58
murine Ym1	GACTATGAAGCATTGAAT	TCTGATAACTGACTGAAT	400 nM	54

2.1.10) Mice

2.1.10.1) Wildtype Mice

Strain	Laboratory
C57BL/6 (B6)	Janvier Labs, Laval (France)
SJL/J	Janvier Labs, Laval (France)

2.1.10.2) Genetically modified mice

Strain	Target Properties	Reference/In house breeding
B6.2D2	$CD4^+$ T cells are $MOG_{35–55}$ specific	(Bettelli et al., 2003)
B6.2D2.CFP	$CD4^+$ T cells are $MOG_{35–55}$ specific and labeled in blue	B6.2D2 x B6.CRFP

B6.2D2.RFP	$CD4^+$ T cells are $MOG_{35–55}$ specific and labeled in red	B6.2D2 x B6.acRFP
B6.CFP	ubiquitous CPF expression, thus cells are labeled in blue	CK6/ECFP (Hadjantonakis et al., 2002) back-crossed to C57BL/6
B6.acRFP	ubiquitous RPF expression, thus cells are labeled in red	(Luche et al., 2007)
B6.CX3CR1.GFP	$CX3CR1^+$ Microglia are labeled in green	(Jung et al., 2000)
B6.Rag1$^{-/-}$	Mice lack T and B cells	(Mombaerts et al., 1992)
B6.Rag1$^{-/-}$.CX3CR1.GFP	B6.CX3CR1.GFP and $CX3CR1^+$ Microglia are labelled in green	B6.CX3CR1.GFP x B6.Rag1$^{-/-}$

2.1.11) Software

Software	Application	Company
2100 expert software	Analysis of data assessed with the Bioanalyzer 2100	Agilent, Santa Clara (USA)
Beacon Designer 8 Software	Primer design	Premier Biosoft International, Palo Alto (USA)
Bioconductor (R) (v3.2.0) with Bioconductor (R) packages DESeq (v1.2) and EdgeR (v3.10)	Statistical analysis of RNA-Seq data	Bioconductor (Anders and Huber, 2010) (Robinson et al., 2009)
Bio-Rad CFX Manager	Assessment of qRT-PCR data	Bio-Rad Laboratories, München (Germany)
CLC Genomic Workbench 7.0	Assessment of RNA-Seq data	Qiagen, Hilden (Germany)
FACSDiva	FACS Analysis	BD Bioscience, Franklin Lakes (USA)
FlowJo	FACS Analysis	Tree Star, Ashland (USA)
GraphPad Prism 6	Statistical Analysis	GraphPad Software, Inc., La Jolla (USA)
ImageJ	Analysis of histological stainings	National Institutes of Health, Bethesda (USA)
Imaris (v. 8.1.2)	Analysis and Video preparation of two-photon images	Bitplane AG, Zurich (Switzerland)
NanoDrop 2000 / 2000c Operating Software	Determination of RNA concentrations	Thermo Fisher Scientific, Waltham (USA)
Office 2007/2010	Text preperations, Calculations, Figure preparations	Microsoft Corp., Redmond (USA)

2.2) Methods

2.2.1) Handling of cell culture

All cell culture experiments were handled under a laminar flow hood under sterile conditions. The materials for cell culturing were sterilized or disinfected with 70 % ethanol

before use. Waste was autoclaved at 121 °C for 20 min at 1 bar. Cells were cultured at 37 °C in a 5 % CO_2 atmosphere and 95 % humidity, as enabled by the use of cell culture incubators.

2.2.2) Cell counting

Cells were counted either manually (2.2.2.1) or with the help of a Bio-Rad cell counter (2.2.2.2).

2.2.2.1) Manual cell counting

Cells were taken up in a defined volume and an aliquot of the cell suspension was mixed with trypan blue in a ratio of 1:2, 1:5 or 1:10, depending on the expected cell count. The mixture was applied to a Neubauer counting chamber. The cells of the four quadrants of the chamber were counted under a light microscope and divided by four to evaluate the cell number of one quadrant. Trypan blue traverses only through the damaged cell membrane of dead cells, and not through the intact cell membrane of living cells and therefore allows the visual differentiation between living (colorless) and dead (blue) cells (Strober, 2001). The total number of living cells was calculated according to the following formula:

Total cell number = counted cells/quadrant x 10^4 (chamber coefficient) x dilution factor (in trypan blue) x volume cell suspension

2.2.2.2) Counting with Biorad cell counter

Cells were taken up in a defined volume and an aliquot of the cell suspension was mixed with trypan blue in a ratio of 1:2. The mixture was applied to a Bio-Rad counting chamber. The Bio-Rad counting chamber was transferred into the Bio-Rad cell counter and automatic cell counting was started. The Bio-Rad cell counter provided the concentration of total and living cells per milliliter cell suspension. To determine the absolute cell count, the concentration was multiplied by the volume of cell suspension.

2.2.3) Magnetic activated cell sorting (MACS)

MACS allows the separation of distinct cell populations depending on their surface antigens (Miltenyi et al., 1990). This method takes advantage of antibodies tagged with magnetic beads in order to magnetically label distinct surface molecules and therefore to label specific cells populations. For the MACS mediated separation of distinct cell populations, kits from Miltenyi Biotec were used according to the manufacturer's instructions if not otherwise described. Cells were incubated with the appropriate magnetically labeled antibodies for 5-

15 minutes (depending on the surface antigens) at 4 °C in MACS buffer. Subsequently, 35 mL MACS buffer was added to wash the cell suspension and to remove the remaining magnetic beads. Cells were centrifuged (5 min, 550 g, 4 °C) and the cell pellet was resuspended in 1 mL of MACS buffer per $3x10^8$ cells. The cell suspension was then transferred through a pre-separation filter (30 µm) onto a pre-rinsed MACS column in the magnetic field of a MACS separator. To pre-rinse the MACS column, 3 mL of MACS buffer were applied on the column. The nylon mesh was used to avoid clustering of cells and plugging of the column. A maximum of $3x10^8$ cells were added on one MACS column to ensure highest efficiencies of the sorts. After transferring the labeled cells onto the MACS column with a 1 mL-pipet, the pipet tip was rinsed in an Eppendorf tube containing 1 mL of MACS buffer to collect cells for a purity check of the sort ("pre MACS sample"). Once the cell suspension was completely infiltrated into the column, the column was washed three times, each with 3 mL MACS buffer. To prevent the loss of cells in the original tube, the first two washing steps were performed with MACS buffer, which was at the same time used to rinse the original tube. The third washing step was performed with pure MACS buffer. Thus, the rinsed column contained only the magnetically labeled target cells within its magnetic field. Depending on the sorting strategy, either the labeled cell fraction in the magnetic field (positive sort) or the unlabeled cells in the flow-through (negative sort, untouched) were used for further experiments. Since negative sorts usually require a variety of different antibodies to exclude all non-target cells, it is common to use a mixture of biotinylated antibodies for those negative sorts prior to the labeling of these antibodies with anti-biotin antibodies coupled to magnetic beads. After the negative sort, the flow though contains the untouched target cell population, with no bead-coupled antibodies on its surface. In case of the positive sort, the target population is retained in the magnetic field. To elute these cells after the positive sort, the MACS column was removed from the magnetic field and transferred onto a 15 mL tube. 5 mL MACS buffer were added onto the column and a sterile stamp was used to push the labeled cells out of the MACS column. Positively sorted target cells were still labeled with the magnetic beads on its surface. Those beads are usually released after several days in culture. To evaluate the purity of the target cell population and the sort efficiency, 100 µL of cells suspension were taken from the eluate and transferred to an Eppendorf tube containing 1 mL of MACS buffer ("post MACS sample"). The "pre MACS samples" and "post MACS samples" were analyzed with flow cytometric analyses (2.2.4) to evaluate the sort efficiency.

2.2.4) Analysis and separation of cells with FACS

FACS is a flow cytometric method to analyze cell morphologies as well as the expression of surface molecules or intracellular molecules of cells, which allows not only the characterization of cell populations but also the ultrapure separation of cell populations according to their specific characteristics (Hulett et al., 1973). Morphological characteristics are assessed via the interpretation of the light scattering mediated by the cell structures. The forward scatter (FSC) reflects the relative cell size (a higher FSC correlates with a larger cell size) and the sideward scatter (SSC) mirrors the relative granularity of a cell (a high SSC correlates with a high granularity). In addition to scattering properties, cells can be fluorescently labeled using specific fluorophore-labeled antibodies. In the experiments described in this thesis, a FACS Canto II was used for the flow cytometric analysis of cells. A FACS Aria II was used for the analysis of distinct cell populations followed by the separation of cells.

To stain the surface (2.2.4.1) or intracellular molecules (2.2.4.2) of cell populations, the following staining procedures were used. The subsequent analysis of FACS data was performed using the FlowJo analysis software.

2.2.4.1) Surface staining

To stain the surface of cell populations, cell suspensions were centrifuged (550 g, 5 min, 4 °C), supernatants were removed and the cell pellets were washed twice with 1 mL of FACS buffer. After these washing steps the cell pellets were taken up in a staining solution, prepared with fluorescently labeled antibodies directed to the target antigens diluted in FACS buffer. If not otherwise mentioned, 100 µL of staining solution was used for up to $10x10^6$ cells. Cells were incubated with the staining solution for 10 min at 4 °C in the dark. After incubation, 1 mL of FACS buffer was added to the cell suspension to wash the cells. Cell suspensions were centrifuged (550 g, 5 min, 4 °C) and cell pellets were taken up in 200-1000 µL FACS buffer, depending on cell number. The cell suspensions were then transferred in FACS tubes. If propidium iodide (PI) was used to stain dead cells, it was added at a concentration of 1:1000 into the cell suspension directly before acquisition at the flow cytometer. If fixable live/dead staining was used to stain dead cells, washing steps and preparation of staining solutions were performed with PBS instead of FACS buffer to avoid unspecific bindings.

The surface stained cell suspension could be either directly analyzed in the flow cytometer or used for further intracellular staining.

2.2.4.2) Intracellular staining

For intracellular staining, cells had to be fixed and permeabilized. Therefore cell suspensions were centrifuged (550 g, 5 min, 4 °C) and washed with PBS. For fixation, cells were incubated in 1 mL of 2 % PFA buffer (500 µL PBS + 500 µL 4 % PFA buffer) for 20 min at 4 °C in the dark. After fixation, all subsequent centrifugation steps were performed at 1000 g for 5 minutes at 4 °C. Following fixation, cells were washed with PBS. For membrane permeabilization, 2 mL Saponine buffer were added to the cells and cell suspensions were centrifuged. The cell pellets were then washed with another 2 mL Saponine buffer to complete permeabilization. Cells were centrifuged and the supernatants were removed. For Fc-blocking, 70 µL Fc-blocking solution (αCD16/αCD32, 1:70 in Saponine buffer) was added and incubated for 10 min at 4 °C in the dark. For the intracellular staining 20 µL of staining solution, prepared with fluorescently labeled antibodies directed to the intracellular target antigens diluted in Saponine buffer were added. The dilution of the target antibodies were calculated for 100 µL of total staining volume (70 µL + 20 µL + cell pellet and Saponine residues). Incubation occurred for 20 min at 4 °C in the dark. After the intracellular staining, cells were washed with 2 mL Saponine buffer and in a second washing step with 2 mL FACS buffer. The washed cells were then resuspended in 200-300 µL FACS buffer, depending on the cell number. The cell suspensions were transferred to FACS tubes and acquired at the flow cytometer.

2.2.5) Mouse dissections

Prior to dissection of the target organs, surgery instruments were wiped with ethanol (70 %). Mice were either sacrificed via cervical dislocation or lethally anesthetized by the application of 1 mL/mouse anesthesia solution, containing Ketamine and Rompun in sterile NaCl solution (0.9 %). As soon as no reflexes were detectable, the surgery was started. The abdominal skin was opened and detached from the abdominal cavity.

2.2.5.1) Spleen preparation

To dissect the spleen, the abdominal cavity was opened with sterile scissors. Sterile pincettes were used to take out the spleen and to remove the attached pancreas.

2.2.5.2) Lymph node preparation

For all lymph node experiments carried out in this thesis, the inguinal, axial and brachial lymph nodes were dissected and pooled. To dissect these lymph nodes, sterile pincettes were used.

2.2.5.3) CNS preparation

Prior to CNS dissection, mice were perfused with PBS to remove the whole blood from the mouse in order to avoid the presence of blood cells in the dissected CNS. Therefore the thorax of the mice was opened. The diaphragm was removed to enable access to the heart. A small incision was made into the right atrium. A syringe of PBS was used to inject 20-30 mL PBS into the left ventricle. After perfusion, the CNS and spinal cord were removed and transferred into a 15 mL tube containing 5 mL of IMDM.

2.2.6) T cell culture

For Th17 and Th2 cultures, naïve T cells (2.2.6.2) were co-cultured with antigen presenting cells (APC, 2.2.6.1) in the presence of αCD3e and polarizing cytokines (2.2.6.3) as described below.

2.2.6.1) Isolation of APC

For the isolation of APC, spleens (2.2.5.1) from cervically dislocated C57BL/6 mice (6 to 12 weeks old) were dissected and transferred into a 15 mL tube containing 5 mL Wash medium (WM). Cells were put through a nylon mesh (100 µm) and resuspended in 50 mL WM. After centrifugation (550 g, 5 min, 4 °C), erythrocytes were lysed by resuspending the cell pellet in 10 mL Lysis buffer. To stop the lysis, 5 mL WM were added. The cells were centrifuged again (550 g, 5 min, 4 °C) and taken up in 50 mL MACS buffer. Cells were counted manually (2.2.2.1) to determine the most appropriate reagent volume for the magnetic bead-based cell sort of CD90.2 negative cells. MACS was performed as described in 2.2.3. Thereby, the cell pellet was resuspended in 95 µL of MACS buffer and 5 µL of CD90.2 beads for every $1x10^7$ cells. The incubation occurred for 15 min at 4 °C. CD90.2-directed microbeads were used to label splenic lymphocytes without the capacity of antigen presentation. Throughout the magnetic cell sort, all CD90.2 positive cells were removed from the APC fraction, due to fixation in the magnetic field. The flow-through containing the unlabeled APC was centrifuged and the APC were taken up in 10 mL of sterile filtered mouse medium (MM). In order to avoid proliferation of APC in the co-culture with T cells and to limit APC lifetime

during culturing, APC were irradiated in a gamma irradiator, applying 3000 rad. Cells were then centrifuged (550 g, 5 min, 4 °C), taken up in 20-50 mL depending on the pellet size and counted manually (2.2.2.1).

2.2.6.2) Isolation of naïve CD4$^+$ T cells

For the isolation of naïve CD4$^+$ T cells, spleens (2.2.5.1) and lymph nodes (2.2.5.2) from cervically dislocated B6.2D2 mice, B6.2D2.CFP mice or B6.2D2.RFP mice (6 to 9 weeks old) were dissected and transferred into a 15 mL Tube, containing 5 mL WM. Cells were put through a nylon mesh (100 µm) and resuspended in 50 mL WM. After centrifugation (550 g, 5 min, 4 °C), erythrocytes were lysed by resuspending the cell pellet in 10 mL Lysis buffer. To stop the lysis, 5 mL WM was added. The cells were centrifuged again (550 g, 5 min, 4 °C) and taken up in 20-50 mL MACS buffer, depending on the pellet size. Cells were counted manually (2.2.2.1) to determine the most appropriate reagent volume for the magnetic bead-based cells sort of naïve CD4$^+$CD62L^{hi} cells. The magnetic bead-based sort of murine CD4$^+$CD62L^{hi} T cells was performed using a Miltenyi CD4 isolation kit followed by a CD62L positive sort according to the manufacturer's instructions and as described in 2.2.3. Thereby 40 µL MACS buffer and 10 µL of the CD4 T cell biotin antibody cocktail were applied for every 10^7 cells. The pellet was resuspended in the corresponding volume and incubated for 10 min at 4 °C in the dark. According to manufacturer`s instructions, 30 µL MACS buffer and 20 µL anti-biotin microbeads were added after this incubation. An additional incubation time of 5 min followed. At this step 5 µL CD8 microbeads were added in addition to the anti-biotin microbeads to reduce the amount of contaminating CD8$^+$ cells in the target fraction, which are hard to remove by purely applying the CD4 isolation kit. After this untouched sort of CD4$^+$ cells, the efficiency was evaluated via flow cytometry (2.2.4). Therefore, αCD4-Horizon (1:400) and αCD3-APC (1:600) were used to stain these surface molecules. Usually, CD3$^+$/CD4$^+$ purity reached about > 90 % of the lymphocytes. The CD62L positive sort was performed subsequently. Therefore 960 µL of MACS buffer and 40 µL of CD62L microbeads were added to the cell pellet of enriched CD4-expressing cells. The incubation occurred for 15 min at 4 °C in the dark. The efficiency of the cell sort was routinely analyzed via flow cytometry using αCD4-Horizon (1:400) and αCD62L-APC (1:200) antibodies. Only naïve T cells with purity better than 96 % were used for further experiments. Flow cytometry was also used to confirm the expression of Vβ11 of 2D2 cells with αVβ11-FITC (1:400).

2.2.6.3) T cell culture and differentiation

To differentiate the naïve T cells (2.2.6.2) into Th17 cells or Th2 cells, cells were cultured on a 24 well plate in 2 mL MM in the presence of 2 µg/mL αCD3e and with the irradiated $CD90^+$-depleted C57BL/6 splenic APC (2.2.6.1), at a one-to-ten ratio. The following cytokines were added for the initial stimulation into Th17 or Th2 differentiation.

Th17	3 ng/mL TGF-β
	20 ng/mL IL-23
	20 ng/mL IL-6
Th2	10 ng/mL IL-4
	10 µg/mL αIFN-γ
	10 µg/mL αIL-12

After 3 and 5 days of culture, T cells were split and fed with the following cytokines.

Th17	50 U/mL IL-2 (d3); 25 U/mL IL-2 (d5)
	10 ng/mL IL-23 (d3 and d5)
Th2	100 U/mLIL-2 (d3)
	10 ng/mL IL-4 (d5)

Th2 cells were used for co-cultures with hippocampal slices (2.2.15) after 5 days of culture. Th17 cells were either used for co-cultures after 5 days of culture or restimulated after one week. For the restimulation, Th17 were harvested, counted and seeded on 24-well plates with freshly isolated, irradiated $CD90^+$-depleted C57BL/6 splenic APC (2.2.6.1), at a one-to-five ratio and in the presence of 2 µg/mL αCD3e. The following cytokines where added for the restimulation.

Th17	0.75 ng/mL TGFβ
	20 ng/mL IL-23
	10 ng/mL IL-6

Restimulated cells were used three days after the restimulation for further experiments (co-culture with organotypic hippocampal slices or induction of passive transfer EAE).

2.2.6.4) Cytokine check in T cell cultures

Cytokine expression was routinely checked on day 5 and day 10 of culture using flow cytometry to detect successful T cell polarization. 24 h prior to the cytokine check, one well per culture was coated on a 48-well plate with αCD3e and αCD28 antibodies. Therefore 120 µL PBS, containing 3 µg/mL αCD3e and 2.5 µg/mL αCD28 were applied per well. The 48-well plate was covered with a cling film pre-sprinkled with 70 % EtOH and incubated at 4 °C

overnight. For stimulation, the coating solution was removed. 2 mL of the T cell culture were resuspended and divided into each 1 mL cell suspension, which was transferred to either the coated or to an uncoated control well of the 48-well plate. Brefeldin A was added with a final concentration of 5 µg/mL into each well to block the cytokine secretion of the cells. After 4h of stimulation, cells were harvested for the FACS staining which was performed according to (2.2.4) using CD4-PECy7 (1:1000) for extracellular staining, Fc-blocking solution (1:100) and IFN-γ-Horizon (1:200), IL-17-APC (1:200) and TNFa-AF700 (1:200) for intracellular staining analyzing Th17 cells. If Th2 cells were analyzed, an additional intracellular staining of IL-10-APC (1:200) was performed. Th17 cells usually yielded 30-40 % IL-17 and no IFN-γ expression, while Th2 cells lacked the expression of both IFN-γ and IL-17 but showed low IL-10 expression.

2.2.7) EAE

All animal experiments were conducted according to the German Animal Protection Law. For active C57BL/6 EAE, mice were immunized subcutaneously with 200 µL of a myelin oligodendrocyte protein $(MOG)_{35–55}$ emulsion in complete Freund adjuvant (CFA) (Hooke kit). Additionally, C57BL/6 mice received 200 ng pertussis toxin (PTX) intraperitoneally (i.p.) at the time of immunization and after 24 h. For active SJL/J EAE, mice were immunized subcutaneously (s.c.) with 200 µL a proteolipid protein $(PLP)_{139\text{-}151}$ emulsion in 200 µL CFA (Hooke kit). SJL/J mice received 500 ng PTX i.p. at the time of immunization.

For adoptive transfer EAE, 10-30x10^6 2D2.RFP Th17 cells (2.2.6) were injected intravenously (i.v.) into B6.CX3CR1.GFP mice and PTX (400 ng/mouse) was injected on the day of transfer as well as on day 2 following transfer.

Mice were checked for clinical symptoms daily, and signs of EAE were translated into a clinical score as follows. Classical disease: 0, no detectable signs of EAE; 0.5, tail weakness; 1, complete tail paralysis; 2, partial hind limb paralysis; 2.5, unilateral complete hind limb paralysis; 3, complete bilateral hind limb paralysis; 3.5, complete hind limb paralysis and partial forelimb paralysis; 4, total paralysis of forelimbs and hind limbs; 5, moribund or day after death. Atypical disease: 0, no detectable signs of EAE; 1: tail paralysis, hunched appearance, unsteady walk; 2: ataxia, head tilt 3: severe ataxia, spasticity or knuckling; 4 moribund.

2.2.8) Isolation of CD11c$^+$ myeloid cells for RNA-Sequencing

CD11c$^+$ myeloid cells were purified out of freshly isolated mononuclear cells from the CNS (2.2.8.1) and from splenocytes (2.2.8.2) of EAE-diseased mice. In order to enrich CD11c$^+$ cells, a positive MACS was performed (2.2.8.3). Highly pure CD11c$^+$ cells were finally obtained using FACS (2.2.8.4). These cells were taken up in 350 µL RLT buffer (implemented in RNA isolation kits) and resuspended carefully by up and down pipetting (at least ten times) using a syringe (20 G) in order to allow complete lysis of the cells. Lysed cells were stored at -80 °C until RNA isolation (2.2.9.1).

2.2.8.1) Isolation of myeloid cells from the CNS

Dissected CNS tissue was transferred into a 15 mL tube containing 5 mL IMDM (2.2.5.3). Up to three CNS samples were pooled in one tube. To cut the CNS into small pieces, samples were transferred into cell culture dishes and fragmented with a scalpel. CNS fragments and IMDM were then retransferred into the 15 mL tube. To allow the isolation of single CNS-derived cells, CNS samples were treated with 10 mg/mL Collagenase/Dispase, 10 mg/mL Collagenase and 200 U/mL DNase to remove intrinsic collagen fibers, DNA and fibronectin. Digestion was performed for 30 min at 37 °C in a water bath, while the samples were swirled every 5 min. After digestion, the CNS tissue was put through a nylon mesh (70-100 µm), washed with 45 mL IMDM and centrifuged (550 g, 5 min, 4 °C). CNS mononuclear cells were separated by a 30/70 Percoll gradient. Therefore, CNS cell pellets were resuspended in 5 mL 30 % Percoll (in IMDM) per CNS. 5 mL of 70 % Percoll (in PBS) was then carefully overlayed with each 5 mL of the cell suspension. Density centrifugation was performed at 750 g for 30 min with an acceleration- and deceleration-unit of 1 each. Light and fatty compartments on top of the 30 % Percoll were removed with a 1 mL pipet and discarded. To collect mononuclear cells, the cell layer at the interface between the 30 % Percoll layer and the 70 % Percoll layer was collected and transferred to a 50 mL tube containing 40 mL MM. At this step, samples from up to seven mice were pooled. Cells were centrifuged (550 g, 5 min, 4 °C) and taken up in 1 mL MM for automatic cell counting using the Bio-Rad cell counter (2.2.2.2).

2.2.8.2) Isolation of splenic myeloid cells

Dissected spleens were transferred into a 15 mL tube containing 5 mL WM (2.2.5.1). Up to three spleens were pooled in one tube. To cut the spleens into small pieces, spleens and

WM were transferred into cell culture dishes and fragmented with a scalpel. Spleen fragments and WM were retransferred to the 15 mL tube. To allow the isolation of single spleen cells, splenic collagen was digested via treatment with 10 mg/mL Collagenase for 30 min at 37 °C, while the samples were swirled every 5 min. After digestion, spleen tissue was put through a nylon mesh (70-100 µm), washed with 45 mL WM and centrifuged (550 g, 5 min, 4 °C). Erythrocytes were lysed by resuspending the cell pellet in 10 mL lysis buffer. Following resuspension, the lysis was stopped by the addition of 5 mL WM. Spleen cells were then centrifuged (550 g, 5 min, 4 °C) and the cell pellet was taken up in 50 mL WM. Cells were automatically counted using a Bio-Rad cell counter (2.2.2.2).

2.2.8.3) MACS CD11c$^+$-cell enrichment

For CD11c$^+$-cell enrichment, single cells from the CNS (2.2.8.1) and the spleen (2.2.8.2) were labeled with αCD11c microbeads to perform bead-based MACS according to manufacturer's instructions (2.2.3). For all experiments, the total amount of the CNS-derived mononuclear cells obtained were used for the MACS enrichment, while a maximum of $1x10^8$ splenocytes were enriched for one experiment. According to the cell count, 100 µL of αCD11c beads and 400 µL MACS buffer per 10^8 cells were used for the sort. The incubation time was 15 min. In order to optimize the sort efficiency, αCD16/CD32-antibodies (1:100) were added before the incubation with the αCD11c microbeads.

2.2.8.4) FACS of CD11c$^+$ cells

After the CD11c positive MACS enrichment (2.2.8.3), cell suspensions were centrifuged (550 g, 5 min, 4 °C) to proceed with a FACS surface staining (2.2.4.1). During FACS surface staining, the cell pellets were each stained with 1 mL of an antibody cocktail containing fluorescently labeled antibodies against CD11c, CD45, CD45.1, CD90.2, I-A[b] and I-A[K], depending on the target cell population. Staining was performed in 15 mL tubes, which were filled with MACS buffer for the washing steps. Subsequently, target cell populations ($CD45^+CD90^-CD11c^+$ myeloid cells or $CD45^+CD90^-CD11c^+MHCII^+$ myeloid cells) were sorted using the FACS Aria II. 1 mL of MM was prefilled in the collection tube to host the sorted cells. The purity of the sorted populations ranged from 90 to 99 % of living cells. Finally, the cell suspensions were centrifuged to remove the supernatant. The sorted cells were stored in 250 µL RLT buffer at -80 °C.

2.2.9) RNA Isolation

RNA from less than 5 x 10^5 cells was isolated using RNeasy® Micro Kit (2.2.9.1); RNA from more than 5 x 10^5 cells was isolated using RNeasy® Mini Kit (2.2.9.2). The first resuspension steps were performed by up and down pipetting (at least ten times) in RLT buffer using a syringe (20 G) in order to allow complete lysis of the cells.

2.2.9.1) RNA isolation using RNeasy® Micro Kit

The RNA isolation was performed according to the manufacturer's instructions. Consequently, cells were resuspended and homogenized in 350 µL RLT buffer. 350 µL of 70 % ethanol (freshly prepared from 100 % ethanol and RNAse-free water) were added to the lysate and the sample was mixed by pipetting. The sample was then transferred to an RNeasy MinElute spin column in a 2 mL collection tube and centrifuged (8000 g, 15-60 s, at room temperature (RT)). The flow-through was discarded before the column was washed with 350 µL RW1 buffer. The sample was centrifuged (8000 g, 15-60 s, RT) and the flow-through was again discarded. 10 µL DNase I stock solution was diluted in 70 µL RDD buffer to freshly prepare 80 µL of a DNase I incubation mix, which was transferred to the column membrane. Incubation occurred at RT for 15 min to allow DNA digestion. 350 µL RW1 buffer were then used to wash to the column. After centrifugation (8000 g, 15-60 s, RT), the collection tube was discarded. The column was placed in a new 2 mL collection tube and washed with 500 µL RPE buffer. After centrifugation (8000 g, 15-60 s, RT), the flow-through was discarded. An additional washing step was performed with 500 µL of 80 % ethanol (freshly prepared from 100 % ethanol and RNAse-free water) (8000 g, 15-60 s, RT). The column was again placed in a new 2 mL collection tube. To dry the membrane, the lid of the column was opened before the next centrifugation step (21000 g, 5 min, RT). To elute the RNA, the column was placed in a 1.5 mL collection tube, 20 µL RNase-free water were added directly to the center of the column membrane and the column was centrifuged (21000 g, 1 min, RT). The RNA was either directly used for further experiments or stored at -80 °C.

2.2.9.2) RNA isolation using RNeasy® Mini Kit

The RNA isolation was performed according to the manufacturer's instructions. Consequently, cells were resuspended and homogenized in 350 µL RLT buffer. 350 µL of 70 % ethanol (freshly prepared from 100 % ethanol and RNAse-free water) were added to the lysate and the sample was mixed by pipetting. The sample was transferred to an RNeasy

Mini spin column placed in a 2 mL collection tube and centrifuged (8000 g, 15-60 s, RT). The flow-through was discarded before the column was washed with 500 µL RPE buffer. The sample was centrifuged (8000 g, 15-60 s, RT) and the flow-through again discarded. This washing step was repeated using 500 RPE buffer (8000 g, 2 min, RT). The column was placed in a new 2 mL collection tube and centrifuged to dry the membrane (21000 g, 1 min, RT). To elute the RNA, the column was placed in a 1.5 mL collection tube, 87 µL RNase-free water were added directly to the center of the column membrane and the column was centrifuged (21000 g, 1 min, RT). For DNA digestion, the sample was treated with 10 µL 10x incubation buffer and 2 µL DNAse from the Roche DNase kit. 1 µL RNAseOUT from the Superscript III First Strand Synthesis System was additionally applied in order to prevent RNA degradation. This mixture was incubated for 20 min at 37 °C. The reaction was stopped using 2 µL 0.2 M EDTA. 350 µL RLT buffer (containing 10 µL β-mercaptoethanol per 1 mL) were added and mixed well with the sample. Additionally, 250 µL ethanol (96-100 %) was added. Divergent from the manufacturer's instructions, the well-mixed sample (700 µL) was then transferred to an RNeasy MinElute spin column instead of an RNeasy Mini spin column. After centrifugation (21000 g, 30 s, RT), the column was transferred to a new 2 mL collection tube. The sample was washed with 500 µL RPE buffer and centrifuged (21000 g, 30 s, RT). An additional washing step was performed using 500 µL ethanol (80 %). After centrifugation (21000 g, 2 min, RT), the column was again transferred to a new 2 mL collection tube, opened and centrifuged again to dry the membrane (21000 g, 5 min, RT). To elute the RNA, the column was placed in a 1.5 mL collection tube, 20 µL RNase-free water were added directly to the center of the column membrane and the column was centrifuged (21000 g, 1 min, RT). The RNA was either directly used for further experiments or stored at -80 °C.

2.2.10) RNA quantification and quality assessment

RNA samples destined for qRT-PCR analyses were quantified using the NanoDrop. For this, 1 µL of the diluted RNA samples was applied on the spectrophotometer and the NanoDrop software was used to determine RNA quantity.

RNA samples planned for RNA sequencing (RNA-Seq) analyses were quantified using a Qubit® 2.0 fluorometer and the Qubit RNA assay kit. According to the manufacturer's instructions, the Qubit™ working solution was prepared by diluting the Qubit™ RNA reagent 1:200 in Qubit™ RNA buffer in a 1.5 mL Eppendorf tube. 199 µL Qubit™ working solution were transferred into a thin-wall, clear 0.5 mL optical-grade real-time PCR tube (Qubit™

Assay Tube) and 1 µL of the RNA sample were added. The sample was mixed well by vortexing 2–3 seconds, before it was incubated at room temperature for 2 minutes. The sample tube was then inserted into the Qubit® 2.0 fluorometer and the detection process was started. Dependent on the RNA concentration, a part of the RNA sample was diluted in RNAse-free water to avoid a final concentration above 3 ng/µL during quality assessment.

To assess RNA quality, the Bioanalyzer 2100 was used with the Agilent RNA 6000 pico kit according to the manufacturer's instructions. Consequently, the required gel-dye mix was prepared by adding 1 µL of RNA 6000 Pico dye concentrate to a 65 µL aliquot of filtered gel. The sample was then vortexed thoroughly and centrifuged (13000 g, 10 min, RT). The gel-dye mix was equilibrated to RT for 30 minutes in the dark before use. The chip was placed on the chip priming station and 9.0 µL of the gel-dye mix were pipetted at the bottom of the marked well and dispensed. The chip priming station was closed and the plunger of the syringe was pressed from the 1 mL position down until it was held by the clip. After 30 s the plunger was released and pulled back to the 1 mL position after additional 5 s. The chip priming station was then opened and 9.0 µL of the gel-dye mix was pipetted in each of the accordingly marked wells. Then 9 µL of the RNA 6000 Pico conditioning solution were pipetted into the respective marked well. Further, 5 µL of the RNA 6000 Pico marker were pipette into the respective wells. 1 µL of the diluted RNA 6000 Pico ladder were pipetted into the accordingly marked well. Lastly, 1 µL of each sample were transferred into the sample wells. The chip was placed horizontally in the adapter of the IKA vortex mixer and vortexed for 60 s at 2400 rpm. After vortexing, the chip was transferred into the Bioanalyzer and RNA quality was assessed using the 2100 expert software. Only samples with an RNA integrity number (RIN) >7.4 were used for the library preparation for RNA-Seq.

2.2.11) mRNA Sequencing (mRNA-Seq)

Deep mRNA sequencing (mRNA-Seq) is a fulminant tool, allowing the analysis of the whole cell transcriptome, with a highly precise detection of transcript levels and their isoforms superior to other methods (Wang et al., 2009). Taking advantage of mRNA-Seq allows the identification of changes in gene expression patterns in cells (Wang et al., 2009) and thus enables the identification of gene expression patterns controlling myeloid cell function and potentially influencing disease states, such as exacerbation and remission of EAE or MS. For mRNA-Seq, RNA samples with an RIN >7.4 were used. The cDNA was synthesized from RNA as described by Picelli et al. (Picelli et al., 2014)(2.2.11.1). After the determination of the

cDNA quantity (2.2.11.2), 1 ng of the cDNA was used for the library preparation (2.2.11.3). The library size distribution was assessed (2.2.11.4) before sequencing was performed using the MiSeq (2.2.11.5).

2.2.11.1) cDNA synthesis

According to Picelli et al. (Picelli et al., 2014), the respective amount of RNA was pipetted into a 0.2 mL PCR tube containing 1 µL RNAse-free water from the RNA isolation kits, 1 µL RNAseOUT from the Superscript III First Strand Synthesis System, 1 µL of oligo-dT primer (10 µM) and 1 µL of dNTP mix (10 mM). The respective amount of reagents required for all samples was calculated and a reaction mix was prepared, which was then distributed to the sample tubes to guarantee equal reaction conditions for every sample. After adding the RNA, the sample tubes were quickly vortexed, spun down and placed on ice. The samples were then incubated for 3 min at 72 °C to allow oligo-dT primer hybridization to the poly(A) tail of mRNA molecules. After this incubation, the samples were put on ice, spun down, and placed back on ice. For reverse transcription, the reverse transcription mix for all reactions was prepared by combining the reagents listed below.

Component	Volume [µL]	Final concentration
SuperScript II reverse transcriptase (200 U/µL)	0.5	100 U
RNAse inhibitor (40 U/µL)	0.25	10 U
Superscript II first-strand buffer (5x)	2	1x
DTT (100 mM)	0.25	5 mM
Betaine (5 M)	2	1 M
MgCl2 (100 mM)	0.9	6 mM
TSO (10 µM)	1	1 µM
Nuclease-free water	0.1	

7 µL of this mix was then added to the samples. The samples were spun down and incubated in a thermal cycler as described below.

Cycle	Temperature (°C)	Time
1	42	90 min
2-11	50	2 min
	42	2 min
12	70	15 min
13	4	hold

After this incubation 40 µL of the following PCR mix were added.

Component	Volume [µL]	Final
KAPA HiHi HotStart	25	1x
IS PCR primers (10 µM)	1	0.1 µM
Nuclease-free water	14	

To amplify cDNA, PCR was performed using the following program. Dependent on the inserted RNA amount, the number of PCR amplification cycles was altered (usually, 16-17 cycles).

Cycle	Temperature (°C)	Time
1	98	3 min
2-18	98	20 s
	67	15 s
	72	6 min
19	72	5 min
20	4	hold

For cDNA purification, 50 µL of well-mixed Ampure XP beads were added to each sample and mixed by pipetting. Incubation occurred for 8 min at RT to allow DNA binding to the beads. The 96-well plate containing the samples was placed on a magnetic stand for 5 min. Subsequently, the liquid was carefully removed without disturbing the beads. The beads were then washed with 200 µL ethanol (80 %, freshly prepared). After 30 s incubation, the ethanol was removed and washing was repeated with fresh ethanol (80 %, freshly prepared). Following the second washing step, ethanol was completely removed and the beads were dried for 5 min. To elute the purified cDNA, the beads were resuspended in 17.5 µL EB solution and incubated for 2 min. The plate was again placed on the magnetic stand for 2 min. 15 µL of the supernatant were collected. The cDNA was either directly used for DNA quantity- and quality-assessment or stored at -20 °C.

2.2.11.2) cDNA quantification

DNA samples were quantified using a Qubit® 2.0 fluorometer and the Qubit dsDNA HS assay kit. According to the manufacturer's instructions, the Qubit™ working solution was prepared by diluting the Qubit® dsDNA HS reagent 1:200 in Qubit® dsDNA HS buffer in a 1.5 mL Eppendorf tube. 199 µL Qubit™ working solution were transferred into a thin-wall, clear 0.5 mL optical-grade real-time PCR tube (Qubit™ Assay Tubes) and 1 µL of the cDNA sample were added. The sample was mixed well by vortexing 2–3 seconds, before it was incubated at room temperature for 2 minutes. The sample tube was then inserted into the Qubit® 2.0 fluorometer and the detection process was started. Dependent on the DNA concentration, a

part of the cDNA sample was diluted in nuclease-free water from the RNA isolation kits to obtain a final concentration of 0.2 ng/µL.

2.2.11.3) Library preparation

The Nextera xt DNA library preparation kit was used to prepare the cDNA library. According to the manufacturer's instructions 10 µL of TD buffer was pipetted into each sample well of a 96-well plate. 5 µL of the cNDA (0.2 ng/mL) was subsequently added. After additionally adding 5 µL ATM to each well, samples were mixed by pipetting up and down five times. The sample plate was centrifuged (280 g, 1 min, RT) and transferred into a thermal cycler to incubate at 55 °C for 5 min and to then cool down to 10 °C. Once the sample reached 10 °C, 5 µL NT buffer was added to each sample well, mixed with the sample by pipetting, centrifuged (280 g, 1 min, RT) and incubated for 5 min at RT. Subsequently, 15 µL of NPM was added to each well. In every sequencing run, four different samples were compared. To distinguish between samples, different index primers (e.g. n701 and s501, n702 and s502, n703 and s503 or n704 and s504) were applied to each sample and mixed well with the sample by pipetting. The samples were centrifuged (280 g, 1 min, RT) before the following thermal cycle was performed in a thermal cycler.

Cycle	Temperature (°C)	Time
1	72	3 min
2	95	30 s
3-14	95	10 s
	55	30 s
	72	30 s
15	72	5 min
16	10	hold

In order to purify the cDNA libraries, the samples were centrifuged (280 g, 1 min, RT) and transferred into a new 96-well plate. 90 µL of AMPure XP beads were added to each sample well and mixed with the samples by pipetting. Subsequent incubation occurred for 5 min at RT, before the plate was placed on a magnetic stand for 2 min. The supernatant was then discarded and replaced by 200 µL ethanol (80 %, freshly prepared) to wash the beads. After 30 s of incubation, the ethanol was replaced by 200 µL fresh ethanol (80 %, freshly prepared) for a second washing step. The ethanol was again removed after 30 s and the beads were air-dried for 15 min. 52.5 µL RSB were then added, mixed well with the sample and incubated for 2 min. The plate was then placed on the magnetic stand for 2 min. 50 µL of the

clear supernatant containing the purified cDNA libraries were finally transferred into a new 96-well plate. The cDNA was quantified according to (2.2.11.2), before the cDNA library size distribution was assessed (2.2.11.4).

2.2.11.4) cDNA library size distribution assessment

To assess cDNA library size distribution, the Bioanalyzer 2100 was used with a high sensitivity DNA kit according to the manufacturer's instructions. Consequently, the required gel-dye mix was prepared by pipetting 15 µL of the dye concentrate into a high sensitivity DNA gel matrix vial. The tube was vortexed for 10 s and transferred to a spin filter, which was then centrifuged (2240 g, 10 min, RT). The gel-dye mix was equilibrated to RT for 30 minutes in the dark before use. The chip was placed on the chip priming station and 9.0 µL of the gel-dye mix were pipetted at the bottom of the marked well and dispensed. The chip priming station was closed and the plunger of the syringe was pressed from the 1 mL position down until it was held by the clip. After 30 s, the plunger was released and pulled back to the 1 mL position after additional 5 s. The chip priming station was then opened and 9.0 µL of the gel-dye mix was pipetted in each of the accordingly marked wells. Then 5 µL of the high sensitivity DNA marker were pipetted into the respective marked well and into all sample wells. 1 µL of the high sensitivity DNA ladder was pipetted into the accordingly marked well. Finally, 1 µL of each sample was transferred into the sample wells and 1 µL of ladder to every unused sample well. The samples were diluted to a concentration of 2 ng/mL before use. The chip was then placed horizontally in the adapter of the IKA vortex mixer and vortexed for 60 s at 2400 rpm. After vortexing, the chip was transferred into the Bioanalyzer and cDNA quality and library size distribution was assessed using the 2100 expert software. To proof the adequate quality of the cDNA used for the library preparation, cDNA samples were assessed in parallel.

The cDNA library molarity was calculated based on the determined average size according to the following formula: c = c(library) x 1000 x 1/649 x 1/(Average Size) x 1000 nM.

2.2.11.5) Sequencing with Miseq

Sequencing was performed on a MiSeq with MiSeq Reagent Kit v3. Accordingly, 5 µL from each of the target cDNA libraries (pre-diluted to 4 nM) were pooled in a 1.5 mL Eppendorf tube. 5 µL of the pooled library were transferred to a new 1.5 mL Eppendorf tube and 5 µL of NaOH (0.2 N) was added. Incubation occurred for 5 min to allow denaturation before it was

stopped by adding 990 µL HT-1 buffer to obtain a 20 pM library. 540 µL of the library were diluted with 60 µL HT-1 buffer to obtain 600 µL of a 18 pM library, which was finally transferred in a MiSeq chamber into the MiSeq. Sequencing was started and sequencing data were analyzed with CLC Genomic Workbench 7.0.

2.2.12) RNA-Seq statistics

Alignment of RNA-Seq data to the mouse genome (Mm9) and quantification of aligned reads per gene (counts) was conducted using CLC Genomics Workbench software 7.0. All statistical analyses of RNA-Seq data were performed in R (v3.2.0) using Bioconductor routines (Huber et al., 2015) in collaboration with the Institute of Medical Biostatistics Epidemiology and Informatics of the Johannes Gutenberg University Medical Center in Mainz, Germany. After alignment, genes with less than 10 aligned reads in at least one sequencing library were discarded. Significant differences in aligned reads per gene between the different disease conditions and the distinct organs were assessed using the Bioconductor (R) packages DESeq (Anders and Huber, 2010) (v1.2) and EdgeR (Robinson et al., 2009) (v3.10). Differences between the disease conditions were analyzed separately in each mouse model. Normalization for sequencing depth was performed using the normalization procedure implemented in DESeq. Generalized linear models and likelihood ratio tests implemented in EdgeR (McCarthy et al., 2012) were employed to detect genes with significantly different expression between the analyzed conditions. P-values were adjusted for multiple testing using the Benjamini-Hochberg procedure (Benjamini and Hochberg, 1995). Genes with adjusted p-values < 0.05 which is equivalent to a false discovery rate (FDR) of 5 % were flagged as significant in the subsequent analysis. Principal component analysis (PCA) was performed on variance-stabilized expression data. After normalization for sequencing depth, counts per gene were transformed using a variance-stabilizing transformation implemented in DESeq. The 100 most variable genes were used for the PCA. Clustering of samples based on their scores on the two principal components that accounted for the highest amount of expression variability was visually inspected.

2.2.13) qRT-PCR

For qRT-PCR, RNA was transcribed into cDNA using the SuperScript® III First Strand Synthesis System following the manufacturer's instructions. Per reaction, 1 µg RNA was used in a reaction volume of 50 µL. If less material was available all RNA was used. 5 µL of random

hexamer primers (50 ng/µL) were added to 18 µL of the diluted RNA sample. To allow primer hybridization, samples were incubated for 5 min at 65 °C. The tubes were then placed on ice and 27 µL of the following reaction mix was added to each sample:

Component	Volume [µL]
MgCl2	10
10x RT buffer	5
0.1 M DTT	5
dNTP mix (10 mM each)	5
RNaseOUT	1
Superscript III reverse transcriptase	1

The samples were then transferred into a thermal cycler and the following program was started:

Cycle	Temperature (°C)	Time
1	25	10 min
2	50	50 min
3	85	5 min
4	4	hold

If 1 µg RNA was used for cDNA syntheses, the resulting cDNA was diluted with 150 µL nuclease-free water. If less RNA was applied, the cDNA was utilized without dilution for qRT-PCR.

For qRT-PCR, 4 µL of cDNA was amplified using iQ SYBR® Green supermix in a CFX Connect™ Real Time Detection System. Therefore, 100-400 nM of the respective forward and reverse primers (2.1.9; designed using Beacon Designer 8 Software and subsequently tested for amplification efficiency and specificity) were added to 10 µL of the iQ SYBR® Green supermix. Nuclease-free water was used to fill each reaction mix up to 16 µL. The reaction mix was then pipetted into 4 µL of the diluted RNA sample on a clear 96-well plate. The plate was placed in the CFX Connect™ Real Time Detection System and the following thermal cycle was performed:

Cycle	Temperature (°C)	Time	Comment
1	95	3 min	
2-41	95	10 s	
	Tm*	45 s	* Tm varied depending on the target gene (2.1.9)
		Plate read	
42	95	1 min	
43	55	1 min	
44	55-95	Increment: 0.5 °C /10s	Melt curve

Technical triplicates of gene expressions were applied to ensure accuracy of the quantity determination. Data were analyzed using Bio-Rad CFX Manager Software. Only triplicates with an SD < 0.5 were used for the analysis. As described above, amplification was performed for 40 cycles. Samples which were not detectable were included in the analysis with a Cq value of 40. Gene expression was normalized to β-actin expression as described in (Vogelaar et al., 2009).

2.2.14) Generation of bone marrow derived dendritic cells (BMDC) and bone marrow derived macrophages (BMDM)

Bone marrow cells were isolated from the tibias and femurs of C57BL/6 mice. Therefore, the tibias and femurs were flushed with PBS into a petri dish filled with WM. The cells were resuspended in WM and filtered through a nylon mesh (100 µm) to remove remaining bone fragments and fat leftovers. The filtered cells were filled up with WM to 30 mL and centrifuged (550 g, 5 min, 4 °C). The pellet was resuspended and the cell count was determined by manual cell counting (2.2.2.1).

For the *in vitro* generation of BMDC, cells were incubated in 100 mm^2 cell culture dishes at a concentration of 5 x 10^6 cells/cell culture dish. Granulocyte-macrophage colony-stimulating factor (GM-CSF) was added to the culture medium (MM). After 4 days, half of the culture medium was carefully removed and replaced with fresh culture medium containing GM-CSF. For classical activation, LPS was added at a final concentration of 10 µg/mL to the culture. For alternative activation, LPS (final concentration of 10 µg/mL), IL-4 (final concentration of 10 ng/mL) and dexamethasone (final concentration of 5×10^{-7} M) were added to the culture. In such a way the cells were stimulated for 3 days.

For the *in vitro* generation of BMDM, cells were incubated in 75 cm^2 cell culture flasks. Macrophage colony-stimulating factor (M-CSF) was added to the culture medium at a concentration of 20 ng/mL. After 4 days, the culture medium was replaced with fresh culture medium containing M-CSF. For classical activation, LPS was added at a final concentration of 10 µg/mL to the culture. For alternative activation, LPS (final concentration of 10 µg/mL), IL-4 (final concentration of 10 ng/mL) and dexamethasone (final concentration of 5×10^{-7} M) were added to the culture. In such a way the cells were stimulated for 3 days.

2.2.15) Organotypic hippocampal slice (co-)culture

For organotypic hippocampal slice cultures, P2–P6 pups of B6.CX3CR1$^{GFP/GFP}$ mice were decapitated. The brain was rapidly removed and transferred to ice-cold slice preparation medium. Both hemispheres from the brain were separated and the meninges were removed. The hippocampi were isolated with adjacent cortical parts and coronally cut into 300 µm-thick slices using a McILWAIN tissue chopper. Intact hippocampal slices were then transferred onto Millicell cell culture inserts and cultivated for 7 to 14 days in slice culture medium. The medium was changed 24 h after the isolation of the hippocampus and then every other day. After 7 to 14 days of culture, hippocampal slices were used for experiments. For co-cultures either 1 x 10^5 Th17 or 1 x 10^5 Th2 cells were added in a volume of 10 µL on top of the hippocampal slices and cultured for 24 h. To modify the interactions between the T cells and microglia in the slice tissue, the following reagents were added.

Reagent	Final	Application
Annexin V	10 µg/mL	Into T cell medium and slice culture medium on the day the co-culture was started (24 h before imaging)
Wortmannin	2.5-5 µM	Into T cell medium and slice culture medium on the day the co-culture was started (24 h before imaging)
LPS	1 µg/mL	For LPS pre-activation, organotypic slices were treated with LPS for 24 h prior to T cell addition (48 h before imaging). LPS was kept in the medium during the co-culture.
GlcNAc	20-40 mM	Into slice culture medium 24 h before the co-culture was started (48 h before imaging). Additional 20 mM GlcNAc was added to the slice culture medium 20-30 min before the co-culture was started and with the T cells on top of the slices, when the culture was started (24 h before imaging).

2.2.16) Two-photon imaging

2.2.16.1) *In vivo* experiments

Two-photon experiments were performed with EAE-diseased B6.CX3CR1$^{GFP/GFP;+/GFP}$.Rag$^{-/-;-/+}$ mice. EAE was induced by the transfer of pathogenic fluorescently labeled T cells into the recipient mice (s. 2.2.7). Operation procedures and two-photon laser scanning microscopy (TPLSM) for *in vivo* imaging experiments were performed as described previously (Herz et al., 2010; Luchtman et al., 2016; Siffrin et al., 2010a). Briefly, mice were anesthetized with isoflurane and then continuously respirated using 1.5 % isoflurane in oxygen/nitrous oxide (1:2) via a facemask. The anesthetized animal was transferred to a custom-built surgery and

microscopy table and fixed in a hanging position with the head inclined to allow access to regions deeper in the brainstem. The brainstem was exposed for imaging by carefully removing musculature above the dorsal neck area and carefully removing the dura mater. A sterile agarose patch (0.5 % in 0.9 % NaCl solution) was installed on the exposed brain surface which was used to capture a PBS bath that was continuously exchanged by a peristaltic pump. During surgery and imaging, body temperature was maintained at 35-37 °C. The depth of anesthesia was controlled by continuous CO_2 measurements of exhaled gas. Dual near-infrared and infrared excitation of the brainstem was applied at 850 nm by an automatically tunable Ti:Sa laser and at 1110 nm by an optical parametric oscillator (OPO) pumped by the Ti:Sa laser. Volumes of approximately 300 µm x 300 µm x 72 µm were acquired over time using an Olympus XLUMPlanFI 20x/0.95 W objective on a TriMScope I from LaVision Biotec and exported as TIFFs for 3D analyses.

2.2.16.2) *Ex vivo* experiments

Co-cultures of T cells and hippocampal slices were used after 24 h of co-culture for two-photon Imaging. In order to differentiate viable and apoptotic T cells, co-cultures were stained with Image-iT ™ LIVE Red Caspase-3 and -7 Detection Kit prior to imaging. Thus, 1x wash buffer was prepared by diluting 1 part warm 10x apoptosis wash buffer with 9 parts deionized H_2O. A 30-fold dilution of 30x FLICA reagent working solution was prepared in cell-culture medium, mixed well, and added on top of the slice. This was followed by incubation for 30-60 minutes at 37 °C in a 5 % CO_2 atmosphere and 95 % humidity in the dark, as enabled by the use of cell culture incubators. Subsequently, the solution was removed and the slice was gently rinsed with 2 mL of 1x wash buffer.

For imaging, the cell culture inserts with the organotypic hippocampal slices were transferred to 60 mm cell culture dishes. The cell culture dishes were then transferred onto the stage of a Leica TCS-MP5 multi-photon system with a heated and gas perfused (95 % O_2/5 % CO_2) Ludin enclosure. Volumes of 300 µm x 300 µm at variable depth (max. 80 µm) were acquired with a Leica HCX IRAPO L 25x/0.95 W objective, at 1000 nm to visualize the interaction between CX3CR1.GFP microglia and 2D2.RFP Th17 cells. LIF files were exported for analyses. For imaging CX3CR1.GFP microglia and 2D2.CFP.Th17 cells that were alive (blue) or stained with Image-iT® LIVE Red Caspase-3 and -7 (red), as well as for imaging long term (beyond 20 min), the TriMScope I from LaVision Biotec with the Bold-Line

series of stage top incubators from Okolab was used, allowing long uninterrupted imaging while keeping tight control of temperature, humidity and atmospheric gases.

2.2.17) Two-photon imaging analysis

All image analysis was performed using Imaris software. Cell tracks were created using the tracking tool and manually corrected. Contact types and durations were determined manually with 3D rotation and surface analysis to verify contacts. Temporary contacts were defined as contacts lasting less than 10 min, stable contacts consisted of contacts lasting longer than 10 min. Engulfment processes (EPs) were subdivided in engulfment (T cell is fully surrounded by the microglial cell), escape (T cell moves through the microglial cell) and clear attempt to engulf (microglia actively prolongs processes to engulf microglia). Noise reduction was achieved using the software's "medium filter".

2.2.18) Immunohistochemistry

Immunohistochemistry was performed with co-cultures of organotypic hippocampal slices from CX3CR1.GFP mice with 2D2 T cells (2.2.15). Therefore, the slices were first fixated by transferring the slice culture inserts to a 6-well plate containing 1 mL PFA (4 %). 1 mL additional PFA (4 %) was added on top of the slice. Incubation occurred for 20 min at RT. PFA was removed and the fixation step was repeated two times using fresh PFA (4 %) to complete fixation. The slices were then washed with phosphate buffer (PB) three times (each time 20 min at RT), before the slices were cut out of the insert membrane using a scalpel. The cut culture insert was glued onto a block of agarose to enable re-slicing of the slices with a vibratome. The agarose block was glued to a metal plate which was submerged in the PB-water (1:1) bath of the vibratome cooled to 4 °C. Using the vibratome, the original slices were re-sliced into 50-µm-thick slices. These slices were transferred to Netwell inserts (74 µm mesh size) for free-floating immunohistochemistry and either stored in PB at 4 °C or directly used for the immunostaining.

Before immunostaining was started, non-specific binding sites were blocked using a serum blocking buffer containing NGS (5 %) and Triton X-100 (0. 2 %) diluted in PB. Therefore the slices were incubated in 1 mL of this blocking buffer for 1 h. This incubation step and all subsequent incubation steps were performed in the dark on a platform shaker. To stain microglia, 1 mL of a staining solution containing a primary anti-mouse GFP antibody (rabbit) at a dilution of 1:500 in PB with 0.1 % Triton X-100 were applied and incubated at 4 °C

overnight. The staining solution was then removed and the slices were washed 3 times with PB (each time 10 min). The fluorophore-conjugated secondary antibody anti-rabbit-AF488 was then added at a concentration of 1:1000 in PB containing 0.1 % Triton X-100 and incubated at RT for 4 h. The staining solution was removed and the slices were washed 3 times with PB (each time 10 min). To stain $CD4^+$ cells, 1 mL of the fluorescently labeled primary antibody anti-mouse-CD4-AF647 (1:200) were added in PB containing 0.1 % Triton X-100 for 4 h. Subsequently, the staining solution was removed and the slices were washed with PB (10 min). To stain the nucleus DAPI was used at a concentration of 500 ng/mL in PB and incubated for 20 min at RT. Following incubation, slices were washed five times with PB for 7 min at RT. The slices were then mounted on microscope glass slides using ProLong Gold Antifade Mountant. The Confocal Laser Scanning System SP8 from Leica was used to acquire images which were exported as TIFFs for analysis in ImageJ or Imaris software.

2.2.19) Statistical analysis

If not otherwise mentioned, all data were analyzed using GraphPad Prism 6. Mean group differences were investigated by one-way ANOVA followed by Tukey's multiple comparison test, Mann-Whitney test or independent-sample t-tests. Significance level was set at 0.05. The ROUT method implemented in GraphPad was used to identify and exclude outliers. For slice culture experiments, pie charts reflect the mean of the relative interaction distributions per analyzed video. If normalization was performed in slice culture experiments, each parameter was normalized to the mean of the control group from the respective slice preparation.

3) Results

3.1) Increase of alternatively activated antigen myeloid cells (aaMC) in active EAE

In order to understand how activated myeloid cells are involved during different phases of EAE, CD11c$^+$ myeloid cells were isolated from the CNS and the spleen of SJL/J and C57BL/6 mice at different time points during the disease using flow cytometry (**Figure 4**). For this, up to seven mice with a clinical score representing the mean clinical score of the entire group were combined to gain enough cells for the gene expression analysis during the different disease states using RNA-Seq. SJL/J mice were used to analyze the gene expression of myeloid cells during exacerbation, remission, and relapse phase of the disease. Gene expression in myeloid cells from C57BL/6 mice was analyzed on day 15 prior to the

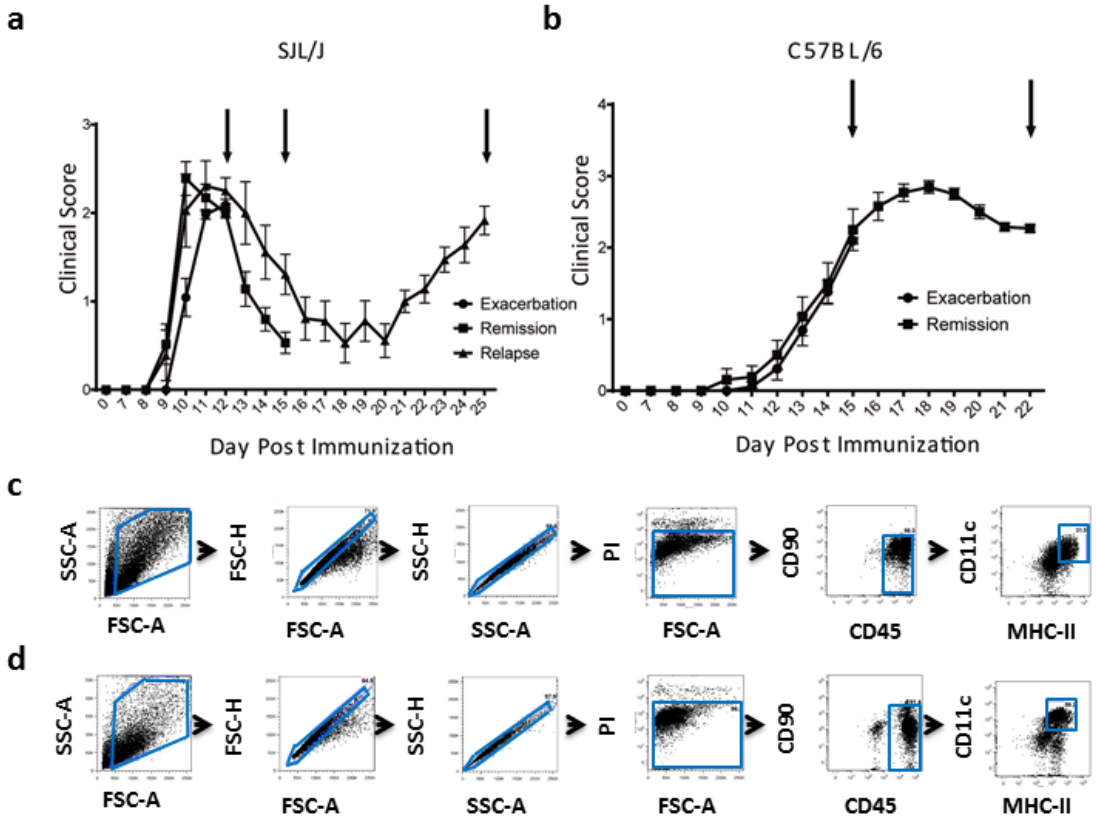

Figure 4: Isolation strategy of CD11c$^+$ myeloid cells during EAE. (a+b) Clinical symptoms of SJL/J mice immunized with $PLP_{139-151}$ **(a)** and C57BL/6 immunized with MOG_{35-55} **(b)** are shown. Data represent the mean clinical score of three independent EAE experiments. CD45$^+$CD90$^-$CD11c$^+$ myeloid cells (SJL/J) or CD45$^+$CD90$^-$CD11c$^+$MHCII$^+$ myeloid cells (C57BL/6) from the CNS and spleen were isolated at the exacerbation of the disease, (partial) remission and relapse, as marked with arrows. **(c+d)** Exemplary gating strategy for the isolation of CD45$^+$CD90$^-$CD11c$^+$MHCII$^+$ myeloid cells from CNS **(c)** and spleen **(d)**. CD45$^+$CD90$^-$CD11c$^+$MHCII$^+$ myeloid cells were sorted by flow cytometry from CD11c$^+$ cells pre-enriched using bead based cell sorting. Debris, doublets, and dead cells were excluded according to the forward and sideward scatter properties of the cells, and using PI. CD45$^+$CD90$^-$CD11c$^+$MHCII$^+$ cells were gated using fluorescent-labeled antibodies. Plots represent sorting from combined C57BL/6 animals.

exacerbation of the disease, when clinical scores were comparable to scores during partial remission. Thus, differences in gene expression in cells isolated from C57BL/6 mice should be related to disease states rather than to differences in the clinical score (**Figure 4b**).

3.1.1) Gene expression during exacerbation and remission is strain specific

A principal component analysis (PCA) based on the variance-stabilized expression data of the 100 most variable genes was performed to identify the main sources of expression variation. The first two principal components (PCs) PC1 and PC2 visualized a clear separation of CNS and spleen samples along the PC1 axis and of SJL/J and C57BL/6 samples along the PC2 axis (**Figure 5**). These data clearly identified the genetic background and the organ tissue as the main sources of variation in gene expression which was much stronger than the additional gene expression variations comparing the different disease states in the CNS. However, CNS samples collected during remission in SJL/J mice seemed to form a cluster which appeared to be distinct from the cluster of exacerbation samples, confirming the expectation of a gene expression regulation during the distinct disease states. In C57BL/6 mice no clearly separated cluster for exacerbation and partial remission samples was observed. It was of interest, which genes were differentially expressed in both mouse models comparing the exacerbation state and the remission despite the strong genetic differences.

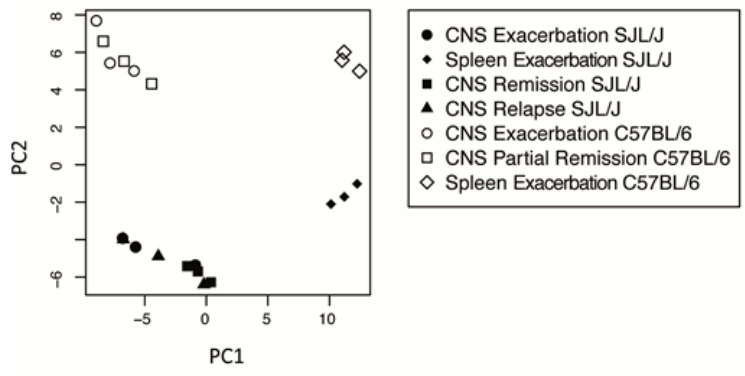

Figure 5: Expression variability depends on mouse strain and target organ. Scores of the RNA-Seq libraries generated from CD11c^{+} myeloid cells on the two principal components (PC1, PC2) that capture the highest amount of expression variability. The PCs are derived from a PCA conducted on the 100 genes with highest expression variation in the RNA-Seq libraries. Each dot corresponds to one RNA-Seq library generated from 3-7 pooled mice from a single experiment. The statistical analyses of RNA-Seq data were performed in collaboration with the Institute of Medical Biostatistics Epidemiology and Informatics of the Johannes Gutenberg University Medical Center in Mainz, Germany.

3.1.2) Genes characterizing aaMC are regulated during EAE

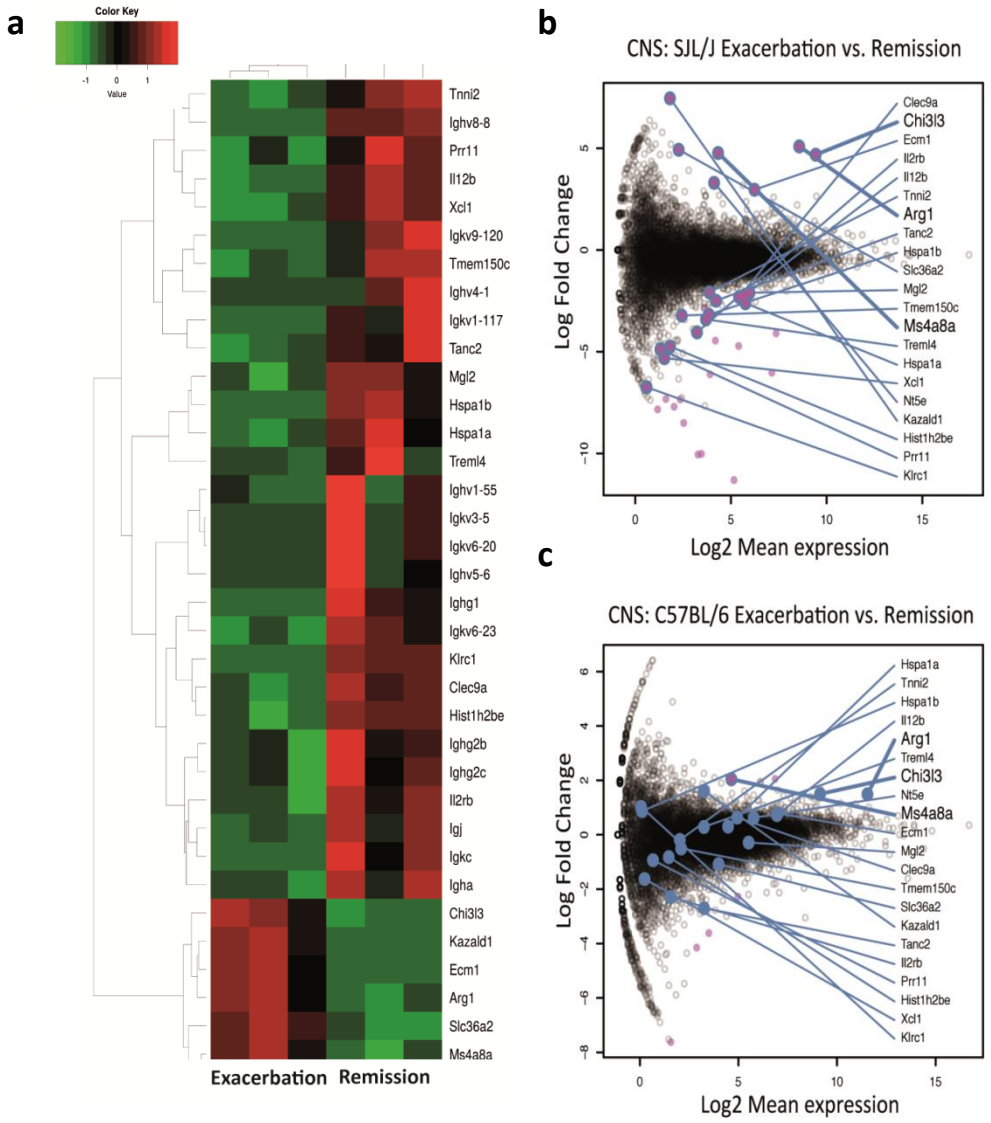

Figure 6: Comparable regulation of gene expression during EAE in SJL/J and C57BL/6 mice show importance of aaMC markers. (a) Gene expression measured by RNA-Seq in CD11c^{+} myeloid cells isolated from the CNS of SJL/J mice during the exacerbation and during the remission of the disease is shown for significantly regulated genes (likelihood- ratio test, FDR < 5%). The results of three independent RNA-Seq experiments are shown. The gene expression data was z-transformed after the variance was stabilized. Relative expression is indicated by color intensity. Green indicates lower while red indicates higher expression compared to the mean expression across all samples. The horizontal dendrogram indicates the relationship between the different samples based on their expression levels inferred by hierarchical clustering. The vertical dendrogram indicates the relationship between genes based on their expression levels inferred by hierarchical clustering. **(b+c)** The log2 fold-change (logFC) between exacerbation and remission of EAE diseased SJL/J mice **(b)** and C57BL/6 mice **(c)** is shown relative to average expression levels (Mean expression (log2 counts per million (CPM)) inferred from each three independent experiments. Positive fold changes indicate higher, negative fold changes indicate lower expression in the exacerbation compared to remission. Significantly regulated genes (likelihood- ratio test, FDR < 5%) are labeled in magenta. Selected genes that are found differentially expressed between exacerbation and remission in SJL/J mice **(**see **a)** are labeled in blue. The statistical analyses of RNA-Seq data were performed in collaboration with the Institute of Medical Biostatistics Epidemiology and Informatics of the Johannes Gutenberg University Medical Center in Mainz, Germany.

Gene expression analysis of CD11c$^+$ myeloid cells isolated from the CNS of SJL/J mice during the different disease states revealed 36 genes to be differentially expressed comparing exacerbation and remission (**Figure 6a+b and Table 1**). Fewer differences were found between exacerbation and relapse, or remission and relapse (**Figure 7**). Genes which were significantly regulated in SJL/J mice comparing exacerbation and remission were considered as genes of interest (**Figure 6**, **Figure 7**, marked in blue). Here, genes coding for antibody immunoglobulin chains originating from CD11c$^+$ B cells (**Figure 6a and Table 1**) were

Table 1: Statistical analysis of RNA sequencing of CNS samples from EAE diseased SJL/J mice. Significantly regulated genes comparing exacerbation and remission of disease are shown. Logarithmic fold-change (logFC)(base2), logarithmic counts per million reads (logCPM), p values, FDR and total read counts for exacerbation, remission and relapse are reported for three experimental repeats. The statistical analyses of RNA-Seq data were performed in collaboration with the Institute of Medical Biostatistics Epidemiology and Informatics of the Johannes Gutenberg University Medical Center in Mainz, Germany.

Gene	logFC	logCPM	PValue	FDR	
Ms4a8a	4.8	4.3	1.73E-08	4.77E-05	**Genes more highly expressed during exacerbation of disease**
Arg1	5.1	8.6	1.66E-07	3.27E-04	
Chi3l3	4.7	9.4	3.28E-06	3.68E-03	
Ecm1	3.0	6.2	8.90E-06	8.01E-03	
Nt5e	3.3	4.1	1.33E-05	1.08E-02	
Kazald1	7.5	1.8	6.82E-05	3.25E-02	
Slc36a2	4.9	2.3	0.000125	4.80E-02	
Igkv6-23	-6.1	3.9	3.63E-09	2.89E-05	**Genes more highly expressed during remission of disease**
Igkc	-4.1	7.4	4.18E-09	2.89E-05	
Igj	-4.7	5.4	7.94E-09	3.66E-05	
Ighg1	-11.3	5.2	1.47E-08	4.77E-05	
Il2rb	-4.0	3.2	1.08E-07	2.49E-04	
Hspa1b	-3.2	3.9	2.70E-07	4.66E-04	
Ighg2b	-6.0	7.1	3.09E-07	4.74E-04	
Ighv5-6	-10.1	3.3	1.30E-06	1.80E-03	
Hspa1a	-2.6	5.8	3.28E-06	3.68E-03	
Mgl2	-2.1	6.0	3.46E-06	3.68E-03	
Il12b	-2.2	5.7	7.09E-06	7.00E-03	
Ighg2c	-4.5	4.2	9.28E-06	8.01E-03	
Igkv6-20	-10.0	3.5	1.46E-05	1.12E-02	
Ighv4-1	-8.5	2.5	1.56E-05	1.13E-02	
Ighv1-55	-7.3	2.3	1.72E-05	1.19E-02	
Igkv1-117	-7.7	2.0	1.89E-05	1.24E-02	
Hist1h2be	-4.7	1.8	2.57E-05	1.61E-02	
Ighv8-8	-6.8	0.5	2.89E-05	1.73E-02	
Treml4	-3.4	3.7	4.38E-05	2.52E-02	
Igha	-2.8	3.6	5.13E-05	2.83E-02	
Prr11	-4.9	1.3	6.25E-05	3.25E-02	
Clec9a	-2.3	5.4	6.55E-05	3.25E-02	
Xcl1	-5.3	1.5	6.65E-05	3.25E-02	
Tanc2	-2.5	4.2	7.20E-05	3.32E-02	
Igkv3-5	-7.8	1.2	8.32E-05	3.65E-02	
Klrc1	-6.7	0.6	8.46E-05	3.65E-02	
Tmem150c	-3.2	2.4	0.000105	4.38E-02	
Tnni2	-2.1	3.9	0.000117	4.75E-02	
Igkv9-120	-7.3	1.6	0.000125	4.80E-02	

excluded from further analysis. Comparing the gene expression regulation of the genes of interest between SJL/J and C57BL/6 mice revealed uniquely Ms4a8a to be significantly regulated in both mouse models (**Figure 6a-c**). Of note, Ms4a8a, Chi3l3 (YM1) and Arginase1, reached the highest significance and the highest fold changes in SJL/J mice (**Table 1 and Figure 6a+b**) and although not significantly, YM1 and Arginase1 were regulated similarly in C57BL/6 mice (**Figure 6c**). Interestingly, Ms4a8a, YM1 and Arginase1 were all described as markers for aaMC (Munder et al., 1998; Raes et al., 2002; Schmieder et al., 2012) and the simultaneous upregulation in the exacerbation suggests a role of this myeloid cell subset during the exacerbation of disease. Tracking Ms4a8a, YM1 and Arginase1 over the disease course in SJL/J mice revealed a reduced expression also during relapse compared to exacerbation (**Figure 7a**). The same genes showed a trend towards a lower expression during remission than during relapse (**Figure 7b**), demonstrating a regulation of these gene expressions over the whole disease course. In the spleen, a significantly lower expression of all three genes was detected compared to CNS suggesting an active role of the respective

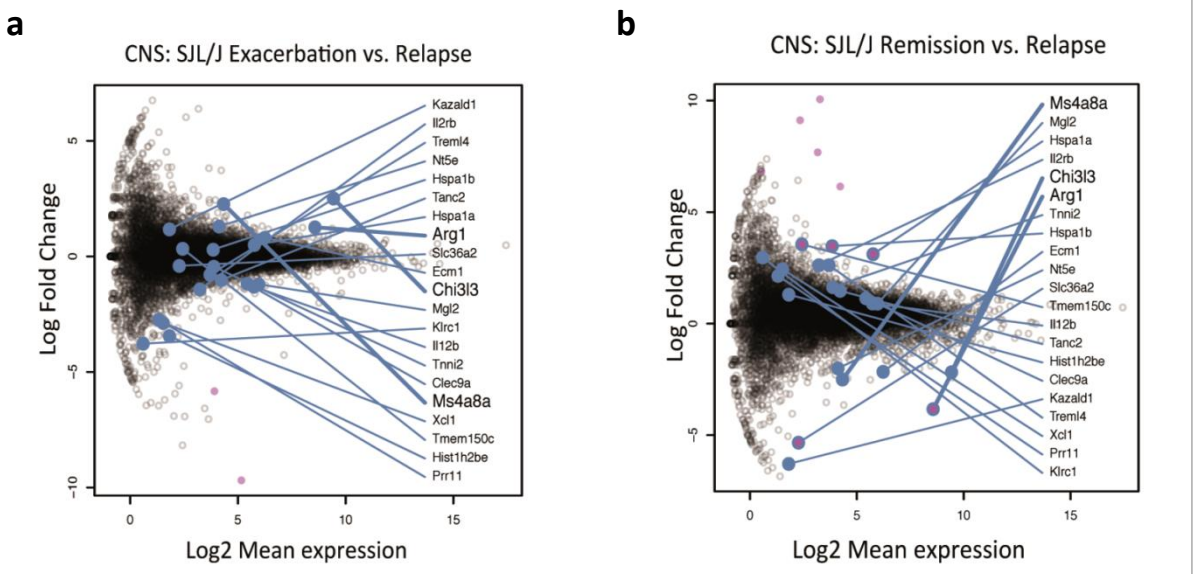

Figure 7: Genes of interest are regulated over the whole disease course. The log2 fold-change (logFC) between gene expression measured by RNA-Seq in CD11c^{+} myeloid cells isolated from the CNS during exacerbation and relapse **(a)** and remission and relapse **(b)** of EAE diseased SJL/J is shown relative to average expression levels (Mean expression (log2 counts per million (CPM)) inferred from each three independent experiments. Positive fold changes indicate higher, negative fold changes indicate lower expression. Significantly regulated genes (likelihood- ratio test, FDR < 5%) are labeled in magenta. Genes of interest are labeled in blue. The statistical analyses of RNA-Seq data were performed in collaboration with the Institute of Medical Biostatistics Epidemiology and Informatics of the Johannes Gutenberg University Medical Center in Mainz, Germany.

proteins in the target organ of the disease (**Figure 8**). These results were independent of the mouse strain as both SJL/J mice (**Figure 8a**) and C57BL/6 mice (**Figure 8b**) showed a significantly lower mRNA expression of all three genes in the spleen.

To confirm the sequencing data, mRNA expression of CD11c$^+$ myeloid cells from the CNS and spleen of EAE diseased mice were additionally analyzed using qRT-PCR. Taking advantage of this technique, gene regulation of Ms4a8a (**Figure 9a+d**), YM1 (**Figure 9b+e**) and Arginase1 (**Figure 9c+f**) was confirmed in the CNS of both SJL/J and C57BL/6 mice. The most prominent expression of Ms4a8a, YM1, and Arginase1 was again found during the exacerbation of the disease, while during remission and relapse a reduced expression of Ms4a8a and YM1 was detected. Although not significantly, Arginase1 showed a slight increase in expression during relapse after remission, as also suggested by the RNA-Seq data, showing the strongest regulation of Arginase1 comparing the three markers of alternatively activated macrophages during remission and relapse (**Figure 7b**). These data indicate a more prominent role of Arginase1 in relapses as compared to Ms4a8a and YM1.

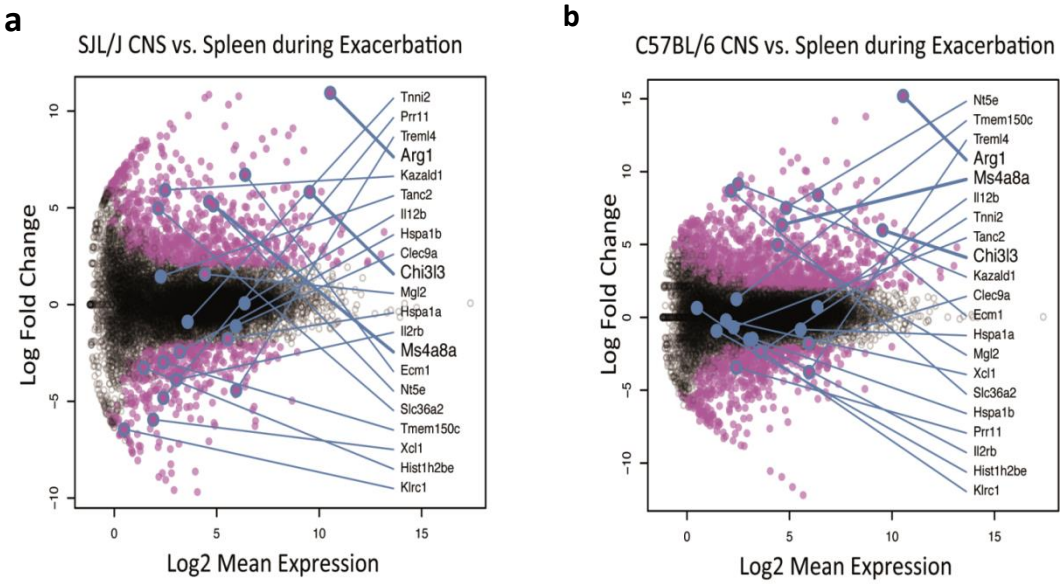

Figure 8: aaMC markers are more highly expressed in the CNS compared to the spleen during the exacerbation of EAE disease. The log2 fold-changes (logFC) between gene expression measured by RNA-Seq in CD11c$^+$ myeloid cells isolated from the CNS and spleen during exacerbation of EAE diseased SJL/J **(a)** and C57BL/6 mice **(b)** are shown relative to average expression levels (Mean expression (log2 CPM)) inferred from three independent experiments. Genes of interest are labeled in blue. Positive fold changes indicate higher, negative fold changes indicate lower expression in the CNS compared to spleen during exacerbation of disease. Significantly regulated genes (likelihood- ratio test, FDR < 5%) are labeled in magenta. The statistical analyses of RNA-Seq data were performed in collaboration with the Institute of Medical Biostatistics Epidemiology and Informatics of the Johannes Gutenberg University Medical Center in Mainz, Germany.

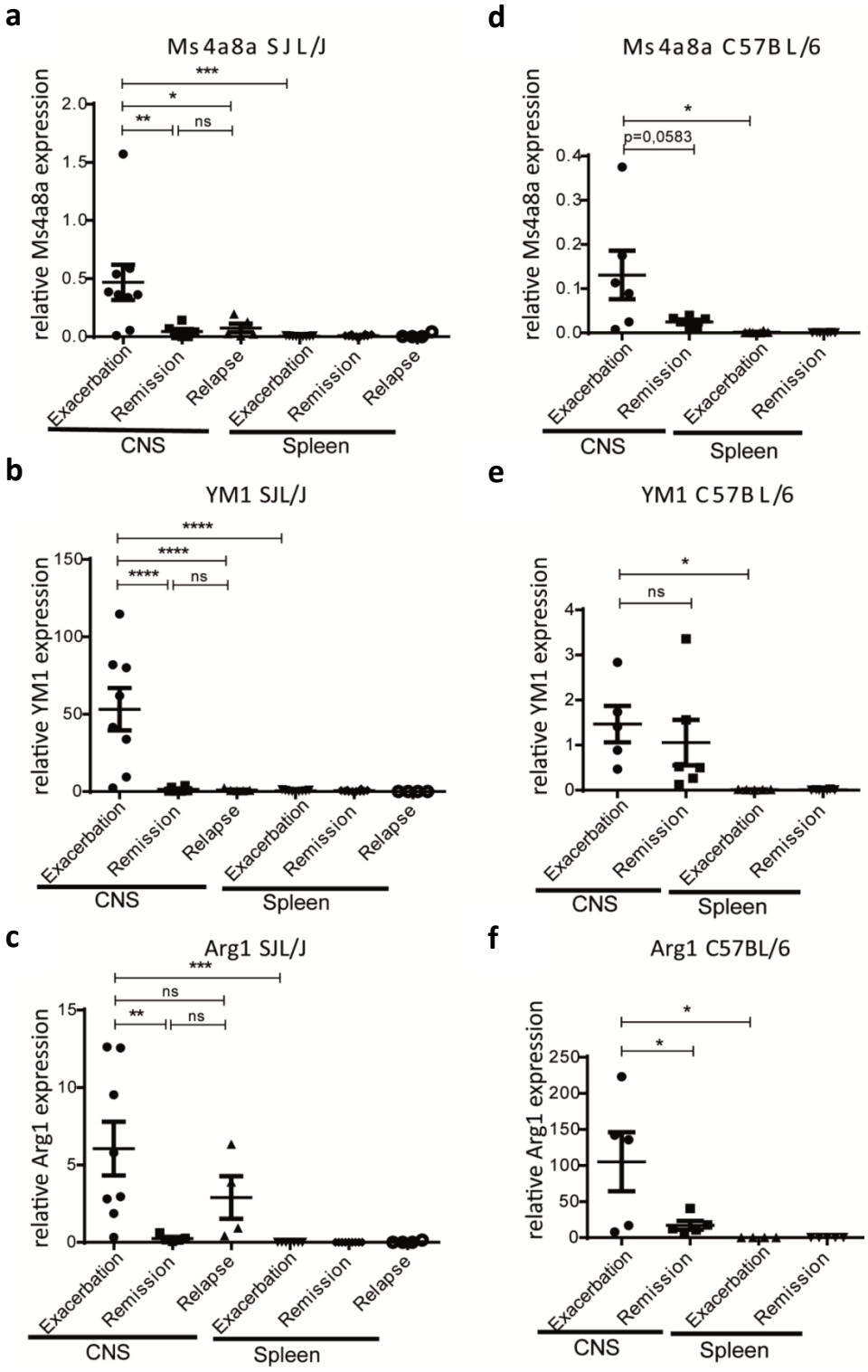

Figure 9: Expression of Ms4a8a, YM1 and Arginase1 genes is higher in myeloid cells from the CNS during the exacerbation of EAE compared to other disease states. qRT-PCR was performed with cDNA from $CD45^+CD90^-CD11c^+MHCII^+$ myeloid cells isolated from the CNS and from the spleen during the exacerbation, (partial) remission and relapse of the EAE in SJL/J (**a-c**) and in C57BL/6 mice (**d-f**). Data represent the expression of Ms4a8a (**a,d**), YM1 (**b,e**) and Arginase1 (**c,f**) in 4–9 samples normalized to β-actin expression. Horizontal lines indicate mean and standard error of the mean (SEM). Differences in gene expression between disease states was investigated by one-way ANOVA and Tukey's multiple comparison test; ns = not significant, * = $p < 0.05$, ** = $p < 0.01$, *** = $p < 0.001$, **** = $p < 0.0001$.

In the spleen, all markers showed lower or no expression and no significant regulation of Ms4a8a, YM1 or Arginase1 mRNA expression was detected tracking the disease course (**Figure 9**).

In order to confirm a role of these genes upon alternative activation of myeloid cells, the induction of Ms4a8a, YM1 and Arginase1 gene expression was further investigated in *in vitro*-generated mouse BMDM and BMDC via treatment with LPS/Dexamethasone/IL-4 for 72 h, which has been previously described to cause an alternatively activated phenotype of myeloid cells (Schmieder et al., 2012).

Treatment with LPS/Dexamethasone/IL-4 induced Ms4a8a, YM1 and Arginase1 gene expression in BMDM (**Figure 10a-c**) and Ms4a8a and YM1 (**Figure 10d+e**) but not Arginase1 (**Figure 10f**) gene expression in BMDC as determined by qRT-PCR. Thus, generally both

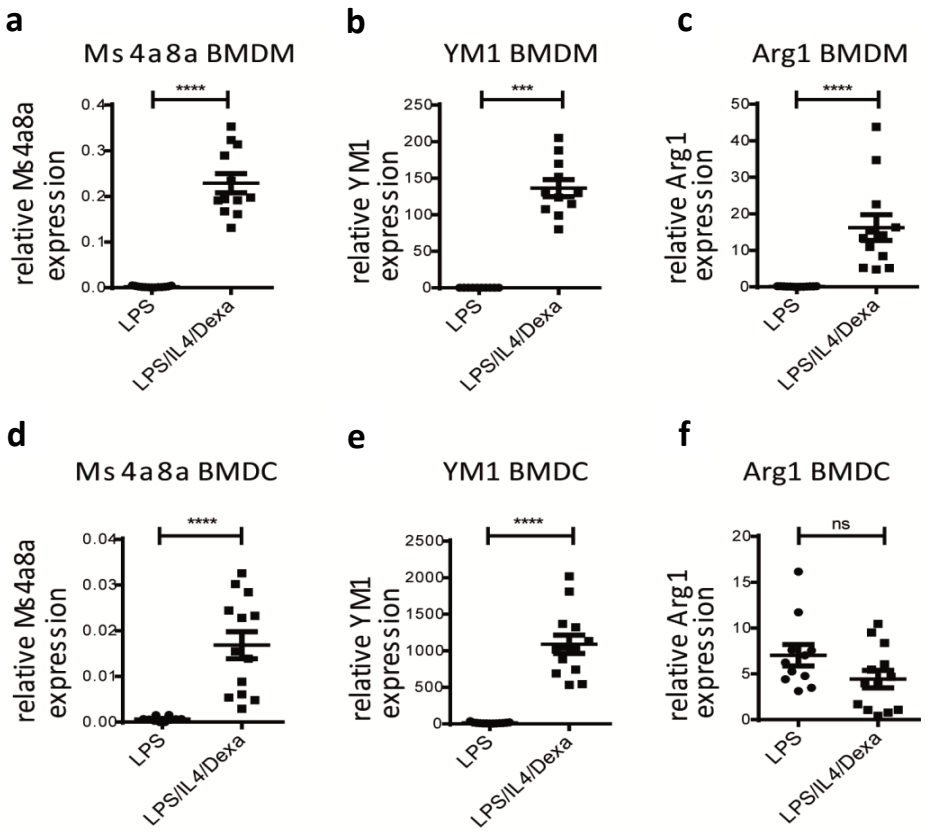

Figure 10: Ms4a8a, YM1 and Arginase 1 expression in BMDM and BMDC following LPS/IL-4 and dexamethasone exposure. BMDMs (**a-c**) and BMDCs (**d-f**) were treated for 72 h with either LPS (10 µg/mL) or a combination of LPS (10 µg/mL), IL-4 (10 ng/mL) and Dexamethasone (5 x 10^{-7} M). RNA expression of Ms4a8a, YM1, and Arginase1 was analyzed by qRT-PCR and normalized to β-actin expression. Data represent the expression of Ms4a8a (**a, d**), YM1 (**b, e**) and Arginase1 (**c, f**) of 10–13 samples from each of four experimental repeats for BMDMs and BMDCs. Horizontal lines indicate mean and SEM. Significance of difference in mean expression was assessed using an unpaired t-test; ns = not significant, *** = $p < 0.001$, **** = $p < 0.0001$.

macrophages and dendritic cells were able to contribute to the higher Ms4a8a and YM1 expression during the exacerbation. However, the gene expression of aaBMDM fit best with the genes found in *ex vivo* myeloid cells during the exacerbation.

3.1.3) Disease state correlates with expression of aaMC markers

To investigate whether the observed higher expression of Ms4a8a, YM1 and Arginase1 in the CNS during the exacerbation of the disease was dependent on the disease phase rather than

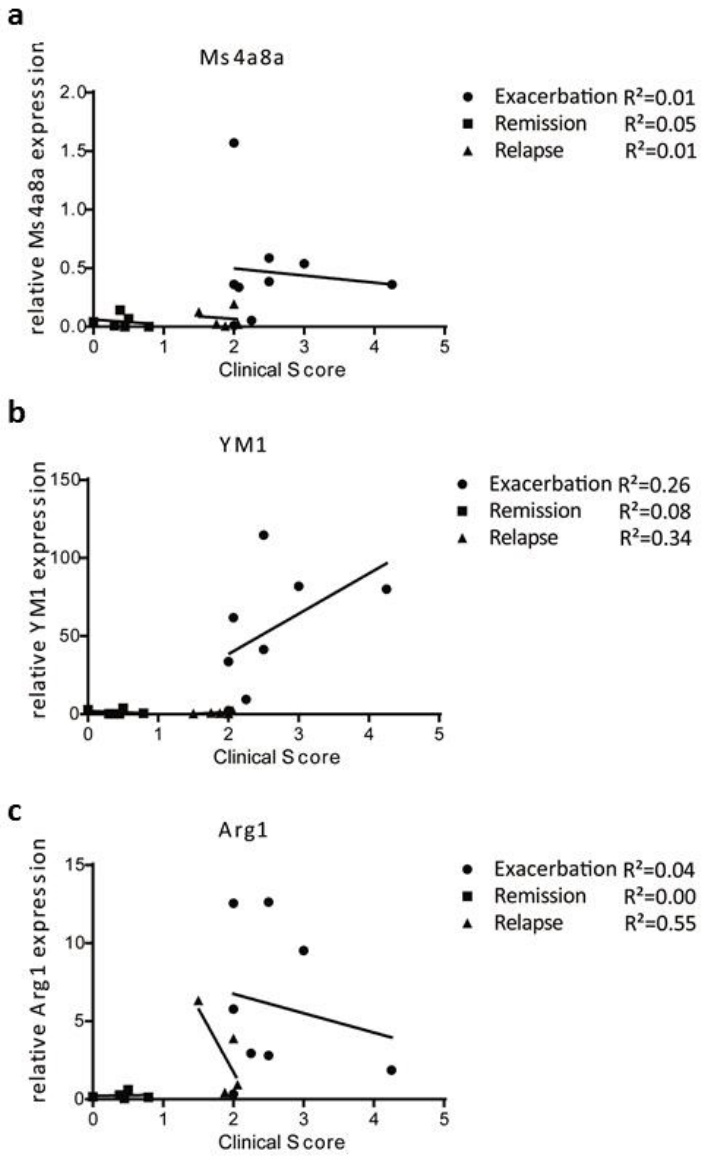

Figure 11: Correlation of aaMC marker expression with clinical score dependent on disease state. qRT-PCR was performed with cDNA from $CD45^{+}CD90^{-}CD11c^{+}MHCII^{+}$ myeloid cells isolated from the CNS of mice varying in clinical score during the exacerbation, remission and relapse of EAE. Dots represent the expression of Ms4a8a **(a)**, YM1 **(b)** and Arginase1 **(c)** normalized to β-actin expression in samples of 1–7 pooled animals, relative to the mean clinical score of all pooled animals. Linear regression was employed to visualize correlation of gene expression with clinical scores separately for the different disease states (solid lines).

on the clinical score, the expression levels of Ms4a8a, YM1 and Arginase1 were determined in relation to the clinical scores. This analysis clearly demonstrated no correlation between the gene expression and the clinical score, neither during the different unique disease states nor when analyzing the data set as a whole (**Figure 11**). Even if equal scores were compared during exacerbation and relapse in SJL/J mice (**Figure 11**), expression of Ms4a8a, YM1 and Arginase1 genes was higher during the exacerbation compared to the relapse state. This may indicate that the activity of Ms4a8a, YM1 and Arginase1 genes counteracted autoimmune inflammation during the first disease wave independent on the disease severity. In order to deeply analyze the function of CNS resident myeloid cells during the active disease state, two-photon imaging was applied to visualize direct microglia-T cell interactions in the CNS.

3.2) Fate of living Th17 cells engulfed by microglia in neuroinflammation

In vivo two-photon imaging is a powerful tool in neuroimmunological research that enables

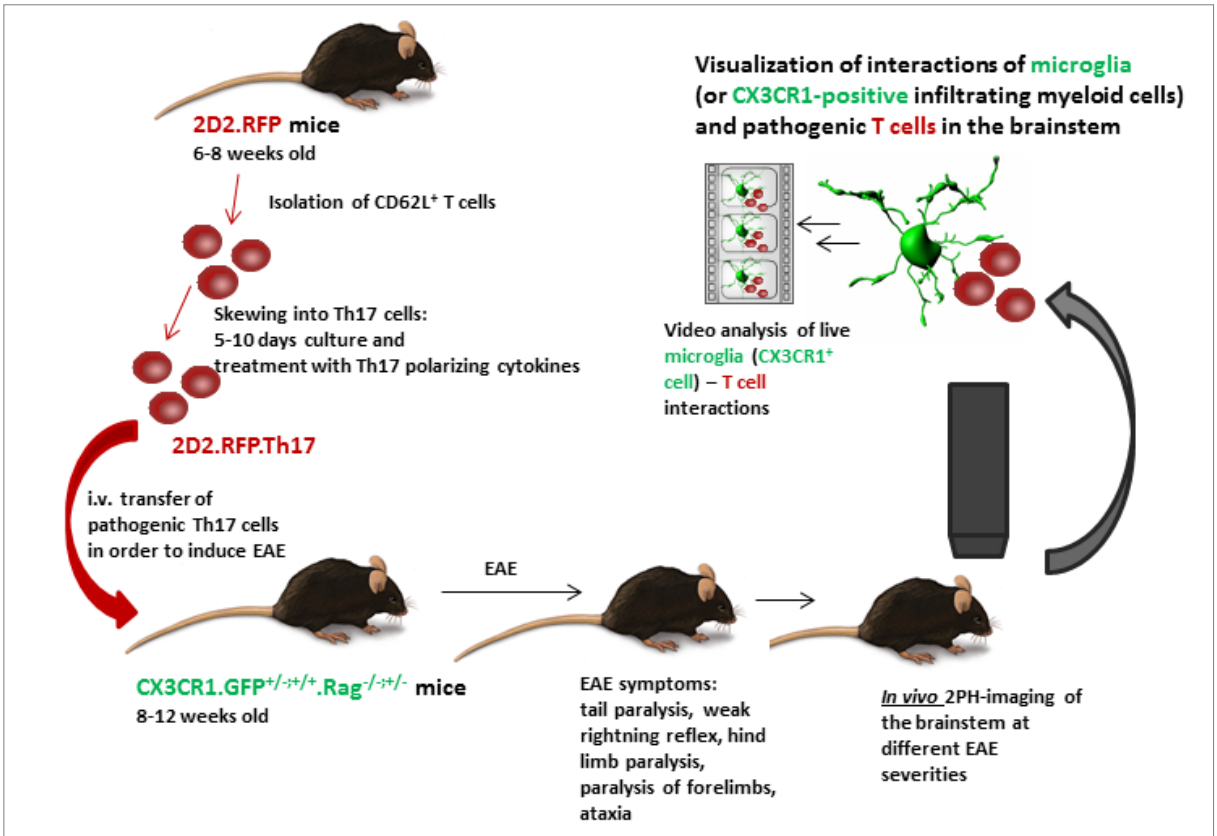

Figure 12: Visualization of microglia-T cell interactions in the CNS *in vivo*. Naïve T cells were isolated from 2D2.RFP mice and skewed into Th17 cells. These pathogenic T cells were injected i.v. into B6.CX3CR1.GFP.Rag mice (either homozygous or heterozygous for GFP and Rag) to induce EAE. The interactions of fluorescently labelled T cells (red) and microglia or other CX3CR1^{+} cells in the CNS (green) were visualized using two-photon (2PH) microscopy during distinct disease severities, allowing the video-preparation of live-interactions as well as the analysis of those interactions.

the direct assessment of disease processes and cellular interactions in the intact CNS tissue (Kawakami and Flügel, 2010; Weigert et al., 2010). In order to analyze the function of CNS resident myeloid cells during the active disease state more precisely, two distinct platforms to investigate microglia-T cell interactions in the CNS were established in this study. In one approach, two-photon imaging was performed *in vivo* in EAE-diseased animals to allow the direct investigation of disease state-dependent processes (**Figure 12**). Therefore EAE was induced by transfer of pathogenic red-fluorescent MOG_{35-55} peptide-specific Th17-skewed

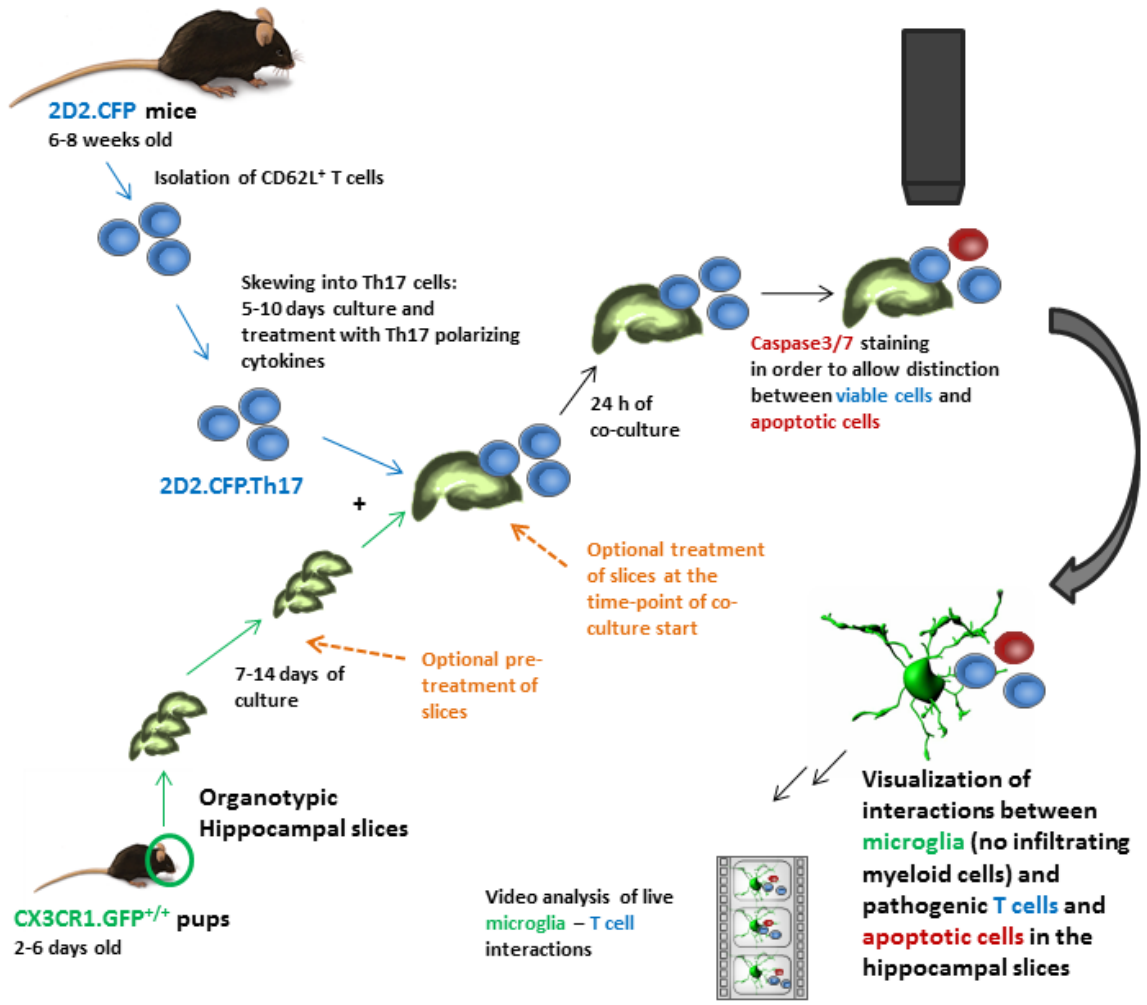

Figure 13: Visualization of microglia-T cell interactions in organotypic hippocampal slices. Naïve T cells were isolated from 2D2.CFP mice, skewed into Th17 cells and co-cultured with organotypic hippocampal slices (7-14 days cultured). Optional pre-treatment of the hippocampal slices was performed 24h before co-culture was started. Co-culture treatment was performed when starting the co-culture. Apoptotic cells were labeled after 24h of co-culture (30 min prior to imaging) with a Caspas3/7 red-staining. The interactions of fluorescently labeled viable T cells (blue) and microglia (green) and apoptotic cells (red) with microglia (green) were visualized using two-photon (2PH) microscopy, allowing the video-preparation of live-interactions as well as the analysis of those interactions.

cells (2D2.RFP) into recipient mice. To enable microglia visualization, EAE was induced in B6.CX3CR1.GFP.Rag recipient mice (either homozygous or heterozygous for GFP and Rag), in which the expression of GFP is driven by the CX3CR1 promoter. Thus, microglia, which have been shown to express CX3CR1 (Goldmann et al., 2013; Jung et al., 2000), were labeled in green and T cells were visualized in red, allowing the investigation of microglia-T cell interactions via two-photon microscopy. In a separate approach, organotypic hippocampal slices (Stoppini et al., 1991) were used to allow targeted modification processes in a stable *ex vivo* model (**Figure 13**). Organotypic hippocampal slice cultures develop largely similar to the *in vivo* tissue, especially when pups around P5 are selected for slicing (De Simoni et al., 2003; De Simoni and My Yu, 2006). After one week *in vitro*, most cells in the slice surface are healthy, receiving and sending inputs from intact axons, thus enabling high-resolution imaging under *in vivo*-like conditions while having the possibility of precise experimental intervention (De Simoni and My Yu, 2006). Here, these hippocampal slices were prepared using B6.CX3CR1.GFP pups in which microglia were labeled in green (Jung et al., 2000). The hippocampal slices were cultured for 7-14 days to allow microglial stabilization after cutting-mediated tissue damage (Vinet et al., 2012) before they were used for further experiments. Blue-fluorescent T cells were then cultured with the hippocampal slices to mimic the *in vivo* situation and T cell infiltration under stable conditions. In addition to the advantages of a stable, targetable system, this *ex vivo* model enabled the specific visualization of microglia, since CNS-infiltrating $CX3CR1^{+}$ myeloid cells which are present in the CNS under EAE conditions (Geissmann et al., 2003; Goldmann et al., 2013; Jung et al., 2000) should be barely present in hippocampal slices prepared from healthy pups. Similar to the *in vivo* model, the fluorescently labeled cells allow the visualization of cellular interactions via two-photon imaging. The exclusive excitation of molecules in the laser focus, the protection of the surrounding tissue from bleaching, and a deep penetration into the tissue reflect major advantages of two-photon microscopy compared to other microscopic approaches (Denk et al., 1990; Theer et al., 2003; Zipfel et al., 2003).

3.2.1) *In vivo* imaging reveals engulfment of viable T cells by microglia in neuroinflammation

To understand how microglia react towards a T cell-driven CNS inflammation, the dynamic interactions of microglia and T cells were visualized in the upper brainstem, which is highly affected by T cell infiltration and inflammation during EAE (Siffrin et al., 2015; Siffrin et al.,

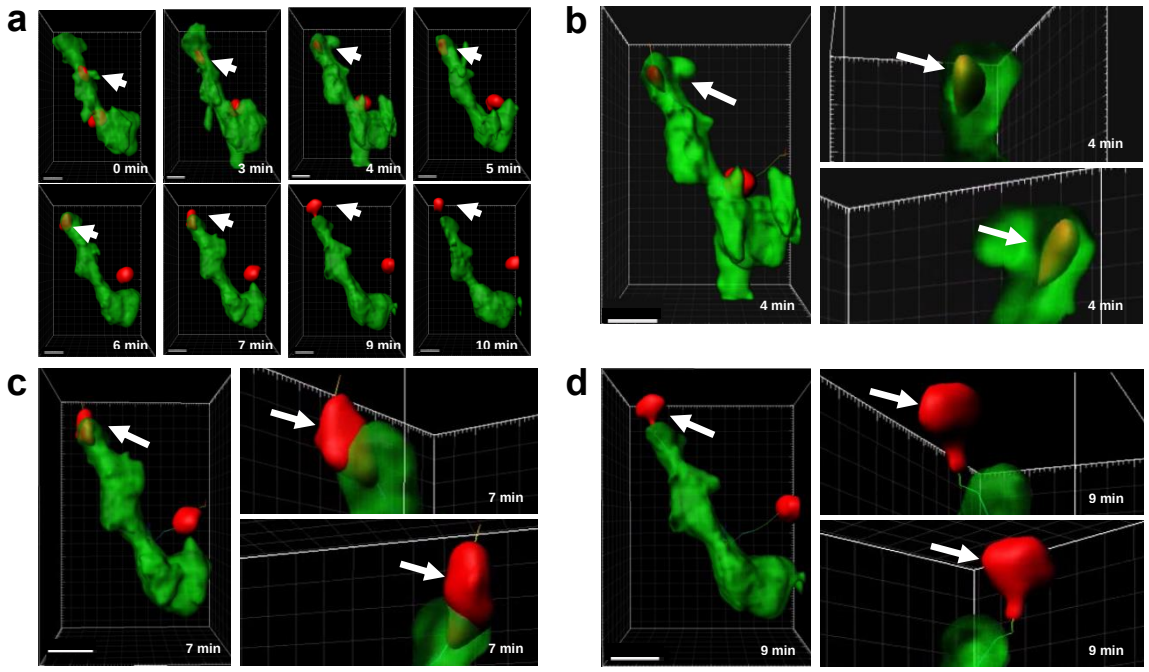

Figure 14: Viable T cells in EAE lesions can be engulfed *in vivo* by CX3CR1^{+} cells without subsequent cell death. EAE was induced in CX3CR1.GFP (microglia green) mice via the passive transfer of 2D2.RFP.Th17 cells (red). At the peak of disease, approximately 11 days post immunization, interactions were imaged *in vivo* with intravital two-photon imaging and analyzed using 3D reconstruction software Imaris. **(a)** Time-lapse surface analysis of the full engulfment (min 3 and 4) of a red fluorescent Th17 cell by a green microglial cell, followed by the escape from this engulfment (min 5-10). Scale bars = 10 µm. (b-d) Magnified and 3D-rotated surface analysis of the sequence from **(b)** full engulfment and **(c)** escape to **(d)** full T cell detachment. Scale bars = 15 µm.

2010a). Infiltrating pathogenic T cells in EAE lesions were found to intensely interact with CX3CR1.GFP cells. In-depth analyses of the surface-reconstructed images revealed multiple types of interactions, including full engulfment of the CNS-infiltrating pathogenic Th17 cells by CX3CR1.GFP microglia (**Figure 14a-d**). Remarkably, two different T cell fates were observed after uptake by microglia. T cells either stayed engulfed or were able to escape this engulfment. These observations point to an active attempt of the CNS-resident microglia to remove invading T cells, although these attempts were only partially successful in the inflamed CNS due to the ability of pathogenic T cells to regularly escape from microglia engulfment.

3.2.2) Resident myeloid cells are responsible for engulfment processes - intravital two-photon imaging in organotypic slice cultures

To exclude a possible contribution of CNS-infiltrating CX3CR1.GFP myeloid cells under EAE conditions (Geissmann et al., 2003; Goldmann et al., 2013; Jung et al., 2000), organotypic hippocampal slice cultures prepared from CX3CR1.GFP mice were co-cultured with

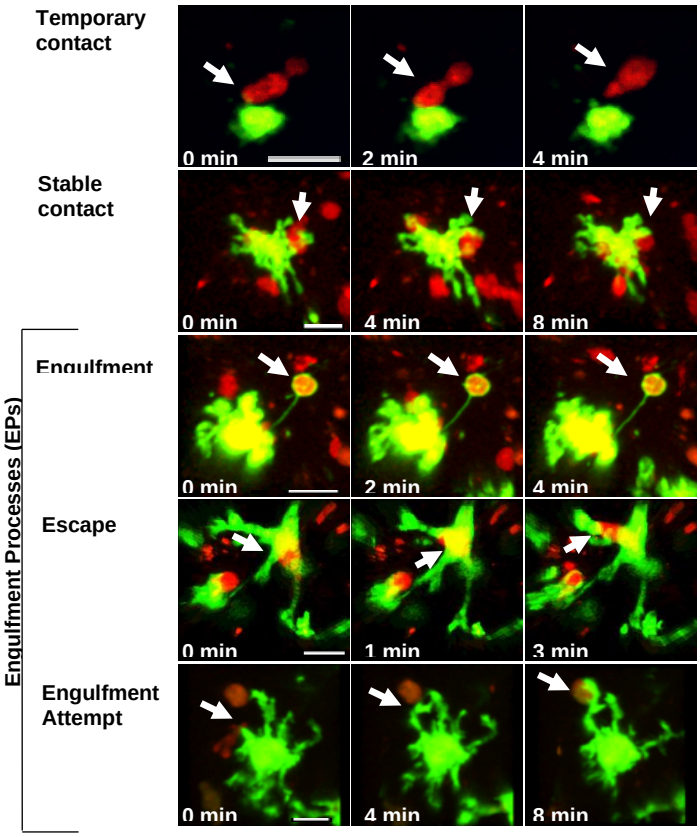

Figure 15: Various interactions between microglia and T cells can be observed in hippocampal slice cultures. 24 h co-cultures of organotypic hippocampal slices from CX3CR1.GFP pups with pathogenic 2D2.RFP.Th17 cells were imaged over a time period of 10 min. The characterization of all detectable interactions between microglia (green) and T cells (red) is shown. All interactions in which a T cell was engulfed, crossing the cytoplasm of a microglial cell during the interaction or in which a microglial cell prolonged it's processes in order to engulf a T cell (Engulfment, Escape and Engulfment attempt) were summarized under the term Engulfment Processes (EPs). Scale bars = 15 µm.

pathogenic T cells for 24 hours, allowing to exclusively focus on microglia-T cell interactions in a controlled *ex vivo* setting, mimicking the *in vivo* condition. As mentioned above, in the hippocampus of healthy, non-immunized CX3CR1.GFP mice, CX3CR1$^+$ infiltrating myeloid cells should be absent or only barely present. In the resulting two-photon time-lapse movies, the observation that microglia cells readily engaged and engulfed T cells *in vivo*, was confirmed (**Figure 15**). The engulfment of CD4$^+$ T cells was further confirmed via immunohistochemistry (**Figure 16**). Based on these detailed observations (**Figures 15+16**), five different types of microglia-T cell interactions were defined: "Temporary" (less than 10 minutes of continuous contact) and "stable" (at least 10 minutes of continuous contact) contacts were most common. In addition to the already described "engulfments" and "escapes" from engulfment following a migration through the microglial cytoplasm (**Figure 14**), the active prolongation of microglial extensions towards and around T cells, either successfully or not ("engulfment attempts"), was also observed (**Figure 15**). These three engulfment-related interactions were summarized under the term "Engulfment Processes" (EPs) (**Figure 15**).

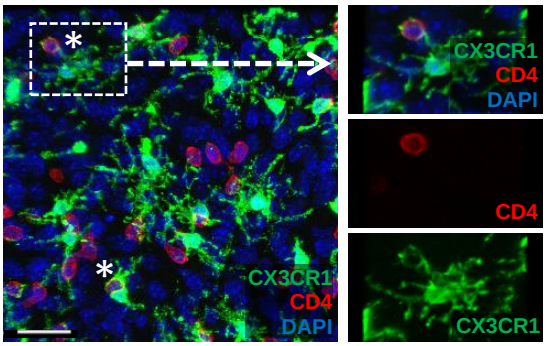

Figure 16: Engulfment of T cells by microglial cells is confirmed via immunohistochemistry. 24 h co-cultures of organotypic hippocampal slices from CX3CR1.GFP pups were co-cultured with pathogenic 2D2.Th17 cells and immunohistochemical staining of microglia (antiGFP, green), $CD4^+$ T cells (antiCD4, red) and cell nucleus (DAPI, blue) was performed to visualize engulfment *ex vivo*. Asterisks mark engulfed T cells. Scale bar = 30 µm. For better visualization, single stainings for one engulfment interaction are shown (right panel).

3.2.3) The interactions of T cells and microglia are regulated over the disease course

The defined interactions between microglial cells and T cells were not static, but depended on the disease severity (**Figure 17**). While the percentage of stable contacts increased in correlation with a higher disease score, temporary contacts were more abundant at lower disease scores (**Figure 17a+b**). Interestingly, the full engulfment of pathogenic T cells was found to be more prevalent in the CNS of EAE-diseased mice exhibiting a low clinical score (**Figure 17a+b**). In the same sense, the T cell motilities were altered over the disease score. Corresponding with the higher amount of temporary contacts compared to stable contacts during a less severe EAE phase, the T cell motility parameters “T cell speed” and “T cell displacement rate” were found to be higher in EAE-diseased mice exhibiting a clinical score below 2 as compared to mice exhibiting a clinical score above 2 (**Figure 17c+d**). Similar results were obtained analyzing the T cell infiltration and migration capacities during the different disease states (**Figure 17e**). During early phases of the disease, T cells showed a higher migration compared to disease states in which a higher disease score was reached (**Figure 17e**).

The interactions of microglia and T cells in organotypic hippocampal slice cultures showed comparable distributions to the interactions of microglia and T cells in the CNS of EAE-diseased mice exhibiting a low clinical score (**Figure 17b**). In terms of T cell motility, T cells in organotypic hippocampal slice cultures showed intermediate T cell motility parameters as compared to T cell motilities in mice exhibiting a clinical score either above or below 2 (**Figure 17d**). The T cell infiltration in organotypic hippocampal slice cultures was comparable to mice exhibiting a clinical score of 1.5 (**Figure 17e**). In summary, the hippocampal slice cultures represented an appropriate model for the *in vivo* system during the early (low

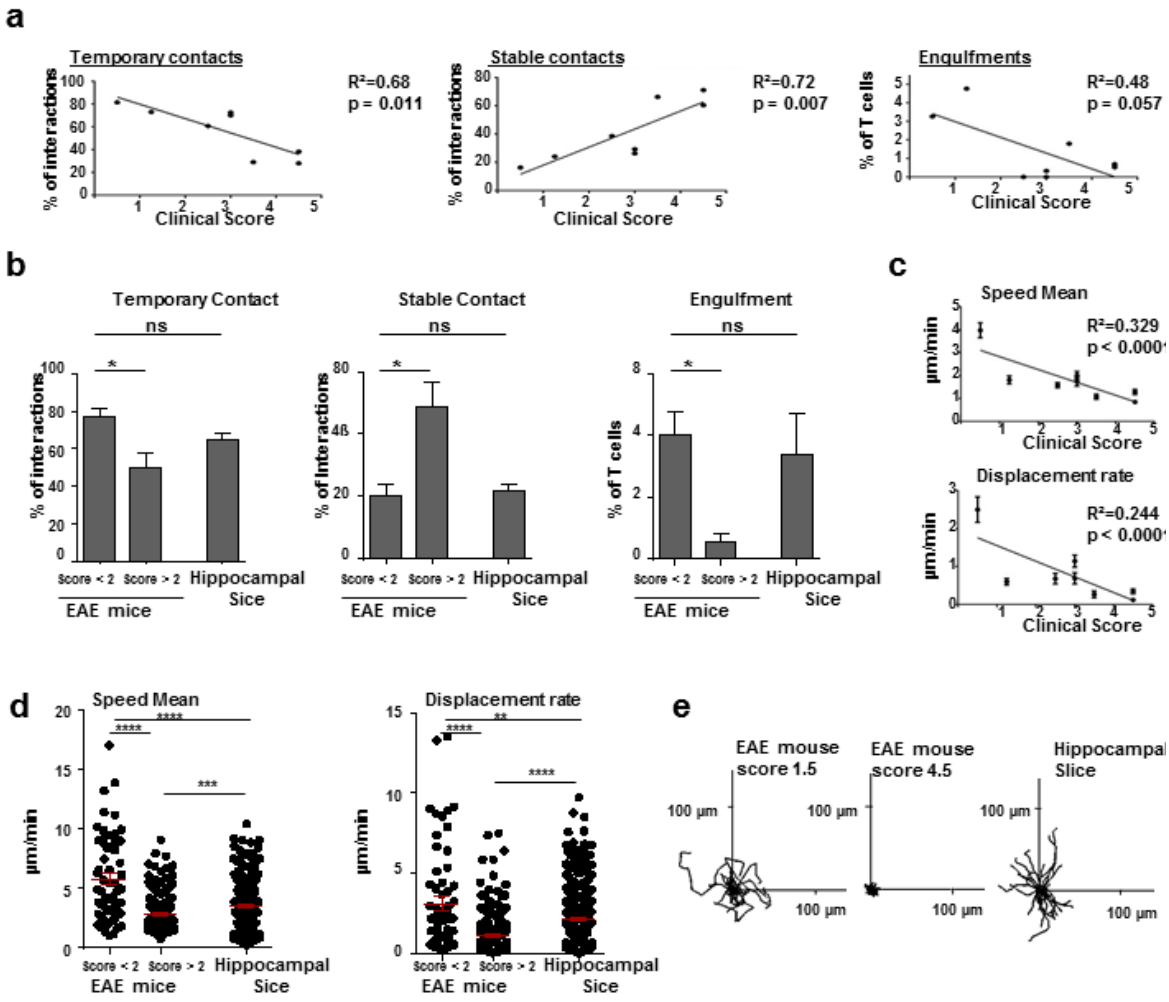

Figure 17: Interactions between microglia and T cells are dependent on disease score. EAE was induced in CX3CR1.GFPxRag$^{-/-}$ and CX3CR1.GFPxRag$^{+/-}$ mice (microglia green) via the passive transfer of 2D2.RFP.Th17 cells (red). Interactions between microglia and T cells as well as T cell motility parameters were imaged *in vivo* with intravital two-photon imaging and analyzed using 3D reconstruction software Imaris during different disease states. For hippocampal slice culture experiments, co-cultures of hippocampal slices from CX3CR1.GFP pups with pathogenic 2D2.CFP.Th17 cells were stained with Image-iT™ LIVE Red Caspase-3 and -7 Detection Kit to identify apoptotic cells and only living T cells were included in further analyses. **(a)** Percentages of temporary contacts, stable contacts and engulfments in the CNS of EAE-diseased mice depending on disease score. p values indicate whether the slope of linear regression is significantly non-zero. (n = 8 mice) **(b)** Mean (± SEM) percentages of temporary contacts, stable contacts and engulfments among the detected interactions or the detectable T cell count per region of interest were compared in mice exhibiting a clinical score below 2 (n = 2 mice), mice exhibiting a score above 2 (n = 6 mice) and hippocampal slice cultures (n = 12 organotypic hippocampal slice cultures). **(c)** Mean (± SEM) of T cell motility parameters in the CNS of EAE-diseased mice in relation to disease score. p values indicate whether the slope of linear regression is significantly non-zero (n = 8 mice, 30 T cells per mouse). **(d)** Mean (± SEM) percentages of T cell motility parameters of representative T cells were compared in mice exhibiting a score below 2 (n = 2 mice, 30 T cells per mouse), mice exhibiting a score above 2 (n = 6 mice, 30 T cells per mouse) and hippocampal slice cultures (n = 13 organotypic hippocampal slice cultures, 17-30 T cells per slice). **(e)** Normalization of all T cell tracks in a representative experiment to a common starting point compared in a mouse exhibiting a clinical score of 1.5, a mouse exhibiting a clinical score of 4.5 and a hippocampal slice co-culture. Each line represents one individual T cell.

clinical score) disease course. In order to investigate the engulfment processes more precisely, the hippocampal slice cultures were used for further experiments.

3.2.4) Dual fate of engulfed living T cells: cell death or escape

In order to determine the fate of engulfed T cells, long-term imaging of the engulfed T cells was performed. To assess the viability of engulfed T cells, Caspase-3/7 activity was stained during live two-photon imaging, to allow the distinction between viable and apoptotic cells. This approach revealed three types of engulfed T cells: living T cells (CFP-positive), early apoptotic T cells (diminished CFP-reporter signal and low Caspase-3/7 expression) and apoptotic T cells (**Figure 18a**). Non-viable cells were expected to lose their genetically-encoded reporter signal (CFP) due to protein degradation. Indeed, in those T cells that did not escape, long-term imaging typically showed a gradual reduction in the CFP fluorescence signal, indicating the degradation of these T cells within microglial cells (**Figure 18b**, false-

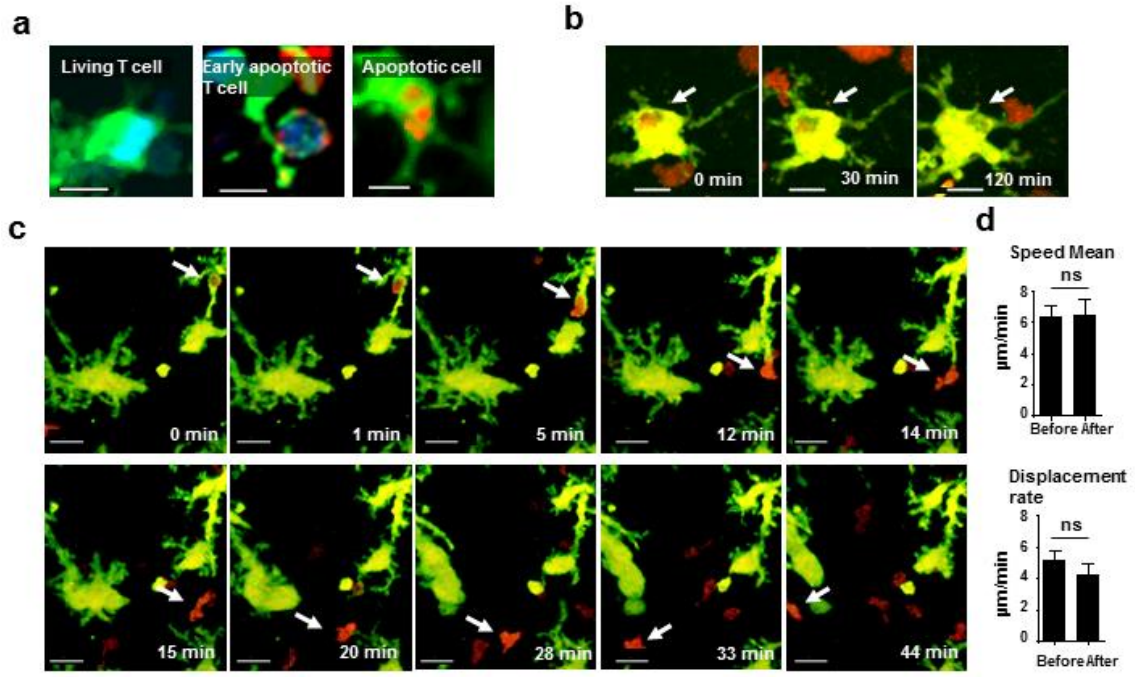

Figure 18: Th17 cell escape from microglia and cell death within microglia after internalization. Co-cultures of hippocampal slices from CX3CR1.GFP pups with pathogenic 2D2.CFP.Th17 cells were stained with Image-iT™ LIVE Red Caspase-3 and -7 Detection Kit to identify apoptotic cells. **(a)** Identification of viable T cells (blue), early apoptotic T cells (blue and red) and apoptotic/dead cells engulfed by microglia (green). Scale bars = 10 µm. **(b)** Representative sequence of an engulfed Caspase-3/7 negative B6.2D2.CFP Th17 cell (viable, false colored in red for better visualization) imaged over a time period of 120 min via two-photon microscopy *ex vivo*. Scale bars = 15 µm **(c)** Representative sequence of an escaped viable T cell (false colored in red for better visualization) for 44 min *ex vivo*. Scale bar = 15 µm. **(d)** Mean (± SEM) T cell motility parameters of viable T cells before (n = 6 cells) and after (n = 6 cells) the interaction with microglia during the escape process *ex vivo*. ns = not significant.

colored in red for better visualization). On the other hand, engulfed T cells which were able to escape the microglial entrapment did not lose their fluorescence intensity or show any indications that the engulfment had an effect on the T cell motility parameters (**Figure 18c+d**). Follow-up of these escaped T cells confirmed them to be viable and actively moving in the tissue for time periods up to at least 45 minutes after escape (**Figure 18c**).

3.2.5) Engulfment of viable cells is not dependent on phosphatidylserine exposure

Since a reversible expression of the "eat-me" signal phosphatidylserine (PS) on stressed (but otherwise viable) cells might already lead to recognition by phagocytic cells (Brown and Neher, 2014), it was of interest whether the here observed engulfment of living T cells was dependent on PS exposure. In order to analyze the effect of an inhibited PS-signaling, Annexin V was applied to co-cultures of organotypic hippocampal slice cultures with B6.2D2.CFP.Th17 cells at a concentration of 10 µg/mL. Treatment with high concentrations of soluble Annexin V has been described to successfully mask PS-signals (Lu et al., 2011). Consistent with the known phagocytic abilities of microglia (Sierra et al., 2013), Caspase-3/7^{+} cells were observed to be more frequently engulfed by microglial cells than viable T cells (**Figure 19a**). However, a detailed quantification of the EPs of living cells showed that the EP frequency accounted to 13 % of all interactions between living T cells and microglia (**Figure 19b**). While the treatment with soluble Annexin V significantly reduced both the total EPs and the engulfment frequencies of apoptotic cells, it had no effect on the EPs and engulfment frequencies of living T cells (**Figure 19c-e**). These data suggest a PS-independent mechanism responsible for the engulfment of viable T cells, in contrast to the PS-dependent phagocytosis of apoptotic cells. Moreover, the Annexin V treatment did not impact T cell motility parameters (**Figure 19f**).

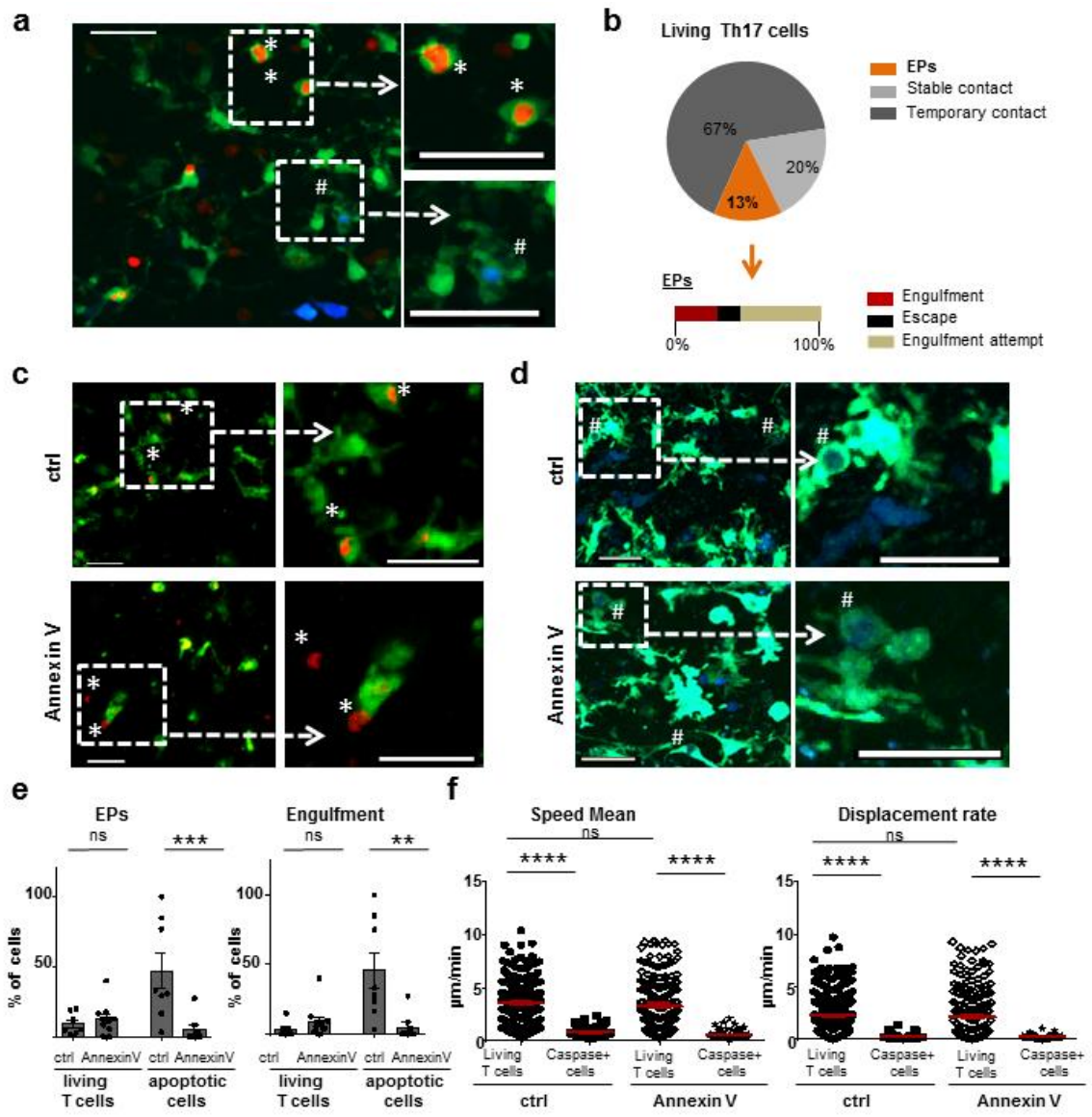

Figure 19: Engulfment of living T cells. 24 h co-cultures of organotypic hippocampal slices from CX3CR1.GFP pups with pathogenic B6.2D2.CFP.Th17 cells were stained with Image-iT™ LIVE Red Caspase-3 and -7 Detection Kit to identify apoptotic cells and imaged over a time period of 20 min with two-photon microscopy. **(a)** Representative example of the Caspase-3 and -7 staining (red) in 24 h co-cultures of organotypic hippocampal slices with B6.2D2.CFP.Th17 cells (blue). Scale bars = 40 µm. **(b)** The pie chart demonstrates the distribution (%) of interaction modes between microglia and viable 2D2.CFP.Th17 cells (n = 19 organotypic slices) and the contingency bar reflects the distribution of engulfment, escape and engulfment attempt. **(c+d)** Representative two-photon images of the 24 h co-cultures of the organotypic hippocampal slices with B6.2D2.CFP.Th17 cells stained with the Caspase-3 and -7 Detection Kit, with or without 10 µg/mL Annexin V treatment (24 h); relevant areas are magnified (right panel); asterisks mark apoptotic cells (red, **c**), hashes mark non-apoptotic T cells (blue, **d**). Scale bars = 40 µm. **(e)** Mean (± SEM) percentages of engulfment-related process (EPs) (left panel) and full engulfments (right panel) among the detectable cell count (viable T cells and apoptotic cells) per region of interest, without (n = 7 organotypic slices for viable cells, n = 8 organotypic slices for apoptotic cells) and with Annexin V treatment (n = 11 organotypic slices for viable cells, n = 8 organotypic slices for apoptotic cells). **: $p < 0.01$; ***: $p < 0.001$; ns = not significant. **(f)** Mean (± SEM) T cell motility parameters compared between Caspase-3/7^{+} and viable 2D2.CFP.Th17 cells without (n = 10 organotypic slices, 276 T cells for viable cells; n = 8 organotypic slices, 185 T cells apoptotic cells) and with (n = 12 organotypic slices, 205 T cells for viable cells; n = 8 organotypic slices, 171 T cells for apoptotic cells) Annexin V treatment. ****: $p < 0.0001$; ns = not significant.

3.2.6) Engulfment is dependent on T cell activity

To determine whether antigen-specificity impacts T cell–microglia interactions, MOG-specific 2D2.Th17 cells and polyclonal B6.Th17 cells were compared (**Figure 20**). Analyzing the interaction modes between these conditions revealed similar EP frequencies among the overall interactions with microglia. Furthermore, the engulfment frequency among EPs was similar for both conditions. Similar results were obtained comparing Th17 and Th2 cells, which represent two distinct T helper cell subtypes with highly dissimilar capacities during the disease (s. 1.2). In order to uncover whether T cell activity per se might be a prerequisite for microglial recognition, the role of the PI3K/Akt pathway as a major regulator of T cell activity was addressed in regard to the engulfment frequencies among the interactions of microglia and T cells. PI3K activity was proposed to influence Th17 effector functions (So and Fruman, 2012; Wan et al., 2011). Indeed, the PI3K inhibitor Wortmannin downregulated the expression of the activation markers CD44 and CD25 in stimulated Th17 cells *in vitro* (**Figure 21a+b)** and further decreased Th17 cell effector functions as could be shown by a significantly lower IL-17 expression in unstimulated and stimulated Th17 cells (**Figure 21c**). Interestingly, Wortmannin treatment was at the same time able to significantly lower the engulfment frequency compared to control conditions (**Figure 21d-f**), indicating an impact of the T cell activation status on engulfment probabilities. The reduced engulfment capacity of microglial cells was not mediated by a reduced T cell migration into the organotypic

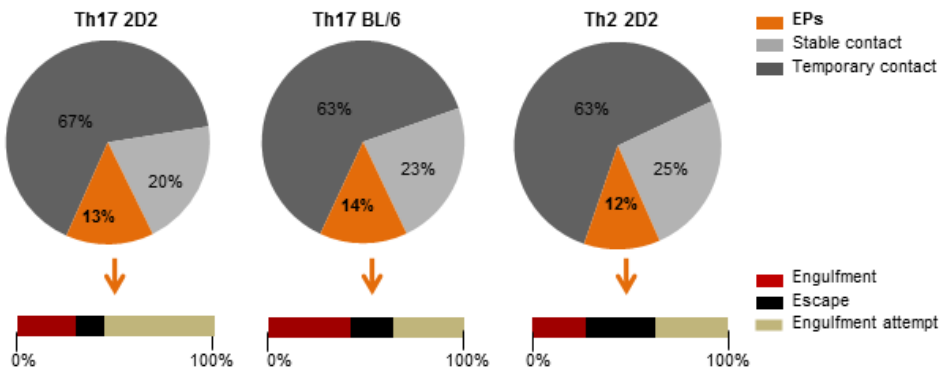

Figure 20: EPs are independent of antigen-specificity and T cell phenotype in organotypic hippocampal slices. 24 h co-cultures of organotypic hippocampal slices from CX3CR1.GFP pups with Th17 cells were stained with Image-iT™ LIVE Red Caspase-3 and -7 Detection Kit to identify apoptotic cells and imaged over a time period of 20 min. Only non-apoptotic T cells were considered for further analyses. Pie charts show the distribution (%) of interaction modes between microglia and viable B6.2D2.CFPTh17 cells (Th17 2D2; n = 19 organotypic slices), polyclonal B6.CFP.Th17 cells (Th17 BL/6; n = 6 organotypic slices) or B6.2D2.CFPTh2 cells (Th2 2D2; n = 3 organotypic slices) (upper panel) and contingency bars reflect the respective distribution of engulfment, escape and attempt to engulf among EPs (lower panel).

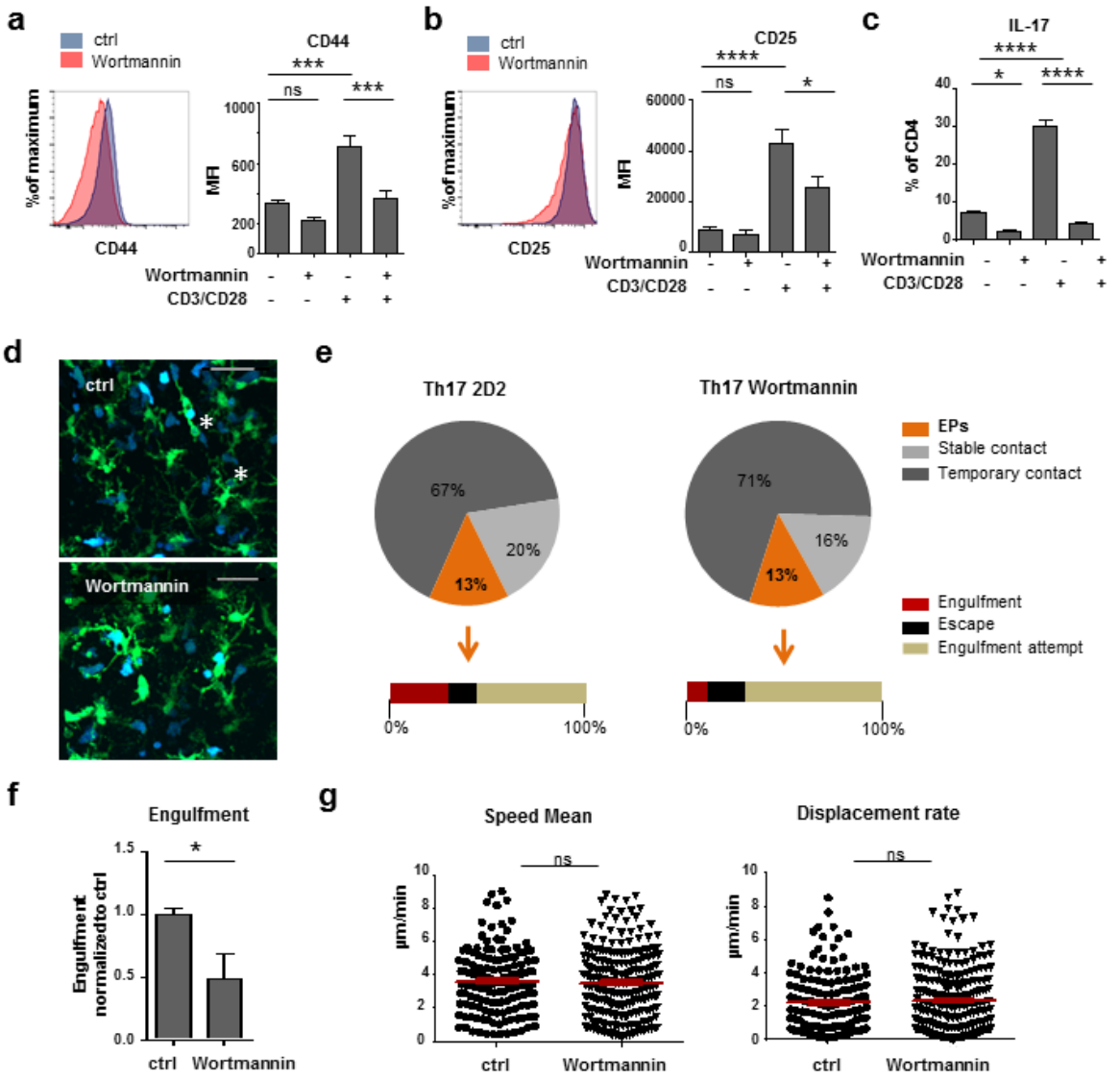

Figure 21: Inhibition of Th17 cells activation and cytokine secretion reduces T cell engulfment. (a-c) Th17-skewed cells (d5 of culture) were either stimulated for 24 h with antiCD3 and antiCD28 or not, each with or without the presence of Wortmannin (2.5 µM). Brefeldin A was used during the last 4h of stimulation to inhibit secretion of IL-17. **(a)** Histogram and quantification (mean ± SEM) of CD44 expression among living $CD4^+$ T cells. n = 6. **(b)** Histogram and quantification (mean ± SEM) of CD25 expression among living $CD4^+$ T cells. n = 6. **(c)** Quantification of IL-17 expression among $CD4^+$ T cells (mean (± SEM). n = 6. **(d-g)** 24 h co-cultures of organotypic hippocampal slices from CX3CR1.GFP pups with pathogenic 2D2.CFP.Th17 cells were stained with Image-iT™ LIVE Red Caspase-3 and -7 Detection Kit to identify apoptotic cells and imaged over a time period of 20 min. Only non-apoptotic T cells were considered for further analyses. **(d)** Representative images of organotypic hippocampal slices with pathogenic B6.2D2.CFP.Th17 cells with and without Wortmannin (2.5-5 µM) treatment. Asterisks mark engulfed cells. Scale bars = 40 µm. **(e)** Pie charts show the distribution (%) of interaction modes between microglia and viable B6.2D2.CFPTh17 cells without (Th17 2D2; n = 19 organotypic slices) and with Wortmannin treatment (2.5-5 µM; n = 8 organotypic slices) and contingency bars reflect the respective distribution of engulfment, escape and attempt to engulf among EPs (lower panel). **(f)** Relative frequency of engulfment compared to control (Mean ± SEM) among the interactions in Wortmannin (2.5-5 µM) treated organotypic hippocampal slices (n = 8 organotypic slices) normalized to the untreated control group (n = 5 organotypic slices). **(g)** T cell motility parameters of viable B6.2D2.CFP.Th17 cells without (n = 5 organotypic slices, 141 T cells) and with (n = 8 organotypic slices, 228 T cells) Wortmannin treatment (2.5-5 µM; mean (±SEM)). *: $p < 0.05$, ***: $p < 0.001$, ****: $p < 0.001$, ns = not significant.

hippocampal slice, as PI3K inhibition had no influence on migration properties of Th17 cells in the organotypic slices (**Figure 21g**). Furthermore, Wortmannin had no obvious impact on microglia structure or morphology (**Figure 21d**).

3.2.7) Microglia activation enhances engulfment of living Th17 cells

Since the engulfment frequency of T cells was found to be dependent on the activation state of T cells, it was of interest whether also the activation status of the microglial cell would impact their ability to engulf living T cells. Migration of T cells into the organotypic slice per se creates an *in vivo*-like inflammatory condition. In order to additionally activate microglia in organotypic slices, the slices were pre-treated with LPS for 24 h prior to the co-culture of the slice with T cells. In parallel to the T cell treatment, fresh LPS was further added to the slice. Indeed, EP frequencies significantly increased upon activation via LPS treatment, indicating that a marked increase in pro-inflammatory activity of microglia supports increased engulfment and thus clearance of invading T cells in neuroinflammation (**Figure 22**).

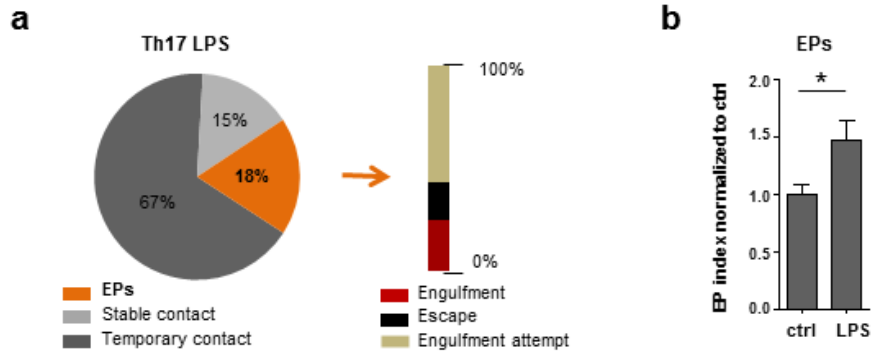

Figure 22: EPs are dependent on pro-inflammatory enhancement of microglia activation. 24 h co-cultures of organotypic hippocampal slices from CX3CR1GFP pups with pathogenic B6.2D2.CFP.Th17 cells were stained with Image-iT™ LIVE Red Caspase-3 and -7 Detection Kit to identify apoptotic cells and imaged over a time period of 20 min. Only non-apoptotic T cells were considered for further analyses. **(a)** The pie chart shows the distribution (%) of interaction modes between microglia and viable T cells in LPS (1 µg/mL) treated co-cultures of organotypic hippocampal slices with B6.2D2.CFPTh17 cells (n = 9 organotypic slices; left panel) and the contingency bar reflects the respective distribution of engulfment, escape and attempt to engulf among EPs (right panel). **(b)** Relative frequency of EP compared to control (Mean ± SEM) among the interactions in LPS (1 µg/mL) treated organotypic hippocampal slices (n = 6 organotypic slices) normalized to the untreated control group (n = 5 organotypic slices). *: $p < 0.05$.

3.2.8) The engulfment of living T cells is mediated by GlcNAc exposure

In order to unravel the mechanism of the engulfment of living T cells, the involvement of N-Acetyl-D-Glucosamine (GlcNAc), which has been previously discussed as an "eat-me" signal on apoptotic thymocytes (Duvall et al., 1985), was examined in this study. Indeed, GlcNAc was found to impact the engulfment of living cells (**Figure 23**). Wheat germ agglutinin (WGA) has been reported to bind and detect GlcNAc (Notter and Leary, 1987). Using fluorescently labeled WGA, stimulated Th17 cells exhibited an increased binding of

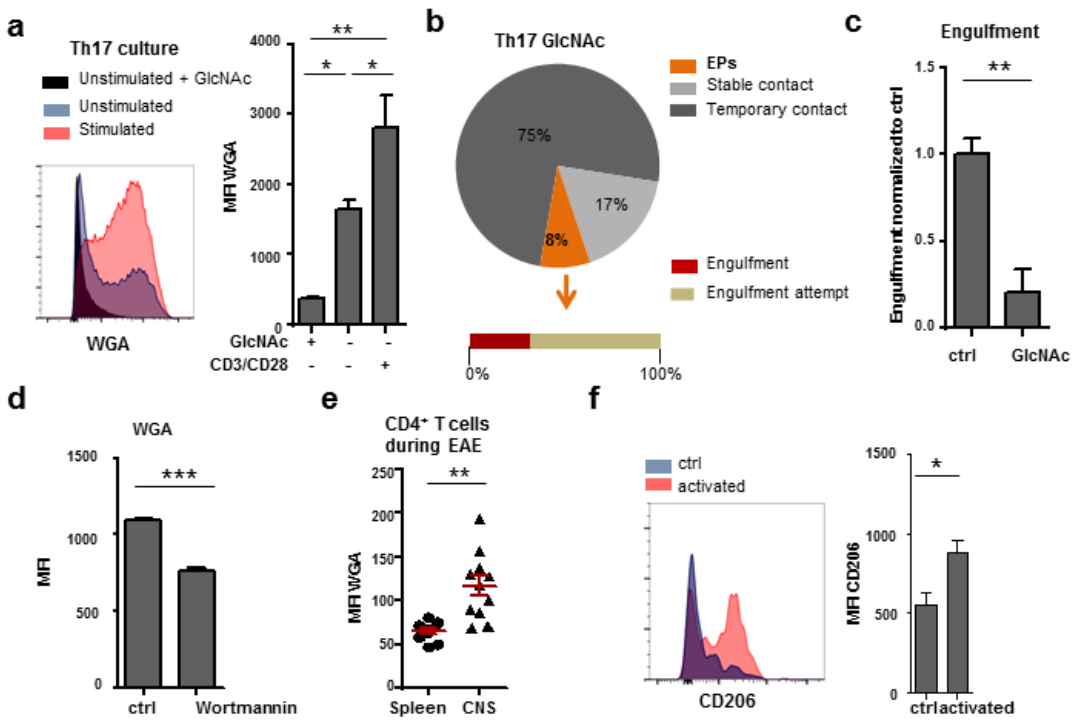

Figure 23: The engulfment of living T cells is dependent on GlcNAc exposure. (a) Th17-skewed cells (d5 of culture) were either stimulated with antiCD3 and antiCD28 or not. After 24 h of stimulation WGA binding was assessed. A control-staining was performed with unstimulated cells in the presence of GlcNAc (200 mM). **(b-c)** 24 h co-cultures of organotypic hippocampal slices from CX3CR1^{GFP} pups with pathogenic 2D2.CFP.Th17 cells were stained with Image-iT™ LIVE Red Caspase-3 and -7 Detection Kit to identify apoptotic cells and imaged over a time period of 20 min. Only non-apoptotic T cells were considered for further analyses. **(b)** The 24 h co-cultures of organotypic hippocampal slices with Th17 cells were treated with GlcNAc (20-40 mM). The pie chart shows the distribution (%) of interaction modes between microglia and viable Th17 cells (n = 4 organotypic slices) (upper panel) and the contingency bar reflects the respective distribution of engulfment and engulfment attempt among EPs (lower panel). **(c)** Relative frequency of engulfment compared to control (Mean ± SEM) among the interactions in GlcNAc (20 mM) treated organotypic hippocampal slices (n = 4 organotypic slices) normalized to the untreated control group (n = 4 organotypic slices). **(d)** Th17-skewed cells (d5 of culture) were stimulated for 24 h with antiCD3 and antiCD28, with or without the presence of Wortmannin. The quantification of the mean fluorescence intensity (mean ± SEM) of WGA binding on stimulated living CD4+ T cells is shown. n = 3. **(e)** Flow cytometric analysis of WGA-binding on living CD4+ T cells in the CNS and spleen of EAE diseased mice in actively immunized C57BL/6 mice. **(f)** Flow cytometric analysis of CD206 in living microglia (PI^{-}GFP^{+}) in organotypic hippocampal slices prepared from CX3CR1^{GFP} pups and treated with/without LPS (24 h, 1 µg/mL) in order to activate microglia.

WGA compared to unstimulated cells, indicating that the reduced engulfment rate of Wortmannin-treated T cells could be mediated by a lower GlcNAc expression on cells which are less activated (**Figure 23a**). The binding of WGA could be inhibited by the presence of competitive GlcNAc during the staining (**Figure 23a**). Importantly, the competitive presence of GlcNAc in the 24 h-co-culture of organotypic hippocampal slices with Th17 cells affected the distribution of interactions and was sufficient to significantly decrease the engulfment of T cells by microglia (**Figure 23b+c**) and Wortmannin was indeed able to reduce WGA-binding on activated T cells (**Figure 23d**). Of note, WGA-binding was higher in T cells invading the CNS compared to peripheral T cells in EAE-diseased mice, suggesting a greater importance of GlcNAc expression in the target organ of EAE and MS (**Figure 23e**). Interestingly, the lectin CD206, which has been described as a marker for aaMC (Franco and Fernández-Suárez, 2015), is able to bind GlcNAc (Taylor et al., 1992; Taylor et al., 2005). The data presented here show an upregulation of CD206 after LPS-mediated microglial activation in organotypic hippocampal slices (**Figure 23f**) and this microglial activation was accompanied by increased engulfment processes (**Figure 22**). Altogether, the engulfment frequency of pathogenic T cells was shown here to be dependent on activity-dependent GlcNAc exposure on T cells.

4) Discussion

Although both beneficial and detrimental roles of myeloid cells have been described during EAE and MS in the literature (1.2.1), the gene expression profile which could be primarily responsible for the different cell fates was only barely considered, thus demanding a more precise and thorough investigation. In this thesis, the gene expression in $CD11c^+$ myeloid cells, including resident activated microglia and infiltrated CD11c-expressing dendritic cells and macrophages, was extensively analyzed as enabled by mRNA sequencing of the whole cell transcriptome. The in-depth analysis of the gene expression profile in $CD11c^+$ myeloid cells revealed a list of genes that were regulated analogously in SJL/J and C57BL/6 mice. This regulation was stable despite the strong genetic differences and despite substantial differences in EAE progression in the two different mouse strains. It was shown for the first time that Ms4a8a, YM1 and Arginase1, characterizing aaMC (Munder et al., 1998; Raes et al., 2002; Schmieder et al., 2012), were the most regulated genes in highly pure $CD11c^+$ CNS myeloid cells comparing the exacerbation and remission phases of EAE. Among myeloid cells, microglia are CNS-resident and therefore particularly relevant for CNS inflammation. Here, microglia were identified for the first time to be able to engulf CNS-invading Th17 cells, a process that appeared most prevalent during less severe disease and which could be overcome during more severe disease states. This microglial engulfment targeted not only apoptotic cells but also fully viable T lymphocytes resulting in stable or temporary cell-in-cell structures. The engulfment of viable T cells was determined to be dependent on T cell activity, microglial activity and GlcNAc exposure and its success also partially depended on the ability of T cells to escape this entrapment. As such, the attempted engulfment of microglia may represent a potentially important pathway in MS disease pathogenesis and thus its modulation a novel therapeutic target. Overall, this thesis presents new knowledge in terms of beneficial myeloid cell involvement during different stages of disease and highlights new therapeutic possibilities.

4.1) aaMC exert beneficial properties during neurological diseases

In contrast to classically activated myeloid cells (caMC), which seem to worsen EAE and MS outcome, aaMC are thought to cause resolution of inflammation, promotion of wound healing and therefore to suppress EAE and MS outcome (Jiang et al., 2014). It was shown

that the enhancement of aaMC responses during EAE promotes amelioration of the disease (Jung et al., 2004; Shin et al., 2000; Tierney et al., 2009). In this context, glatiramer acetate, which is approved for the treatment of RRMS, has been shown to enhance the expression of immunosuppressive IL-10 in myeloid cells (Jung et al., 2004). Thus, the enhancement of aaMC responses represents one of the immunomodulatory mechanisms of glatiramer acetate. Of note, the inhibition of iNOS, which is expressed by caMC, has been shown to ameliorate EAE disease, while the suppression of EAE development by immune complexes was accompanied by elevated IL-10 production in myeloid cells (Shin et al., 2000; Tierney et al., 2009). Furthermore, fumarates which are approved for the treatment of MS, have been described to influence myeloid cell function and to lead to a shift towards type II polarized myeloid cells, favoring Th2 or Treg differentiation (Ghoreschi et al., 2011). The here described upregulation of the aaMC markers during the active disease state might thus represent an endogenous mechanism to counterbalance CNS inflammation, by an endogenous elevation of the aaMC response. Indeed, the high expression of aaMC characterizing genes during the first exacerbation state of the disease was followed by a reduction of disease symptoms during remission. Pharmacological enhancement of this endogenous protective mechanism during chronic disease could thus potentially allow amelioration of the disease also in the chronic phase. Of note, other groups observed aaMC marker expression in the CNS during further neurological diseases, such as spinal cord injury and stroke, emphasizing the great importance of these proteins in the CNS (Hu et al., 2012; Schilling et al., 2003; Schwartz, 2010; Shechter et al., 2009). The upregulation of aaMC markers might thus reflect a general defense mechanism of microglial cells against CNS damage. Therefore, the targeted enhancement of aaMC responses could mediate beneficial effects both in MS and in other neurological diseases. In order to specifically target aaMC functions and to minimize side effects, it would be desirable to identify the pathways which are mainly responsible for the beneficial properties of aaMC. Since the here identified highly regulated proteins of aaMC might exhibit great relevance in mediating aaMC responses, their impact on aaMC function will be discussed more precisely in the following section.

4.2) The identified regulated aaMC markers mediate aaMC functions

Different proteins expressed by aaMC could be crucially responsible for mediating aaMC functions. The strong regulation of the three distinct aaMC markers Ms4a8a, YM1 and

Arginase1 points to a pivotal role of these genes during the disease in order to mediate aaMC function. A disease state-dependent expression of aaMC markers has been described previously during spinal cord injury, whereby some aaMC markers were expressed over a long time period, but others only temporarily (Kigerl et al., 2009). It stands to reason that aaMC markers that are expressed during the active disease state have a strong influence on disease progression. Accordingly, the importance of YM1 and Arginase1 during EAE was suggested previously. Ahn et al. showed higher expression of Arginase1 during the exacerbation of the EAE disease compared to other disease states in total spinal cords of diseased Lewis rats (Ahn et al., 2012). Furthermore, the expression of YM1 and other aaMC markers was described during EAE (Ponomarev et al., 2007). YM1 expression was both detected in resident microglial cells and to a lesser extent in CNS-infiltrating macrophages, thus confirming the contribution of both cell types to the aaMC population in the CNS (Ponomarev et al., 2007). Considering the protein function of YM1, Arginase1 and Ms4a8a more precisely reveals their potential to mediate aaMC properties. Interestingly, it was shown that antibody-mediated neutralization of YM1 was sufficient to inhibit Th2 polarizing effects of the targeted aaMC *in vitro*, thus confirming a key function YM1 to mediate aaMC responses (Arora et al., 2006). Similarly, Arginase1 plays a decisive role in aaMC, as it serves as an enzyme competing with iNOS, the most common marker of caMC, for the substrate L-arginine and thus reduces NO production (Munder et al., 1998; Rauh et al., 2005). Competitive inhibition of iNOS by aminoguanidine has been shown to reduce EAE duration in Lewis rats (Shin et al., 2000; Zhao et al., 1996), pointing to the great potential of the Arginase1/iNOS competing pathways to influence the disease. However, iNOS and its metabolite NO also play a role in various physiological processes such as vasodilation and thrombocyte aggregation (Adams et al., 1995), thus again revealing possible targets for harmful side effects of shifting the Arginase1/iNOS homeostasis. Of note, Ms4a8a was firstly characterized in 2001 by Ishibashi et al. (Ishibashi et al., 2001) and since then has mainly been described as a marker for aaMC (Schmieder et al., 2012; Schmieder et al., 2011; Weitnauer et al., 2014). Specific targeting of Ms4a8a might thus be accompanied by less secondary effects. Although the function of Ms4a8a in aaMC is less well characterized in literature compared to YM1 and Arginase1, the here presented results suggest that Ms4a8a has a comparable key function in aaMC. In a previous study, forced overexpression of Ms4a8a in a macrophage cell line and admixture of these Ms4a8a Raw 264.7 cells

significantly enhanced the tumor growth rate of subcutaneously transplanted mammary carcinomas (Schmieder et al., 2011). Thus, it appears likely that Ms4a8a promotes an anti-inflammatory phenotype of CD11c$^+$ myeloid cells as successfully as YM1 and Arginase1, which could be in turn beneficial during EAE. Support for this notion comes from remitting clinical score soon after the finding that Ms4a8a, as well as Arginase1 and YM1, is strongly expressed during the exacerbation of the EAE disease. In summary, Ms4a8a, YM1 and Arginase1 reveal new specific target proteins in order to alter aaMC effector functions during EAE, whereby especially the effector mechanism of Ms4a8a would merit more comprehensive analysis. In order to better understand their role during EAE progression, the distribution of aaMC-marker expression comparing the CNS and the periphery will be further considered below.

4.3) Myeloid cells in the CNS show a stronger switch to an anti-inflammatory phenotype than peripheral myeloid cells

Interestingly, highly purified CD11c$^+$ splenic myeloid cells yielded only marginal expression of Ms4a8a, YM1 and Arginase1 in the here presented work and the expression of these genes was not altered peripherally over the analyzed time points during disease. This underlines the particular impact of these genes in the CNS, the target organ in EAE and MS. By contrast, a regulation of Arginase1 in peripheral cells has been reported in the past in peripheral blood monocytes of Dark Agouti rats, whereby the highest amount of Arginase1 in the periphery was found during the exacerbation compared to other disease states (Mikita et al., 2011). Similarly, flow cytometric analyses of peripheral splenic myeloid cells from EAE-diseased C57BL/6 mice showed a higher expression of Arginase1 during the disease exacerbation which was decreased during the chronic disease state (Liu et al., 2013). Nevertheless, both Mikita et al. and Liu et al. reported only marginal expression of Arginase1 expression in the periphery and an explanation for the different findings observed here could be related to the small amounts of these genes in highly purified CD11c$^+$ splenic myeloid cells in the current study. Of note, no other study has investigated the transcriptome of highly purified activated CD11c$^+$ myeloid cells *ex vivo* from the CNS of diseased animals yet. Taken together, this work and previous works suggest a low expression of Arginase1 in the periphery of EAE-diseased mice and an accumulation of Arginase1 expressing myeloid cells in the CNS during the active disease state. Similar results were

obtained in this thesis concerning the Ms4a8a and YM1 expressions which were identified to be more highly expressed in the CNS compared to the spleen. These results clearly underline the particular impact of myeloid cells in the CNS during EAE and their capacity to adapt their phenotype according to the challenges of their environment. There are two main explanations for the higher expression of aaMC markers on CNS-infiltrating myeloid cells in comparison to the splenic myeloid cells. Either myeloid cells are alternatively activated in the CNS or polarization into the alternatively activated state facilitates CNS invasion. Importantly, Ms4a8a and YM1 were previously reported to be highly expressed in alternatively activated dendritic cells in the lung and this expression was induced by bronchial epithelial cells in a glucocorticoid-dependent manner (Weitnauer et al., 2014). Weitnauer et al. demonstrated further that both Ms4a8a and YM1 expression was significantly increased in the lung compared to the splenic tissue (Weitnauer et al., 2014). Interestingly, Flügel and colleagues determined in 2012 that T cells become licensed in the lung to enter the CNS (Odoardi et al., 2012). The similar expression profile of aaMC markers on myeloid cells in the CNS and myeloid cells in the lung, suggests that also CNS-invading myeloid cells could migrate into the lung before entering the CNS, where bronchial epithelial cells could promote the expression of aaMC markers on myeloid cells before their invasion to the CNS. To validate this, it would be necessary to analyze aaMC marker expression also during the disease onset. As of yet, the expression of Ms4a8a and YM1 has been not compared during EAE onset and the peak of the disease. However, as described above, the aaMC marker Arginase1 was described to be more highly expressed during the peak compared to the disease onset (Ahn et al., 2012). These data suggest that another or additional pathway in the CNS induces the expression of aaMC markers. In ischemia models it has be shown recently that neurons are rapidly able to secrete IL-4 after unilateral occlusion of the left middle cerebral artery and the left common carotid artery (Zhao et al., 2015). This IL-4 production during ischemia was able to induce alternative activation in myeloid cells (Zhao et al., 2015). Neuronal damage during MS might thus promote IL-4 secretion similarly, especially during the exacerbation of the disease. The specific upregulation of aaMC markers in the target organ of EAE and MS could thereby reveal a protective mechanism, which is directed against damage in the CNS, but not required in peripheral organs such as the spleen, where caMC could further promote immune defense against pathogens. Of note, EAE was more severe in mice with a CNS deficiency in IL-4 and a

higher substantial role of CNS-derived IL-4 was demonstrated compared to peripheral IL-4 in order to counterbalance disease progression (Ponomarev et al., 2007). A CNS-internal mechanism to induce an alternatively activated phenotype is further necessary to polarize CNS-resident microglia. Of note, although both CNS-infiltrating and CNS-resident myeloid cells can contribute to beneficial aaMC effects, CNS-resident microglia express the aaMC marker YM1 not only during EAE but also – to a lesser extent – in non-diseased mice (Ponomarev et al., 2007). Thus, especially microglia, which reside in the CNS tissue during all time points of disease development, could mediate aaMC functions from the onset of the disease. In order to analyze how myeloid cells in the CNS are able to mediate beneficial properties, beside their described aaMC effector functions during the disease, the direct reaction of myeloid cells to the infiltration of pathogenic Th17 cells upon EAE was assessed here using intravital two-photon microscopy. For this, the focus was specifically directed on microglia, the CNS-resident myeloid cells.

4.4) Beneficial properties of CNS-resident myeloid cells can be mediated via the engulfment of invading Th17 cells in the CNS

It is well known that pathogenic Th17 cells invade into the CNS during MS and EAE, mediating inflammation and neuronal degeneration (Dendrou et al., 2015; Goverman, 2009). Nevertheless, although microglia were described to continuously scan their environment and to mediate both detrimental and tissue homeostatic functions (Heneka et al., 2014; Kabba et al., 2017; Nimmerjahn et al., 2005) and even though the great importance of both microglia and T cells during EAE and MS is well accepted, direct interactions of microglia with Th17 cells within the CNS has been poorly defined as of yet. In this work, intravital two-photon imaging was used for the first time to characterize microglia-T cell interactions in the CNS during EAE *in vivo* and in organotypic hippocampal slice cultures *ex vivo*. Two-photon imaging is a powerful tool in neuroimmunological research that enables the direct assessment of disease processes and cellular interactions in the intact CNS tissue (Kawakami and Flügel, 2010; Weigert et al., 2010). Its development enabled the direct observation of cellular processes, such as immunologic and neurologic processes, which led to a better understanding of elementary processes in immune cell regulation (Cahalan and Parker, 2008; Herz et al., 2011). Recently it use has broadened our knowledge by investigating immune cell trafficking processes (Schläger et al., 2016), the initiation of T-cell mediated

neuronal damage (Nikic et al., 2011; Siffrin et al., 2010a) and the role of specific immune cell populations such as dendritic cells (Paterka et al., 2016). Taking advantage of this method, it was observed in this work that microglia intensely contacted pathogenic Th17 cells in inflammatory lesions and that they were able to respond to T cell infiltration by engulfing invading T cells. The engulfment process was thereby characterized to be clearly distinct from the phagocytosis of apoptotic cells. Unexpectedly, some of these engulfed viable pathogenic Th17 cells were able to migrate through the microglia cytoplasm and to escape the engulfment, while others underwent cell death. The capture of T cells was dependent on GlcNAc expression on T cells and lectin expression on microglial cells. Furthermore, engulfment and escape events were independent of antigen presentation or T cell phenotype, but did correlate with T cell activity and pro-inflammatory microglia activation resulting in increased GlcNAc-lectin interactions. GlcNAc has been discussed previously to promote the binding (and subsequent phagocytosis) of apoptotic thymocytes to macrophages (Duvall et al., 1985). Of note, the engulfment of viable T cells was found here to be not driven by phosphatidylserine exposure, clearly identifying this process as distinct from phagocytosis. However, GlcNAc is also expressed by bacteria, where it serves as a target molecule for pattern recognition receptors on phagocytes, resulting in the phagocytosis and removal of harmful CNS intruders (Nadesalingam et al., 2005; Zhang et al., 2015). Thus, it seems that microglia aim to remove CNS-invading T cells in a similar process as compared to the phagocytosis of CNS-invading pathogens. Taken together, these data suggest an active process of microglial cells to remove invading lymphocytes from the brain parenchyma. Given these premises, it appears likely that this T cell removal in the CNS serves as an additional pathway for microglia to limit inflammation beyond the so far reported beneficial effects mediated by the release of anti-inflammatory cytokines such as IL-4, IL-10 or TGF-β and the phagocytosis of myelin debris as a prerequisite for tissue reengineering (Goldmann and Prinz, 2013). Support for this notion comes from the here described observation that microglial engulfment of pathogenic T cells was dependent on disease severity. In this sense, it was shown that microglial engulfment was more prevalent during early inflammation of mice which exhibited a low clinical score compared to mice during chronic disease. Thus, the engulfment of T cells appears to be an early protection mechanism of microglial cells, which is overcome during elevated disease states. T cells that are able to escape the completed microglial engulfment despite their expression of “eat-me”

signals might represent a highly pathogenic subgroup of T cells, critically responsible for EAE manifestation. Of note, the capture of pathogenic cells via engulfment processes could be not only beneficial in EAE, but also in other diseases. Accordingly, in a mouse model of autoimmune hepatitis the engulfment of living T cells by hepatocytes in the periphery has been shown to ameliorate disease outcome (Benseler et al., 2011). During EAE, the assumption of a beneficial impact of the enhanced microglial engulfment capacities is supported by the notion that a high phagocytic capacity of myeloid cells in the CNS has been shown to correlate with a faster CNS regeneration (Lampron et al., 2015). The engulfment of living T cells might contribute to this beneficial effect. Interestingly, glatiramer acetate, which is approved for the treatment of MS, acts on the phagocytic capacity of myeloid cells. Monocytes from the blood of patients with MS who received this therapy exhibited increased phagocytic activity when compared to those from untreated MS patients or healthy controls (Pul et al., 2012). It would be of interest whether glatiramer acetate or other therapeutics could also increase the engulfment of living cells and whether this effect could contribute to the beneficial effects on disease progression. To allow a better understanding of the engulfment processes, it was considered here, how engulfment is effected by the microenvironment in the CNS.

4.5) The microglial engulfment of T cells is dependent on the inflammatory milieu in the CNS

The attempt of microglia to remove non-CNS-resident cells from the brain parenchyma is consistent with the previously reported sensing of the CNS parenchyma and the polarization of microglial processes into the direction of damage in highly localized laser lesions (Nimmerjahn et al., 2005). Indeed, it was confirmed in this work that microglia were highly active even in the absence of T cells, continuously extending and retracting their processes in search of targets to engulf. Strikingly, LPS, which is known to activate microglia in a TLR4-dependent manner (Lehnardt et al., 2002), significantly increased the rate of T cell engulfment, clearly emphasizing the importance of this process in inflammation. The engulfment of living T cells in the CNS may therefore reflect a general defense mechanism of the CNS towards invading activated cells. This concept is supported by the fact that downregulation of T cell activity by treatment with Wortmannin reduced T cell engulfment frequency. Importantly, this was not due to impaired migration of the T cells as the T cell

motility parameters were unchanged. Since GlcNAc exposure was higher in T cells isolated from the CNS compared to peripheral T cells, it could be possible that either highly activated T cells migrate preferentially into the CNS, where they can contribute to the inflammatory milieu, or that the inflammatory milieu in the CNS is stimulating GlcNAc exposure on T cells. Both possibilities would underline that the inflammatory milieu in the CNS is able to enhance engulfment processes during early inflammation. The lectin CD206, which is not only able to bind GlcNAc (Taylor et al., 1992; Taylor et al., 2005) but which is at the same time one of the most prominent aaMC markers (Franco and Fernández-Suárez, 2015), could be one of the microglial proteins which are affected by this microenvironment. As described above, other markers of aaMC such as Msa8a8, YM1 and Arginase1 were expressed more during the first disease exacerbation rather than during chronic disease. Although the regulation of CD206 was not strong enough during the EAE course to be identified by RNA-Seq as one of the most highly regulated genes, the here presented data suggest that also CD206 is more highly expressed during the early disease, possibly even prior to the expression of Ms4a8a, YM1 and Arginase1 at the exacerbation of the disease. Enhancement of aaMC responses could thus mediate beneficial properties not only by the secretion of anti-inflammatory cytokines, but also via a CD206-mediated upregulation of T cell engulfment. Exhaustion of lectin-dependent T cell capture during the chronic state of the disease could be on the other hand mediated via the full establishment of inflammation. In this sense, it has been shown previously that expression of lectins such as CD206 is dependent on the inflammatory milieu and that IFN-γ is able to downregulate CD206 expression on microglia, which is followed by decreased pinocytotic capacities of microglia (Zimmer et al., 2003).

4.6) Microglial T cell engulfment is distinct from cell-in-cell structures between other cell types

While the engulfment and subsequent fate of living T cells in the CNS by microglia *in vivo* has not been reported so far, it has been previously shown that microglia can phagocytose other viable cell types such as neural precursor cells, neutrophils, neurons or synapses mainly in neurodevelopment (Brown and Neher, 2014; Neumann et al., 2008). In very few earlier neuropathological reports based on histological observations, cell-in-cell formation has been mentioned for lymphocytes in neurons (Hughes et al., 1968; Ng and Ling, 1999) and for oligodendrocytes in astrocytes (Shintaku and Yutani, 2004; Wu and Raine, 1992). However,

escape from microglial engulfment has not yet been described and therefore the here reported capability of T cells to break out from glial entrapment despite microglial attempts to engulf, highlights the great pathogenic potential of these T cells. According to *in vitro* observations, cell-in-cell structures have been reported previously also in other cell types, mostly for tumor cells (Yang and Li, 2012). The use of different vaguely defined terms, e.g., entosis, (suicide) emperipolesis, phagoptosis, cytophagocytosis or cannibalism indicate that both the physiological significance and underlying pathways of so-called cell-in-cell structures are still poorly understood (Brown and Neher, 2014; Overholtzer and Brugge, 2008). As a comprehensive understanding and general consensus on the nomenclature in this field is still elusive, the general term "engulfment" was preferentially used in this thesis. Entosis was previously described as a form of cell cannibalism leading either to cell death or sometimes to escape (Krishna and Overholtzer, 2016), thus representing a dual fate of the engulfed cells comparable to the T cell fate described here. Different from activated Th17 cells, however, entosis has so far mostly been assigned to homotypic cell-in-cell interactions (Krishna and Overholtzer, 2016). So far, a potential role of entosis in a non-cancerous context is not clear. Entosis-induced cell death has been shown to predominantly involve lysosomal degradation for the elimination of internalized cells whereas apoptosis of the target cell can compensate to execute cell death only after disruption of lysosomal function (Overholtzer et al., 2007). In the present work, Caspase-3/7 activity was identified in some internalized cells, not capable of escape, which is more in line with so-called suicide emperipolesis. This has been observed in autoimmune hepatitis, where autoreactive $CD8^+$ T cells invade hepatocytes and die by apoptosis after internalization (Benseler et al., 2011). Thus, the here presented engulfment of viable T cells reflects a yet unknown process, clearly distinct from other cell-in-cell formation processes. In addition to the upregulation of typical aaMC responses, enhancement of T cell engulfment could thus serve as a new therapeutic target in MS.

4.7) Targeting the activity of myeloid cells could serve as a new therapeutic strategy

Both the upregulation of aaMC markers during the exacerbation of the disease as well as the engulfment of CNS-invading Th17 cells reflect myeloid cell-mediated mechanisms to counteract neuroinflammation. Thus, promotion of either aaMC functions or the engulfment of Th17 cells could serve as new therapeutic strategies for EAE and MS. A general induction

of the switch from caMC to aaMC would be highly desirable to counteract the disease. However, both IL-4 and glucocorticoids, which are able to mediate aaMC polarization, may partly result in side effects (Jiang et al., 2014; Tischner and Reichardt, 2007; Whitehead et al., 2002) and a more targeted pathway to promote aaMC effector functions may be more effective. Since Ms4a8a, YM1 and Arginase1 are highly regulated during the disease course and are thought to cause cardinal aaMC functions (4.2), a targeting of these proteins would be desirable to support beneficial properties of myeloid cells in the CNS. To translate the reported results from the mouse model to humans, it would be necessary to find human homologs of those genes. Regretfully, Arginase1 and YM1 were only reported to be markers for murine myeloid aaMC, but not for human aaMC (Raes et al., 2005). Similarly, Ms4a8a has not been described in human. Even though Ms4a8b was discussed as a potential functional human homolog of Ms4a8a in differentiated intestinal epithelium (Michel et al., 2013), the expression of Ms4a8b on human aaMC was not described and *in vitro* generation of human M2 macrophages from peripheral blood mononuclear cells did not result in Ms4a8b gene expression as analyzed by qRT-PCR (data not shown). Therefore, the question arises, which human proteins could fulfill the role of Arginase1, YM1 and Ms4a8a in humans to identify new therapeutic target molecules. Many human structural homologs of the Ms4a family are known, which could fulfill the function of the murine Ms4a8a in human. One human member of the Ms4a family which has been described to be expressed by human aaMC is Ms4a4a (Czimmerer et al., 2012; Ishibashi et al., 2001). Ms4a4a was already discussed as a therapeutic target for the treatment of multiple myelomas and could possibly serve also a specific target in MS, as its transcription seems so be limited to hematopoietic cells, mainly macrophages and plasma cells, thus revealing low potential of unfavorable side effects (Sanyal et al., 2017). Future *in vitro* and *in vivo* studies are needed to determine the molecular effector mechanisms of Ms4a8a, YM1 and Arginase1 proteins, and to identify which human genes could be responsible for similar effector mechanisms possibly serving as new therapeutic targets for the treatment of MS. Those studies could use genetic ablation or overexpression to gain new insight into disease mechanisms. Besides targeting the human functional homologues of Ms4a8a, YM1 and Arginase1, the directed manipulation of the beneficial capacities of myeloid cells in the CNS could ameliorate disease outcome. In this sense, it appears likely that the engulfment of living pathogenic T cells in order to protect the CNS tissue would be beneficial not only in mice but also in human, as T cells were also

described in human to invade the CNS during MS (Dendrou et al., 2015). The unique ability of T cells to migrate through microglia without subsequent cell death and to instead escape from those engulfments, which may explain the low overall engulfment rate, reveals a newly discovered mechanism strengthening their pathological potency in CNS inflammation. Thus, inhibiting the escape from microglial engulfment could serve as an additional target during MS. Of note, the lectin CD206, which was identified here to be associated with elevated engulfment capacities of microglia and which is able to bind GlcNAc on activated T cells, is not only expressed on murine but also on human myeloid cells (Franco and Fernández-Suárez, 2015). Pharmacological enhancement of lectin expression on myeloid cells might thus promote T cell clearance during EAE and MS. Comparably to other aaMC markers, CD206 expression is driven by the transcription factor STAT6 and JAK-STAT signaling via binding of IL-4 or IL-13 to their receptor promotes CD206 expression (Lawrence and Natoli, 2011). Furthermore, glucocorticoids also induce CD206 expression (Franco and Fernández-Suárez, 2015). However, it would be of interest whether other pathways impact CD206 with higher specificities compared to IL-4/IL-13- or glucocorticoid-treatment. An increased expression of CD206 could not only increase the engulfment of viable T cells but also the phagocytosis of apoptotic cells via GlcNAc recognition on apoptotic cells (Duvall et al., 1985). As the phagocytosis of apoptotic cells has been shown to promote tissue repair during MS (Neumann et al., 2009), enhancement of CD206 expression on myeloid cells would hence promote two synergic beneficial properties of myeloid cells. CD206 is further involved in the recognition of various pathogenic microorganisms, including bacteria, fungi, virus, and parasites (Azad et al., 2014). Increased CD206 could thus even support immune defense mechanisms.

4.8) Conclusion and Outlook

This work demonstrates the ability of myeloid cells in the CNS of EAE-diseased animals to adapt their phenotype to different disease states and furthermore, to actively react to T cell infiltration during the disease by engulfing the infiltrating cells. Supporting the beneficial properties of myeloid cells in the CNS could thus serve as a new therapeutic target in the treatment of MS. Although available MS therapeutics partially effect myeloid cells already, they are often accompanied by side effects and higher specificities of therapeutics would be desirable. As described here, myeloid cells in the CNS are not only able to engulf invading T

cells, but also to switch to an anti-inflammatory phenotype by adapting their gene expression patterns. In order to investigate whether T cell engulfment is coupled to other beneficial effects of myeloid cells, additional experiments are needed to analyze how beneficial aaMC react to T cell infiltration in comparison to detrimental caMC. Therefore, tissue-resident GFP-labeled microglia in organotypic hippocampal slices could be polarized into alternatively activated microglia by treating the slices with a mixture of IL-4/Dexamethasone and LPS, as it was performed similarly with BMDM in this thesis. Engulfment of fluorescently labeled viable T cells could then be visualized via two-photon imaging and compared to the engulfment capacity of un-polarized or classically activated microglia. In another approach, IL-4/Dexamethasone treatment and subsequent visualization of engulfment processes could be performed *in vivo* in EAE-diseased mice. In addition, the treatment of EAE-diseased animals with MS therapeutics and subsequent analysis of the effect on the engulfment capacities would allow further conclusions concerning the relevance of engulfment processes in MS patients. Since glatiramer acetate and fumarates have been reported previously to affect myeloid cell polarization, these approved MS-therapeutics would be possibly also able to enhance T cell capture. Thus, especially the effect of glatiramer acetate and fumarates on engulfment processes would be worthwhile to analyze in detail. In order to understand the beneficial effects of the engulfment of living cells more precisely in humans, it would be also necessary to investigate engulfment processes in human tissues. Although the visualization of kinetic processes such as microglial T cell engulfment is not feasible in humans, immunohistochemical analysis of human post mortem material from MS patients could be used to visualize the full engulfment of T cells by microglia in human tissue via confocal imaging. Similar to the caspase stainings which were performed here in organotypic hippocampal slices, caspase and other markers for apoptotic cells or dead cells could be used to minimize the consideration of the engulfment of non-viable cells in human post mortem material. To this end, a brief post mortem interval (less than 12 h) would be required to decrease the probability of nonapoptotic DNA strand breaks (Anderson et al., 1996; Tatton, 2000). In order to investigate their relevance for the engulfment process in human, engulfment mediators such as the lectin CD206 could be co-stained in these immunohistochemical stainings as well. Similar immunohistochemical experiments could be also performed *ex vivo* in the CNS tissue of EAE-diseased mice. Since not only the lectin CD206 but also other lectins

could mediate the recognition of GlcNAc-expressing activated T cells, immunohistochemistry could help to screen for other candidates to affect engulfment processes. In order to proof a beneficial capacity of T cell engulfment, antibody-mediated lectin neutralization could be performed *in vivo* in EAE-induced mice prior to the onset of the disease and during the disease course. In case of a beneficial effect of the engulfment processes, inhibition of these processes should result in exacerbated disease courses. However, as lectins such as CD206 are not only expressed by microglia, but also by peripheral myeloid cells (Franco and Fernández-Suárez, 2015), it has to be taken into account that CD206 blockade could also impact peripheral phagocytosis.

To understand the full extent of the impact of engulfment processes during the disease, it is of further interest, whether myeloid cells in the CNS are able to engulf other pathogenic autoimmune cells such as $CD8^+$ T cells or B cells during the disease. In order to answer this question, organotypic hippocampal slices could be co-cultured with various immune cells. *In vivo* two-photon imaging of myeloid cells and T cells in peripheral organs such as the spleen could serve as a control of data obtained in the CNS and could thus provide deeper insight into the relevance of this process in the CNS as the target organ of the disease. These experiments would also determine, whether peripheral myeloid cells are able to contribute to microglial T cell capture. Of note, some T cells were able to escape microglial engulfment and high percentages of T cells were not engulfed in the CNS despite the high expression of GlcNAc in the CNS. In order to determine how T cell capture is circumvented by pathogenic T cells, laser capture microdissection could be used followed by RNA-Seq to compare the gene expression profile of engulfed and freely migrating T cell in the CNS. Differences in the gene expression profile could reveal additional pathways which mediate T cell engulfment or escape, which could in turn reveal more therapeutic targets.

Bibliography

't Hart, B.A., Gran, B., and Weissert, R. (2011). EAE: imperfect but useful models of multiple sclerosis. Trends in Molecular Medicine *17*, 119-125.

Adams, M.R., Forsyth, C.J., Jessup, W., Robinson, J., and Celermajer, D.S. (1995). Oral L-arginine inhibits platelet aggregation but does not enhance endothelium-dependent dilation in healthy young men. J Am Coll Cardiol *26*, 1054-1061.

Ahn, M., Yang, W., Kim, H., Jin, J.-k., Moon, C., and Shin, T. (2012). Immunohistochemical study of arginase-1 in the spinal cords of Lewis rats with experimental autoimmune encephalomyelitis. Brain Research *1453*, 77-86.

Ajami, B., Bennett, J.L., Krieger, C., Tetzlaff, W., and Rossi, F.M.V. (2007). Local self-renewal can sustain CNS microglia maintenance and function throughout adult life. Nature Neuroscience *10*, 1538-1543.

Aktas, O., Smorodchenko, A., Brocke, S., Infante-Duarte, C., Topphoff, U.S., Vogt, J., Prozorovski, T., Meier, S., Osmanova, V., Pohl, E*., et al.* (2005). Neuronal Damage in Autoimmune Neuroinflammation Mediated by the Death Ligand TRAIL. Neuron *46*, 421-432.

Aloisi, F., Ria, F., Columba-Cabezas, S., Hess, H., Penna, G., and Adorini, L. (1999). Relative efficiency of microglia, astrocytes, dendritic cells and B cells in naive CD4+ T cell priming and Th1/Th2 cell restimulation. Eur J Immunol *29*, 2705-2714.

Anders, S., and Huber, W. (2010). Differential expression analysis for sequence count data. Genome Biology *11*, R106.

Anderson, A.J., Su, J.H., and Cotman, C.W. (1996). DNA damage and apoptosis in Alzheimer's disease: colocalization with c-Jun immunoreactivity, relationship to brain area, and effect of postmortem delay. J Neurosci *16*, 1710-1719.

Archambault, A.S., Sim, J., Gimenez, M.A.T., and Russell, J.H. (2005). Defining antigen-dependent stages of T cell migration from the blood to the central nervous system parenchyma. European Journal of Immunology *35*, 1076-1085.

Arora, M., Chen, L., Paglia, M., Gallagher, I., Allen, J.E., Vyas, Y.M., Ray, A., and Ray, P. (2006). Simvastatin promotes Th2-type responses through the induction of the chitinase family member Ym1 in dendritic cells. Proceedings of the National Academy of Sciences *103*, 7777-7782.

Azad, A.K., Rajaram, M.V., and Schlesinger, L.S. (2014). Exploitation of the Macrophage Mannose Receptor (CD206) in Infectious Disease Diagnostics and Therapeutics. J Cytol Mol Biol *1*.

Bailey, S.L., Schreiner, B., McMahon, E.J., and Miller, S.D. (2007). CNS myeloid DCs presenting endogenous myelin peptides 'preferentially' polarize CD4+ TH-17 cells in relapsing EAE. Nature Immunology *8*, 172-180.

Belbasis, L., Bellou, V., Evangelou, E., Ioannidis, J.P.A., and Tzoulaki, I. (2015). Environmental risk factors and multiple sclerosis: an umbrella review of systematic reviews and meta-analyses. The Lancet Neurology *14*, 263-273.

Benjamini, Y., and Hochberg, Y. (1995). Controlling the False Discovery Rate - a Practical and Powerful Approach to Multiple Testing. J Roy Stat Soc B Met *57*, 289-300.

Benseler, V., Warren, A., Vo, M., Holz, L.E., Tay, S.S., Le Couteur, D.G., Breen, E., Allison, A.C., van Rooijen, N., McGuffog, C.*, et al.* (2011). Hepatocyte entry leads to degradation of autoreactive CD8 T cells. Proceedings of the National Academy of Sciences *108*, 16735-16740.

Bettelli, E., Das, M.P., Howard, E.D., Weiner, H.L., Sobel, R.A., and Kuchroo, V.K. (1998). IL-10 is critical in the regulation of autoimmune encephalomyelitis as demonstrated by studies of IL-10- and IL-4-deficient and transgenic mice. J Immunol *161*, 3299-3306.

Bettelli, E., Pagany, M., Weiner, H.L., Linington, C., Sobel, R.A., and Kuchroo, V.K. (2003). Myelin Oligodendrocyte Glycoprotein–specific T Cell Receptor Transgenic Mice Develop Spontaneous Autoimmune Optic Neuritis. The Journal of Experimental Medicine *197*, 1073-1081.

Bhasin, M., Wu, M., and Tsirka, S.E. (2007). Modulation of microglial/macrophage activation by macrophage inhibitory factor (TKP) or tuftsin (TKPR) attenuates the disease course of experimental autoimmune encephalomyelitis. BMC Immunology *8*, 10.

Birkner, K., Wasser, B., Loos, J., Plotnikov, A., Seger, R., Zipp, F., Witsch, E., and Bittner, S. (2017). The Role of ERK Signaling in Experimental Autoimmune Encephalomyelitis. International Journal of Molecular Sciences *18*, 1990.

Bogie, J.F.J., Stinissen, P., Hellings, N., and Hendriks, J.J.A. (2011). Myelin-phagocytosing macrophages modulate autoreactive T cell proliferation. Journal of Neuroinflammation *8*, 85.

Brocker, T., Riedinger, M., and Karjalainen, K. (1997). Targeted expression of major histocompatibility complex (MHC) class II molecules demonstrates that dendritic cells can induce negative but not positive selection of thymocytes in vivo. J Exp Med *185*, 541-550.

Brown, G.C., and Neher, J.J. (2014). Microglial phagocytosis of live neurons. Nature Reviews Neuroscience *15*, 209-216.

Bruck, W., Bruck, Y., and Friede, R.L. (1992). TNF-alpha suppresses CR3-mediated myelin removal by macrophages. J Neuroimmunol *38*, 9-17.

Cahalan, M.D., and Parker, I. (2008). Choreography of Cell Motility and Interaction Dynamics Imaged by Two-Photon Microscopy in Lymphoid Organs. Annual Review of Immunology *26*, 585-626.

Carson, M.J. (2002). Microglia as liaisons between the immune and central nervous systems: Functional implications for multiple sclerosis. Glia *40*, 218-231.

Chastain, E.M.L., and Miller, S.D. (2012). Molecular mimicry as an inducing trigger for CNS autoimmune demyelinating disease. Immunological Reviews *245*, 227-238.

Chen, Z., Jalabi, W., Hu, W., Park, H.J., Gale, J.T., Kidd, G.J., Bernatowicz, R., Gossman, Z.C., Chen, J.T., Dutta, R., and Trapp, B.D. (2014). Microglial displacement of inhibitory synapses provides neuroprotection in the adult brain. Nat Commun *5*, 4486.

Compston, A., and Coles, A. (2008). Multiple sclerosis. Lancet *372*, 1502-1517.

Croxford, A.L., Kurschus, F.C., and Waisman, A. (2011). Mouse models for multiple sclerosis: Historical facts and future implications. Biochimica et Biophysica Acta (BBA) - Molecular Basis of Disease *1812*, 177-183.

Czimmerer, Z., Varga, T., Poliska, S., Nemet, I., Szanto, A., and Nagy, L. (2012). Identification of novel markers of alternative activation and potential endogenous PPARγ ligand production mechanisms in human IL-4 stimulated differentiating macrophages. Immunobiology *217*, 1301-1314.

Darrasse-Jèze, G., Deroubaix, S., Mouquet, H., Victora, G.D., Eisenreich, T., Yao, K.-h., Masilamani, R.F., Dustin, M.L., Rudensky, A., Liu, K., and Nussenzweig, M.C. (2009). Feedback control of regulatory T cell homeostasis by dendritic cells in vivo. The Journal of Experimental Medicine *206*, 1853-1862.

de Jong, E.C., Smits, H.H., and Kapsenberg, M.L. (2005). Dendritic cell-mediated T cell polarization. Springer Seminars in Immunopathology *26*, 289-307.

De Simoni, A., Griesinger, C.B., and Edwards, F.A. (2003). Development of Rat CA1 Neurones in AcuteVersusOrganotypic Slices: Role of Experience in Synaptic Morphology and Activity. The Journal of Physiology *550*, 135-147.

De Simoni, A., and My Yu, L. (2006). Preparation of organotypic hippocampal slice cultures: interface method. Nature Protocols *1*, 1439-1445.

de Vos, A.F., van Meurs, M., Brok, H.P., Boven, L.A., Hintzen, R.Q., van der Valk, P., Ravid, R., Rensing, S., Boon, L., Hart, B.A.t., and Laman, J.D. (2002). Transfer of Central Nervous System Autoantigens and Presentation in Secondary Lymphoid Organs. The Journal of Immunology *169*, 5415-5423.

Dendrou, C.A., Fugger, L., and Friese, M.A. (2015). Immunopathology of multiple sclerosis. Nature Reviews Immunology *15*, 545-558.

Denk, W., Strickler, J.H., and Webb, W.W. (1990). Two-photon laser scanning fluorescence microscopy. Science *248*, 73-76.

Diebold, S.S. (2008). Determination of T-cell fate by dendritic cells. Immunology and Cell Biology *86*, 389-397.

Ding, A.H., Nathan, C.F., and Stuehr, D.J. (1988). Release of reactive nitrogen intermediates and reactive oxygen intermediates from mouse peritoneal macrophages. Comparison of activating cytokines and evidence for independent production. J Immunol *141*, 2407-2412.

Dogan, R.N., Long, N., Forde, E., Dennis, K., Kohm, A.P., Miller, S.D., and Karpus, W.J. (2011). CCL22 regulates experimental autoimmune encephalomyelitis by controlling inflammatory macrophage accumulation and effector function. J Leukoc Biol *89*, 93-104.

Duraes, F.V., Lippens, C., Steinbach, K., Dubrot, J., Brighouse, D., Bendriss-Vermare, N., Issazadeh-Navikas, S., Merkler, D., and Hugues, S. (2016). pDC therapy induces recovery from EAE by recruiting endogenous pDC to sites of CNS inflammation. Journal of Autoimmunity *67*, 8-18.

Duvall, E., Wyllie, A.H., and Morris, R.G. (1985). Macrophage recognition of cells undergoing programmed cell death (apoptosis). Immunology *56*, 351-358.

Falcone, M., Rajan, A.J., Bloom, B.R., and Brosnan, C.F. (1998). A critical role for IL-4 in regulating disease severity in experimental allergic encephalomyelitis as demonstrated in IL-4-deficient C57BL/6 mice and BALB/c mice. J Immunol *160*, 4822-4830.

Fischer, M.T., Sharma, R., Lim, J.L., Haider, L., Frischer, J.M., Drexhage, J., Mahad, D., Bradl, M., van Horssen, J., and Lassmann, H. (2012). NADPH oxidase expression in active multiple sclerosis lesions in relation to oxidative tissue damage and mitochondrial injury. Brain *135*, 886-899.

Fletcher, J.M., Lalor, S.J., Sweeney, C.M., Tubridy, N., and Mills, K.H.G. (2010). T cells in multiple sclerosis and experimental autoimmune encephalomyelitis. Clinical & Experimental Immunology *162*, 1-11.

Flügel, A., Berkowicz, T., Ritter, T., Labeur, M., Jenne, D.E., Li, Z., Ellwart, J.W., Willem, M., Lassmann, H., and Wekerle, H. (2001). Migratory activity and functional changes of green fluorescent effector cells before and during experimental autoimmune encephalomyelitis. Immunity *14*, 547-560.

Franco, R., and Fernández-Suárez, D. (2015). Alternatively activated microglia and macrophages in the central nervous system. Progress in Neurobiology *131*, 65-86.

Friese, M.A., Schattling, B., and Fugger, L. (2014). Mechanisms of neurodegeneration and axonal dysfunction in multiple sclerosis. Nature Reviews Neurology *10*, 225-238.

Fujinami, R.S., von Herrath, M.G., Christen, U., and Whitton, J.L. (2006). Molecular Mimicry, Bystander Activation, or Viral Persistence: Infections and Autoimmune Disease. Clinical Microbiology Reviews *19*, 80-94.

Geissmann, F., Jung, S., and Littman, D.R. (2003). Blood Monocytes Consist of Two Principal Subsets with Distinct Migratory Properties. Immunity *19*, 71-82.

Germain, R.N., and Margulies, D.H. (1993). The biochemistry and cell biology of antigen processing and presentation. Annu Rev Immunol *11*, 403-450.

Ghoreschi, K., Brück, J., Kellerer, C., Deng, C., Peng, H., Rothfuss, O., Hussain, R.Z., Gocke, A.R., Respa, A., Glocova, I.*, et al.* (2011). Fumarates improve psoriasis and multiple sclerosis by inducing type II dendritic cells. The Journal of Experimental Medicine *208*, 2291-2303.

Ginhoux, F., Greter, M., Leboeuf, M., Nandi, S., See, P., Gokhan, S., Mehler, M.F., Conway, S.J., Ng, L.G., Stanley, E.R.*, et al.* (2010). Fate Mapping Analysis Reveals That Adult Microglia Derive from Primitive Macrophages. Science *330*, 841-845.

Goldmann, T., and Prinz, M. (2013). Role of Microglia in CNS Autoimmunity. Clinical and Developmental Immunology *2013*, 1-8.

Goldmann, T., Wieghofer, P., Müller, P.F., Wolf, Y., Varol, D., Yona, S., Brendecke, S.M., Kierdorf, K., Staszewski, O., Datta, M.*, et al.* (2013). A new type of microglia gene targeting shows TAK1 to be pivotal in CNS autoimmune inflammation. Nature Neuroscience *16*, 1618-1626.

Goverman, J. (2009). Autoimmune T cell responses in the central nervous system. Nature Reviews Immunology *9*, 393-407.

Greter, M., Heppner, F.L., Lemos, M.P., Odermatt, B.M., Goebels, N., Laufer, T., Noelle, R.J., and Becher, B. (2005). Dendritic cells permit immune invasion of the CNS in an animal model of multiple sclerosis. Nature Medicine *11*, 328-334.

Gross, C.C., Schulte-Mecklenbeck, A., Klinsing, S., Posevitz-Fejfár, A., Wiendl, H., and Klotz, L. (2015). Dimethyl fumarate treatment alters circulating T helper cell subsets in multiple sclerosis. Neurology - Neuroimmunology Neuroinflammation *3*, e183.

Guo, K., and Janigro, D. (2013). New immunological approaches in treating and diagnosing CNS diseases. Pharmaceutical Patent Analyst *2*, 361-371.

Hadjantonakis, A.K., Macmaster, S., and Nagy, A. (2002). Embryonic stem cells and mice expressing different GFP variants for multiple non-invasive reporter usage within a single animal. BMC Biotechnol *2*, 11.

Haghikia, A., Hohlfeld, R., Gold, R., and Fugger, L. (2013). Therapies for multiple sclerosis: translational achievements and outstanding needs. Trends in Molecular Medicine *19*, 309-319.

Hanisch, U.-K. (2002). Microglia as a source and target of cytokines. Glia *40*, 140-155.

Harding, F.A., McArthur, J.G., Gross, J.A., Raulet, D.H., and Allison, J.P. (1992). CD28-mediated signalling co-stimulates murine T cells and prevents induction of anergy in T-cell clones. Nature *356*, 607-609.

Hashimoto, D., Chow, A., Noizat, C., Teo, P., Beasley, Mary B., Leboeuf, M., Becker, Christian D., See, P., Price, J., Lucas, D.*, et al.* (2013). Tissue-Resident Macrophages Self-Maintain Locally throughout Adult Life with Minimal Contribution from Circulating Monocytes. Immunity *38*, 792-804.

Hendriks, J.J.A., Teunissen, C.E., de Vries, H.E., and Dijkstra, C.D. (2005). Macrophages and neurodegeneration. Brain Research Reviews *48*, 185-195.

Heneka, M.T., Kummer, M.P., and Latz, E. (2014). Innate immune activation in neurodegenerative disease. Nature Reviews Immunology *14*, 463-477.

Heppner, F.L., Greter, M., Marino, D., Falsig, J., Raivich, G., Hövelmeyer, N., Waisman, A., Rülicke, T., Prinz, M., Priller, J.*, et al.* (2005). Experimental autoimmune encephalomyelitis repressed by microglial paralysis. Nature Medicine *11*, 146-152.

Herz, J., Paterka, M., Niesner, R.A., Brandt, A.U., Siffrin, V., Leuenberger, T., Birkenstock, J., Mossakowski, A., Glumm, R., Zipp, F., and Radbruch, H. (2011). In vivo imaging of lymphocytes in the CNS reveals different behaviour of naïve T cells in health and autoimmunity. Journal of Neuroinflammation *8*, 131.

Herz, J., Siffrin, V., Hauser, A.E., Brandt, A.U., Leuenberger, T., Radbruch, H., Zipp, F., and Niesner, R.A. (2010). Expanding Two-Photon Intravital Microscopy to the Infrared by Means of Optical Parametric Oscillator. Biophysical Journal *98*, 715-723.

Hu, X., Li, P., Guo, Y., Wang, H., Leak, R.K., Chen, S., Gao, Y., and Chen, J. (2012). Microglia/macrophage polarization dynamics reveal novel mechanism of injury expansion after focal cerebral ischemia. Stroke *43*, 3063-3070.

Huang, Y.M., Xiao, B.G., Ozenci, V., Kouwenhoven, M., Teleshova, N., Fredrikson, S., and Link, H. (1999). Multiple sclerosis is associated with high levels of circulating dendritic cells secreting pro-inflammatory cytokines. J Neuroimmunol *99*, 82-90.

Huber, W., Carey, V.J., Gentleman, R., Anders, S., Carlson, M., Carvalho, B.S., Bravo, H.C., Davis, S., Gatto, L., Girke, T.*, et al.* (2015). Orchestrating high-throughput genomic analysis with Bioconductor. Nat Methods *12*, 115-121.

Hughes, D., Raine, C.S., and Field, E.J. (1968). Invasion of neurones in vitro by non immune lymphocytes. An electron microscopic study. Br J Exp Pathol *49*, 356-359.

Hughes, J.E., Srinivasan, S., Lynch, K.R., Proia, R.L., Ferdek, P., and Hedrick, C.C. (2008). Sphingosine-1-Phosphate Induces an Antiinflammatory Phenotype in Macrophages. Circulation Research *102*, 950-958.

Hulett, H.R., Bonner, W.A., Sweet, R.G., and Herzenberg, L.A. (1973). Development and application of a rapid cell sorter. Clin Chem *19*, 813-816.

Ishibashi, K., Suzuki, M., Sasaki, S., and Imai, M. (2001). Identification of a new multigene four-transmembrane family (MS4A) related to CD20, HTm4 and beta subunit of the high-affinity IgE receptor. Gene *264*, 87-93.

Jiang, Z., Jiang, J.X., and Zhang, G.-X. (2014). Macrophages: A double-edged sword in experimental autoimmune encephalomyelitis. Immunology Letters *160*, 17-22.

Jolivel, V., Luessi, F., Masri, J., Kraus, S.H.P., Hubo, M., Poisa-Beiro, L., Klebow, S., Paterka, M., Yogev, N., Tumani, H.*, et al.* (2013). Modulation of dendritic cell properties by laquinimod as a mechanism for modulating multiple sclerosis. Brain *136*, 1048-1066.

Jung, S., Aliberti, J., Graemmel, P., Sunshine, M.J., Kreutzberg, G.W., Sher, A., and Littman, D.R. (2000). Analysis of fractalkine receptor CX(3)CR1 function by targeted deletion and green fluorescent protein reporter gene insertion. Mol Cell Biol *20*, 4106-4114.

Jung, S., Siglienti, I., Grauer, O., Magnus, T., Scarlato, G., and Toyka, K. (2004). Induction of IL-10 in rat peritoneal macrophages and dendritic cells by glatiramer acetate. Journal of Neuroimmunology *148*, 63-73.

Kabba, J.A., Xu, Y., Christian, H., Ruan, W., Chenai, K., Xiang, Y., Zhang, L., Saavedra, J.M., and Pang, T. (2017). Microglia: Housekeeper of the Central Nervous System. Cellular and Molecular Neurobiology.

Karman, J., Chu, H.H., Co, D.O., Seroogy, C.M., Sandor, M., and Fabry, Z. (2006). Dendritic Cells Amplify T Cell-Mediated Immune Responses in the Central Nervous System. The Journal of Immunology *177*, 7750-7760.

Karni, A., Abraham, M., Monsonego, A., Cai, G., Freeman, G.J., Hafler, D., Khoury, S.J., and Weiner, H.L. (2006). Innate Immunity in Multiple Sclerosis: Myeloid Dendritic Cells in Secondary Progressive Multiple Sclerosis Are Activated and Drive a Proinflammatory Immune Response. The Journal of Immunology *177*, 4196-4202.

Kawakami, N., and Flügel, A. (2010). Knocking at the brain's door: intravital two-photon imaging of autoreactive T cell interactions with CNS structures. Seminars in Immunopathology *32*, 275-287.

Kawakami, N., Lassmann, S., Li, Z., Odoardi, F., Ritter, T., Ziemssen, T., Klinkert, W.E.F., Ellwart, J.W., Bradl, M., Krivacic, K.*, et al.* (2004). The Activation Status of Neuroantigen-specific T Cells in the Target Organ Determines the Clinical Outcome of Autoimmune Encephalomyelitis. The Journal of Experimental Medicine *199*, 185-197.

Kawamoto, H., and Minato, N. (2004). Myeloid cells. The International Journal of Biochemistry & Cell Biology *36*, 1374-1379.

Kerschensteiner, M., Stadelmann, C., Dechant, G., Wekerle, H., and Hohlfeld, R. (2003). Neurotrophic cross-talk between the nervous and immune systems: implications for neurological diseases. Ann Neurol *53*, 292-304.

Kigerl, K.A., Gensel, J.C., Ankeny, D.P., Alexander, J.K., Donnelly, D.J., and Popovich, P.G. (2009). Identification of Two Distinct Macrophage Subsets with Divergent Effects Causing either Neurotoxicity or Regeneration in the Injured Mouse Spinal Cord. Journal of Neuroscience *29*, 13435-13444.

Kim, H.J., Ifergan, I., Antel, J.P., Seguin, R., Duddy, M., Lapierre, Y., Jalili, F., and Bar-Or, A. (2004). Type 2 Monocyte and Microglia Differentiation Mediated by Glatiramer Acetate Therapy in Patients with Multiple Sclerosis. The Journal of Immunology *172*, 7144-7153.

Korn, T., and Kallies, A. (2017). T cell responses in the central nervous system. Nature Reviews Immunology *17*, 179-194.

Kotter, M.R. (2006). Myelin Impairs CNS Remyelination by Inhibiting Oligodendrocyte Precursor Cell Differentiation. Journal of Neuroscience *26*, 328-332.

Kozovska, M.E., Hong, J., Zang, Y.C., Li, S., Rivera, V.M., Killian, J.M., and Zhang, J.Z. (1999). Interferon beta induces T-helper 2 immune deviation in MS. Neurology *53*, 1692-1697.

Krishna, S., and Overholtzer, M. (2016). Mechanisms and consequences of entosis. Cellular and Molecular Life Sciences *73*, 2379-2386.

Kutzelnigg, A. (2005). Cortical demyelination and diffuse white matter injury in multiple sclerosis. Brain *128*, 2705-2712.

Lampron, A., Larochelle, A., Laflamme, N., Préfontaine, P., Plante, M.-M., Sánchez, M.G., Yong, V.W., Stys, P.K., Tremblay, M.-È., and Rivest, S. (2015). Inefficient clearance of myelin debris by microglia impairs remyelinating processes. The Journal of Experimental Medicine *212*, 481-495.

Larochelle, C., Uphaus, T., Prat, A., and Zipp, F. (2016). Secondary Progression in Multiple Sclerosis: Neuronal Exhaustion or Distinct Pathology? Trends in Neurosciences *39*, 325-339.

Lawrence, T., and Natoli, G. (2011). Transcriptional regulation of macrophage polarization: enabling diversity with identity. Nature Reviews Immunology *11*, 750-761.

Legge, K.L., Gregg, R.K., Maldonado-Lopez, R., Li, L., Caprio, J.C., Moser, M., and Zaghouani, H. (2002). On the Role of Dendritic Cells in Peripheral T Cell Tolerance and Modulation of Autoimmunity. The Journal of Experimental Medicine *196*, 217-227.

Lehnardt, S. (2010). Innate immunity and neuroinflammation in the CNS: The role of microglia in Toll-like receptor-mediated neuronal injury. Glia, NA-NA.

Lehnardt, S., Lachance, C., Patrizi, S., Lefebvre, S., Follett, P.L., Jensen, F.E., Rosenberg, P.A., Volpe, J.J., and Vartanian, T. (2002). The toll-like receptor TLR4 is necessary for lipopolysaccharide-induced oligodendrocyte injury in the CNS. J Neurosci *22*, 2478-2486.

Li, H., Zhang, G.X., Chen, Y., Xu, H., Fitzgerald, D.C., Zhao, Z., and Rostami, A. (2008). CD11c+CD11b+ dendritic cells play an important role in intravenous tolerance and the suppression of experimental autoimmune encephalomyelitis. J Immunol *181*, 2483-2493.

Lill, C.M., Luessi, F., Alcina, A., Sokolova, E.A., Ugidos, N., de la Hera, B., Guillot-Noel, L., Malhotra, S., Reinthaler, E., Schjeide, B.M.*, et al.* (2015). Genome-wide significant association with seven novel multiple sclerosis risk loci. J Med Genet *52*, 848-855.

Liu, C., Li, Y., Yu, J., Feng, L., Hou, S., Liu, Y., Guo, M., Xie, Y., Meng, J., Zhang, H*., et al.* (2013). Targeting the shift from M1 to M2 macrophages in experimental autoimmune encephalomyelitis mice treated with fasudil. PLoS One *8*, e54841.

Lobo-Silva, D., Carriche, G.M., Castro, A.G., Roque, S., and Saraiva, M. (2017). Interferon-β regulates the production of IL-10 by toll-like receptor-activated microglia. Glia.

Lovett-Racke, A.E., Yang, Y., and Racke, M.K. (2011). Th1 versus Th17: Are T cell cytokines relevant in multiple sclerosis? Biochimica et Biophysica Acta (BBA) - Molecular Basis of Disease *1812*, 246-251.

Lu, Z., Elliott, M.R., Chen, Y., Walsh, J.T., Klibanov, A.L., Ravichandran, K.S., and Kipnis, J. (2011). Phagocytic activity of neuronal progenitors regulates adult neurogenesis. Nature Cell Biology *13*, 1076-1083.

Lublin, F.D., and Reingold, S.C. (1996). Defining the clinical course of multiple sclerosis: results of an international survey. National Multiple Sclerosis Society (USA) Advisory Committee on Clinical Trials of New Agents in Multiple Sclerosis. Neurology *46*, 907-911.

Luche, H., Weber, O., Nageswara Rao, T., Blum, C., and Fehling, H.J. (2007). Faithful activation of an extra-bright red fluorescent protein in "knock-in" Cre-reporter mice ideally suited for lineage tracing studies. European Journal of Immunology *37*, 43-53.

Luchtman, D., Gollan, R., Ellwardt, E., Birkenstock, J., Robohm, K., Siffrin, V., and Zipp, F. (2016). In vivo and in vitro effects of multiple sclerosis immunomodulatory therapeutics on glutamatergic excitotoxicity. Journal of Neurochemistry *136*, 971-980.

Lüssi, F., Zipp, F., and Witsch, E. (2016). Dendritic cells as therapeutic targets in neuroinflammation. Cellular and Molecular Life Sciences *73*, 2425-2450.

Marckmann, S., Wiesemann, E., Hilse, R., Trebst, C., Stangel, M., and Windhagen, A. (2004). Interferon-beta up-regulates the expression of co-stimulatory molecules CD80, CD86 and CD40 on monocytes: significance for treatment of multiple sclerosis. Clinical and Experimental Immunology *138*, 499-506.

Martin, C.J., Peters, K.N., and Behar, S.M. (2014). Macrophages clean up: efferocytosis and microbial control. Current Opinion in Microbiology *17*, 17-23.

Matzinger, P., and Guerder, S. (1989). Does T-cell tolerance require a dedicated antigen-presenting cell? Nature *338*, 74-76.

McCarthy, D.J., Chen, Y., and Smyth, G.K. (2012). Differential expression analysis of multifactor RNA-Seq experiments with respect to biological variation. Nucleic Acids Research *40*, 4288-4297.

McMahon, E.J., Bailey, S.L., Castenada, C.V., Waldner, H., and Miller, S.D. (2005). Epitope spreading initiates in the CNS in two mouse models of multiple sclerosis. Nature Medicine *11*, 335-339.

McRae, B.L., Kennedy, M.K., Tan, L.J., Dal Canto, M.C., Picha, K.S., and Miller, S.D. (1992). Induction of active and adoptive relapsing experimental autoimmune encephalomyelitis (EAE) using an encephalitogenic epitope of proteolipid protein. J Neuroimmunol *38*, 229-240.

Mendel, I., Kerlero de Rosbo, N., and Ben-Nun, A. (1995). A myelin oligodendrocyte glycoprotein peptide induces typical chronic experimental autoimmune encephalomyelitis in

H-2b mice: fine specificity and T cell receptor V beta expression of encephalitogenic T cells. Eur J Immunol *25*, 1951-1959.

Menges, M., Rossner, S., Voigtlander, C., Schindler, H., Kukutsch, N.A., Bogdan, C., Erb, K., Schuler, G., and Lutz, M.B. (2002). Repetitive injections of dendritic cells matured with tumor necrosis factor alpha induce antigen-specific protection of mice from autoimmunity. J Exp Med *195*, 15-21.

Merson, T.D., Binder, M.D., and Kilpatrick, T.J. (2010). Role of Cytokines as Mediators and Regulators of Microglial Activity in Inflammatory Demyelination of the CNS. NeuroMolecular Medicine *12*, 99-132.

Michel, J., Schönhaar, K., Schledzewski, K., Gkaniatsou, C., Sticht, C., Kellert, B., Lasitschka, F., Géraud, C., Goerdt, S., and Schmieder, A. (2013). Identification of the novel differentiation marker MS4A8B and its murine homolog MS4A8A in colonic epithelial cells lost during neoplastic transformation in human colon. Cell Death and Disease *4*, e469.

Mikita, J., Dubourdieu-Cassagno, N., Deloire, M.S.A., Vekris, A., Biran, M., Raffard, G., Brochet, B., Canron, M.-H., Franconi, J.-M., Boiziau, C., and Petry, K.G. (2011). Altered M1/M2 activation patterns of monocytes in severe relapsing experimental rat model of multiple sclerosis. Amelioration of clinical status by M2 activated monocyte administration. Multiple Sclerosis Journal *17*, 2-15.

Miller, A., Shapiro, S., Gershtein, R., Kinarty, A., Rawashdeh, H., Honigman, S., and Lahat, N. (1998). Treatment of multiple sclerosis with copolymer-1 (Copaxone): implicating mechanisms of Th1 to Th2/Th3 immune-deviation. J Neuroimmunol *92*, 113-121.

Miltenyi, S., Muller, W., Weichel, W., and Radbruch, A. (1990). High gradient magnetic cell separation with MACS. Cytometry *11*, 231-238.

Mombaerts, P., Iacomini, J., Johnson, R.S., Herrup, K., Tonegawa, S., and Papaioannou, V.E. (1992). RAG-1-deficient mice have no mature B and T lymphocytes. Cell *68*, 869-877.

Munder, M., Eichmann, K., and Modolell, M. (1998). Alternative metabolic states in murine macrophages reflected by the nitric oxide synthase/arginase balance: competitive regulation by CD4+ T cells correlates with Th1/Th2 phenotype. J Immunol *160*, 5347-5354.

Nadesalingam, J., Dodds, A.W., Reid, K.B.M., and Palaniyar, N. (2005). Mannose-Binding Lectin Recognizes Peptidoglycan via the N-Acetyl Glucosamine Moiety, and Inhibits Ligand-Induced Proinflammatory Effect and Promotes Chemokine Production by Macrophages. The Journal of Immunology *175*, 1785-1794.

Napoli, I., and Neumann, H. (2010). Protective effects of microglia in multiple sclerosis. Experimental Neurology *225*, 24-28.

Neumann, H., Kotter, M.R., and Franklin, R.J.M. (2009). Debris clearance by microglia: an essential link between degeneration and regeneration. Brain *132*, 288-295.

Neumann, J., Sauerzweig, S., Ronicke, R., Gunzer, F., Dinkel, K., Ullrich, O., Gunzer, M., and Reymann, K.G. (2008). Microglia Cells Protect Neurons by Direct Engulfment of Invading Neutrophil Granulocytes: A New Mechanism of CNS Immune Privilege. Journal of Neuroscience *28*, 5965-5975.

Ng, Y.K., and Ling, E.A. (1999). Emperipolesis of lymphoid cells in vagal efferent neurons following an intraneural injection of ricin into the vagus nerve in rats. Neurosci Lett *270*, 153-156.

Nikic, I., Merkler, D., Sorbara, C., Brinkoetter, M., Kreutzfeldt, M., Bareyre, F.M., Bruck, W., Bishop, D., Misgeld, T., and Kerschensteiner, M. (2011). A reversible form of axon damage in experimental autoimmune encephalomyelitis and multiple sclerosis. Nat Med *17*, 495-499.

Nimmerjahn, A., Kirchhoff, F., and Helmchen, F. (2005). Resting microglial cells are highly dynamic surveillants of brain parenchyma in vivo. Science *308*, 1314-1318.

Notter, M.F., and Leary, J.F. (1987). Surface glycoproteins of differentiating neuroblastoma cells analyzed by lectin binding and flow cytometry. Cytometry *8*, 518-525.

Odoardi, F., Sie, C., Streyl, K., Ulaganathan, V.K., Schläger, C., Lodygin, D., Heckelsmiller, K., Nietfeld, W., Ellwart, J., Klinkert, W.E.F*., et al.* (2012). T cells become licensed in the lung to enter the central nervous system. Nature *488*, 675-679.

Olah, M., Amor, S., Brouwer, N., Vinet, J., Eggen, B., Biber, K., and Boddeke, H.W.G.M. (2012). Identification of a microglia phenotype supportive of remyelination. Glia *60*, 306-321.

Ousman, S.S., and Kubes, P. (2012). Immune surveillance in the central nervous system. Nature Neuroscience *15*, 1096-1101.

Overholtzer, M., and Brugge, J.S. (2008). The cell biology of cell-in-cell structures. Nature Reviews Molecular Cell Biology *9*, 796-809.

Overholtzer, M., Mailleux, A.A., Mouneimne, G., Normand, G., Schnitt, S.J., King, R.W., Cibas, E.S., and Brugge, J.S. (2007). A Nonapoptotic Cell Death Process, Entosis, that Occurs by Cell-in-Cell Invasion. Cell *131*, 966-979.

Park, H.J., Park, O.J., and Shin, J. (2005). Receptor activator of NF-kappaB ligand enhances the activity of macrophages as antigen presenting cells. Exp Mol Med *37*, 524-532.

Paterka, M., Siffrin, V., Voss, J.O., Werr, J., Hoppmann, N., Gollan, R., Belikan, P., Bruttger, J., Birkenstock, J., Jung, S*., et al.* (2016). Gatekeeper role of brain antigen-presenting CD11c+ cells in neuroinflammation. The EMBO Journal *35*, 89-101.

Paterka, M., Voss, J.O., Werr, J., Reuter, E., Franck, S., Leuenberger, T., Herz, J., Radbruch, H., Bopp, T., Siffrin, V., and Zipp, F. (2017). Dendritic cells tip the balance towards induction of regulatory T cells upon priming in experimental autoimmune encephalomyelitis. Journal of Autoimmunity *76*, 108-114.

Pennock, N.D., White, J.T., Cross, E.W., Cheney, E.E., Tamburini, B.A., and Kedl, R.M. (2013). T cell responses: naive to memory and everything in between. AJP: Advances in Physiology Education *37*, 273-283.

Picelli, S., Faridani, O.R., Björklund, Å.K., Winberg, G., Sagasser, S., and Sandberg, R. (2014). Full-length RNA-seq from single cells using Smart-seq2. Nature Protocols *9*, 171-181.

Politis, M., Giannetti, P., Su, P., Turkheimer, F., Keihaninejad, S., Wu, K., Waldman, A., Malik, O., Matthews, P.M., Reynolds, R*., et al.* (2012). Increased PK11195 PET binding in the cortex of patients with MS correlates with disability. Neurology *79*, 523-530.

Ponomarev, E.D., Maresz, K., Tan, Y., and Dittel, B.N. (2007). CNS-Derived Interleukin-4 Is Essential for the Regulation of Autoimmune Inflammation and Induces a State of Alternative Activation in Microglial Cells. Journal of Neuroscience *27*, 10714-10721.

Ponomarev, E.D., Shriver, L.P., Maresz, K., and Dittel, B.N. (2005). Microglial cell activation and proliferation precedes the onset of CNS autoimmunity. Journal of Neuroscience Research *81*, 374-389.

Ponomarev, E.D., Veremeyko, T., Barteneva, N., Krichevsky, A.M., and Weiner, H.L. (2011). MicroRNA-124 promotes microglia quiescence and suppresses EAE by deactivating macrophages via the C/EBP-α–PU.1 pathway. Nature Medicine *17*, 64-70.

Popovic, N., Schubart, A., Goetz, B.D., Zhang, S.-C., Linington, C., and Duncan, I.D. (2002). Inhibition of autoimmune encephalomyelitis by a tetracycline. Annals of Neurology *51*, 215-223.

Prodinger, C., Bunse, J., Krüger, M., Schiefenhövel, F., Brandt, C., Laman, J.D., Greter, M., Immig, K., Heppner, F., Becher, B., and Bechmann, I. (2011). CD11c-expressing cells reside in the juxtavascular parenchyma and extend processes into the glia limitans of the mouse nervous system. Acta Neuropathologica *121*, 445-458.

Pul, R., Morbiducci, F., Skuljec, J., Skripuletz, T., Singh, V., Diederichs, U., Garde, N., Voss, E.V., Trebst, C., and Stangel, M. (2012). Glatiramer acetate increases phagocytic activity of human monocytes in vitro and in multiple sclerosis patients. PLoS One *7*, e51867.

Raes, G., De Baetselier, P., Noel, W., Beschin, A., Brombacher, F., and Hassanzadeh Gh, G. (2002). Differential expression of FIZZ1 and Ym1 in alternatively versus classically activated macrophages. J Leukoc Biol *71*, 597-602.

Raes, G., Van den Bergh, R., De Baetselier, P., Ghassabeh, G.H., Scotton, C., Locati, M., Mantovani, A., and Sozzani, S. (2005). Arginase-1 and Ym1 Are Markers for Murine, but Not Human, Alternatively Activated Myeloid Cells. The Journal of Immunology *174*, 6561-6562.

Ramgolam, V.S., Sha, Y., Jin, J., Zhang, X., and Markovic-Plese, S. (2009). IFN- Inhibits Human Th17 Cell Differentiation. The Journal of Immunology *183*, 5418-5427.

Ransohoff, R.M. (2007). Microgliosis: the questions shape the answers. Nat Neurosci *10*, 1507-1509.

Ransohoff, R.M. (2016). A polarizing question: do M1 and M2 microglia exist? Nature Neuroscience *19*, 987-991.

Ransohoff, R.M., and Brown, M.A. (2012). Innate immunity in the central nervous system. Journal of Clinical Investigation *122*, 1164-1171.

Ransohoff, R.M., and Cardona, A.E. (2010). The myeloid cells of the central nervous system parenchyma. Nature *468*, 253-262.

Ransohoff, R.M., and Perry, V.H. (2009). Microglial Physiology: Unique Stimuli, Specialized Responses. Annual Review of Immunology *27*, 119-145.

Rauh, M.J., Ho, V., Pereira, C., Sham, A., Sly, L.M., Lam, V., Huxham, L., Minchinton, A.I., Mui, A., and Krystal, G. (2005). SHIP Represses the Generation of Alternatively Activated Macrophages. Immunity *23*, 361-374.

Rescigno, M., Citterio, S., Thery, C., Rittig, M., Medaglini, D., Pozzi, G., Amigorena, S., and Ricciardi-Castagnoli, P. (1998). Bacteria-induced neo-biosynthesis, stabilization, and surface

expression of functional class I molecules in mouse dendritic cells. Proc Natl Acad Sci U S A *95*, 5229-5234.

Robinson, M.D., McCarthy, D.J., and Smyth, G.K. (2009). edgeR: a Bioconductor package for differential expression analysis of digital gene expression data. Bioinformatics *26*, 139-140.

Sanyal, R., Polyak, M.J., Zuccolo, J., Puri, M., Deng, L., Roberts, L., Zuba, A., Storek, J., Luider, J.M., Sundberg, E.M.*, et al.* (2017). MS4A4A: a novel cell surface marker for M2 macrophages and plasma cells. Immunol Cell Biol *95*, 611-619.

Schilling, M., Besselmann, M., Leonhard, C., Mueller, M., Ringelstein, E.B., and Kiefer, R. (2003). Microglial activation precedes and predominates over macrophage infiltration in transient focal cerebral ischemia: a study in green fluorescent protein transgenic bone marrow chimeric mice. Experimental Neurology *183*, 25-33.

Schläger, C., Körner, H., Krueger, M., Vidoli, S., Haberl, M., Mielke, D., Brylla, E., Issekutz, T., Cabañas, C., Nelson, P.J.*, et al.* (2016). Effector T-cell trafficking between the leptomeninges and the cerebrospinal fluid. Nature *530*, 349-353.

Schmieder, A., Schledzewski, K., Michel, J., Schönhaar, K., Morias, Y., Bosschaerts, T., Van den Bossche, J., Dorny, P., Sauer, A., Sticht, C.*, et al.* (2012). The CD20 homolog Ms4a8a integrates pro- and anti-inflammatory signals in novel M2-like macrophages and is expressed in parasite infection. European Journal of Immunology *42*, 2971-2982.

Schmieder, A., Schledzewski, K., Michel, J., Tuckermann, J.P., Tome, L., Sticht, C., Gkaniatsou, C., Nicolay, J.P., Demory, A., Faulhaber, J.*, et al.* (2011). Synergistic activation by p38MAPK and glucocorticoid signaling mediates induction of M2-like tumor-associated macrophages expressing the novel CD20 homolog MS4A8A. International Journal of Cancer *129*, 122-132.

Schwartz, M. (2010). “Tissue-repairing” blood-derived macrophages are essential for healing of the injured spinal cord: From skin-activated macrophages to infiltrating blood-derived cells? Brain, Behavior, and Immunity *24*, 1054-1057.

Serafini, B., Columba-Cabezas, S., Di Rosa, F., and Aloisi, F. (2000). Intracerebral recruitment and maturation of dendritic cells in the onset and progression of experimental autoimmune encephalomyelitis. Am J Pathol *157*, 1991-2002.

Serafini, B., Rosicarelli, B., Magliozzi, R., Stigliano, E., Capello, E., Mancardi, G.L., and Aloisi, F. (2006). Dendritic cells in multiple sclerosis lesions: maturation stage, myelin uptake, and interaction with proliferating T cells. J Neuropathol Exp Neurol *65*, 124-141.

Shechter, R., London, A., Varol, C., Raposo, C., Cusimano, M., Yovel, G., Rolls, A., Mack, M., Pluchino, S., Martino, G.*, et al.* (2009). Infiltrating Blood-Derived Macrophages Are Vital Cells Playing an Anti-inflammatory Role in Recovery from Spinal Cord Injury in Mice. PLoS Medicine *6*, e1000113.

Shin, T., Kim, S., Moon, C., Wie, M., and Kim, H. (2000). Aminoguanidine-Induced Amelioration of Autoimmune Encephalomyelitis is Mediated by Reduced Expression of Inducible Nitric Oxide Synthase in the Spinal Cord. Immunological Investigations *29*, 233-241.

Shintaku, M., and Yutani, C. (2004). Oligodendrocytes within astrocytes (?emperipolesis?) in the white matter in Creutzfeldt-Jakob disease. Acta Neuropathologica *108*.

Sierra, A., Abiega, O., Shahraz, A., and Neumann, H. (2013). Janus-faced microglia: beneficial and detrimental consequences of microglial phagocytosis. Frontiers in Cellular Neuroscience *7*.

Siffrin, V., Birkenstock, J., Luchtman, D.W., Gollan, R., Baumgart, J., Niesner, R.A., Griesbeck, O., and Zipp, F. (2015). FRET based ratiometric Ca2+ imaging to investigate immune-mediated neuronal and axonal damage processes in experimental autoimmune encephalomyelitis. Journal of Neuroscience Methods *249*, 8-15.

Siffrin, V., Radbruch, H., Glumm, R., Niesner, R., Paterka, M., Herz, J., Leuenberger, T., Lehmann, S.M., Luenstedt, S., Rinnenthal, J.L.*, et al.* (2010a). In Vivo Imaging of Partially Reversible Th17 Cell-Induced Neuronal Dysfunction in the Course of Encephalomyelitis. Immunity *33*, 424-436.

Siffrin, V., Vogt, J., Radbruch, H., Nitsch, R., and Zipp, F. (2010b). Multiple sclerosis – candidate mechanisms underlying CNS atrophy. Trends in Neurosciences *33*, 202-210.

Singh, S., Metz, I., Amor, S., van der Valk, P., Stadelmann, C., and Brück, W. (2013). Microglial nodules in early multiple sclerosis white matter are associated with degenerating axons. Acta Neuropathologica *125*, 595-608.

So, L., and Fruman, David A. (2012). PI3K signalling in B- and T-lymphocytes: new developments and therapeutic advances. Biochemical Journal *442*, 465-481.

Sprent, J. (1995). Antigen-presenting cells. Professionals and amateurs. Curr Biol *5*, 1095-1097.

Steinman, R.M., and Nussenzweig, M.C. (2002). Avoiding horror autotoxicus: The importance of dendritic cells in peripheral T cell tolerance. Proceedings of the National Academy of Sciences *99*, 351-358.

Stoppini, L., Buchs, P.A., and Muller, D. (1991). A simple method for organotypic cultures of nervous tissue. J Neurosci Methods *37*, 173-182.

Strober, W. (2001). Trypan blue exclusion test of cell viability. Curr Protoc Immunol *Appendix 3*, Appendix 3B.

Takahashi, K., Prinz, M., Stagi, M., Chechneva, O., and Neumann, H. (2007). TREM2-transduced myeloid precursors mediate nervous tissue debris clearance and facilitate recovery in an animal model of multiple sclerosis. PLoS Med *4*, e124.

Takeuchi, H., Jin, S., Wang, J., Zhang, G., Kawanokuchi, J., Kuno, R., Sonobe, Y., Mizuno, T., and Suzumura, A. (2006). Tumor Necrosis Factor- Induces Neurotoxicity via Glutamate Release from Hemichannels of Activated Microglia in an Autocrine Manner. Journal of Biological Chemistry *281*, 21362-21368.

Tatton, N.A. (2000). Increased Caspase 3 and Bax Immunoreactivity Accompany Nuclear GAPDH Translocation and Neuronal Apoptosis in Parkinson's Disease. Experimental Neurology *166*, 29-43.

Taylor, M.E., Bezouska, K., and Drickamer, K. (1992). Contribution to ligand binding by multiple carbohydrate-recognition domains in the macrophage mannose receptor. J Biol Chem *267*, 1719-1726.

Taylor, P.R., Gordon, S., and Martinez-Pomares, L. (2005). The mannose receptor: linking homeostasis and immunity through sugar recognition. Trends Immunol *26*, 104-110.

Thakker, P., Leach, M.W., Kuang, W., Benoit, S.E., Leonard, J.P., and Marusic, S. (2007). IL-23 Is Critical in the Induction but Not in the Effector Phase of Experimental Autoimmune Encephalomyelitis. The Journal of Immunology *178*, 2589-2598.

Theer, P., Hasan, M.T., and Denk, W. (2003). Two-photon imaging to a depth of 1000 microm in living brains by use of a Ti:Al2O3 regenerative amplifier. Opt Lett *28*, 1022-1024.

Tierney, J.B., Kharkrang, M., and La Flamme, A.C. (2009). Type II-activated macrophages suppress the development of experimental autoimmune encephalomyelitis. Immunology and Cell Biology *87*, 235-240.

Tischner, D., and Reichardt, H.M. (2007). Glucocorticoids in the control of neuroinflammation. Molecular and Cellular Endocrinology *275*, 62-70.

Tompkins, S.M., Padilla, J., Dal Canto, M.C., Ting, J.P.Y., Van Kaer, L., and Miller, S.D. (2002). De Novo Central Nervous System Processing of Myelin Antigen Is Required for the Initiation of Experimental Autoimmune Encephalomyelitis. The Journal of Immunology *168*, 4173-4183.

Tran, E.H., Hoekstra, K., van Rooijen, N., Dijkstra, C.D., and Owens, T. (1998). Immune invasion of the central nervous system parenchyma and experimental allergic encephalomyelitis, but not leukocyte extravasation from blood, are prevented in macrophage-depleted mice. J Immunol *161*, 3767-3775.

Ulges, A., Witsch, E.J., Pramanik, G., Klein, M., Birkner, K., Bühler, U., Wasser, B., Luessi, F., Stergiou, N., Dietzen, S.*, et al.* (2016). Protein kinase CK2 governs the molecular decision between encephalitogenic TH17 cell and Tregcell development. Proceedings of the National Academy of Sciences *113*, 10145-10150.

Vaknin-Dembinsky, A., Balashov, K., and Weiner, H.L. (2006). IL-23 Is Increased in Dendritic Cells in Multiple Sclerosis and Down-Regulation of IL-23 by Antisense Oligos Increases Dendritic Cell IL-10 Production. The Journal of Immunology *176*, 7768-7774.

Vinet, J., Weering, H.R., Heinrich, A., Kalin, R.E., Wegner, A., Brouwer, N., Heppner, F.L., Rooijen, N., Boddeke, H.W., and Biber, K. (2012). Neuroprotective function for ramified microglia in hippocampal excitotoxicity. J Neuroinflammation *9*, 27.

Vogelaar, C.F., Gervasi, N.M., Gumy, L.F., Story, D.J., Raha-Chowdhury, R., Leung, K.-M., Holt, C.E., and Fawcett, J.W. (2009). Axonal mRNAs: Characterisation and role in the growth and regeneration of dorsal root ganglion axons and growth cones. Molecular and Cellular Neuroscience *42*, 102-115.

Wan, Q., Kozhaya, L., ElHed, A., Ramesh, R., Carlson, T.J., Djuretic, I.M., Sundrud, M.S., and Unutmaz, D. (2011). Cytokine signals through PI-3 kinase pathway modulate Th17 cytokine production by CCR6+human memory T cells. The Journal of Experimental Medicine *208*, 1875-1887.

Wang, Z., Gerstein, M., and Snyder, M. (2009). RNA-Seq: a revolutionary tool for transcriptomics. Nature Reviews Genetics *10*, 57-63.

Wasser, B., Pramanik, G., Hess, M., Klein, M., Luessi, F., Dornmair, K., Bopp, T., Zipp, F., and Witsch, E. (2016). Increase of Alternatively Activated Antigen Presenting Cells in Active Experimental Autoimmune Encephalomyelitis. Journal of Neuroimmune Pharmacology *11*, 721-732.

Weigert, R., Sramkova, M., Parente, L., Amornphimoltham, P., and Masedunskas, A. (2010). Intravital microscopy: a novel tool to study cell biology in living animals. Histochemistry and Cell Biology *133*, 481-491.

Weitnauer, M., Schmidt, L., Ng Kuet Leong, N., Muenchau, S., Lasitschka, F., Eckstein, V., Hubner, S., Tuckermann, J., and Dalpke, A.H. (2014). Bronchial Epithelial Cells Induce Alternatively Activated Dendritic Cells Dependent on Glucocorticoid Receptor Signaling. The Journal of Immunology *193*, 1475-1484.

Whitehead, R.P., Lew, D., Flanigan, R.C., Weiss, G.R., Roy, V., Glode, M.L., Dakhil, S.R., and Crawford, E.D. (2002). Phase II trial of recombinant human interleukin-4 in patients with advanced renal cell carcinoma: a southwest oncology group study. J Immunother *25*, 352-358.

Wiendl, H., Toyka, K.V., Rieckmann, P., Gold, R., Hartung, H.P., and Hohlfeld, R. (2008). Basic and escalating immunomodulatory treatments in multiple sclerosis: Current therapeutic recommendations. Journal of Neurology *255*, 1449-1463.

Wilms, H., Sievers, J., Rickert, U., Rostami-Yazdi, M., Mrowietz, U., and Lucius, R. (2010). Dimethylfumarate inhibits microglial and astrocytic inflammation by suppressing the synthesis of nitric oxide, IL-1β, TNF-α and IL-6 in an in-vitro model of brain inflammation. Journal of Neuroinflammation *7*, 30.

Wu, E., and Raine, C.S. (1992). Multiple sclerosis. Interactions between oligodendrocytes and hypertrophic astrocytes and their occurrence in other, nondemyelinating conditions. Lab Invest *67*, 88-99.

Wuest, S.C., Edwan, J.H., Martin, J.F., Han, S., Perry, J.S.A., Cartagena, C.M., Matsuura, E., Maric, D., Waldmann, T.A., and Bielekova, B. (2011). A role for interleukin-2 trans-presentation in dendritic cell–mediated T cell activation in humans, as revealed by daclizumab therapy. Nature Medicine *17*, 604-609.

Yamasaki, R., Lu, H., Butovsky, O., Ohno, N., Rietsch, A.M., Cialic, R., Wu, P.M., Doykan, C.E., Lin, J., Cotleur, A.C*., et al.* (2014). Differential roles of microglia and monocytes in the inflamed central nervous system. The Journal of Experimental Medicine *211*, 1533-1549.

Yang, Y.-Q., and Li, J.-C. (2012). Progress of Research in Cell-in-Cell Phenomena. The Anatomical Record: Advances in Integrative Anatomy and Evolutionary Biology *295*, 372-377.

Yogev, N., Frommer, F., Lukas, D., Kautz-Neu, K., Karram, K., Ielo, D., von Stebut, E., Probst, H.-C., van den Broek, M., Riethmacher, D*., et al.* (2012). Dendritic Cells Ameliorate Autoimmunity in the CNS by Controlling the Homeostasis of PD-1 Receptor+ Regulatory T Cells. Immunity *37*, 264-275.

Zhang, X.-H., Shi, Y.-H., and Chen, J. (2015). Molecular characterization of a transmembrane C-type lectin receptor gene from ayu (Plecoglossus altivelis) and its effect on the recognition of different bacteria by monocytes/macrophages. Molecular Immunology *66*, 439-450.

Zhao, W., Tilton, R.G., Corbett, J.A., McDaniel, M.L., Misko, T.P., Williamson, J.R., Cross, A.H., and Hickey, W.F. (1996). Experimental allergic encephalomyelitis in the rat is inhibited by aminoguanidine, an inhibitor of nitric oxide synthase. J Neuroimmunol *64*, 123-133.

Zhao, X., Wang, H., Sun, G., Zhang, J., Edwards, N.J., and Aronowski, J. (2015). Neuronal Interleukin-4 as a Modulator of Microglial Pathways and Ischemic Brain Damage. Journal of Neuroscience *35*, 11281-11291.

Zimmer, H., Riese, S., and Régnier-Vigouroux, A. (2003). Functional characterization of mannose receptor expressed by immunocompetent mouse microglia. Glia *42*, 89-100.

Zipfel, W.R., Williams, R.M., and Webb, W.W. (2003). Nonlinear magic: multiphoton microscopy in the biosciences. Nature Biotechnology *21*, 1369-1377.

Appendix

Abbreviations

Abbreviation	Meaning
aaBMDM	alternatively activated Bone Marrow-Derived Macrophages
aaMC	alternatively activated Myeloid Cell(s)
APC	Antigen Presenting Cell(s)
ANOVA	Analysis Of Variance
BMDC	Bone Marrow-derived Dendritic Cells
BMDM	Bone Marrow-Derived Macrophages
BME	Basal Medium Eagle
BSA	Bovine Serum Albumin
caMC	classically activated Myeloid Cell(s)
cDNA	Complementary Deoxyribonucleic Acid
CFA	Complete Freund Adjuvant
CFP	Cyan Fluorescent Protein
CNS	Central Nervous System
DAPI	4,6-diamidino-2phenylindole, dihydrochloride
DNA	Deoxyribonucleic Acid
DNase	Deoxyribonuclease
dNTP	deoxy Nucleoside Triphosphate
DTT	Dithiothreitol
EAE	Experimental Autoimmune Encephalomyelitis
EB	Elution Buffer
EDTA	Ethylenediaminetetraacetic acid
EPs	Engulfment Processes
FACS	Fluorescence-Activated Cell Sorting
FBS	Fetal Bovine Serum
FCS	Fetal Calf Serum
FDR	False Discovery Rate
FSC	Forward Scatter
GFP	Green Fluorescent Protein
GM-CSF	Granulocyte-Macrophage Colony-Stimulating Factor
IFN	Interferon
IgG	Immunoglobulin G
IL	Interleukin
i.p.	Intraperitoneally
i.v.	Intravenously
logCPM	logarithmic counts per million
logFC	logarithmic Fold-Change
LPS	Lipopolysaccharide
MACS	Magnetic-Activated Cell Sorting
M-CSF	Macrophage Colony-Stimulating Factor

MEM	Minimum Essential Medium
MHC	Major Histocompatibility Complex
MM	Mouse Medium
MOG	Myelin Oligodendrocyte Glycoprotein
mRNA	messenger Ribonucleic Acid
mRNA-Seq	messenger Ribonucleic Acid Sequencing
MS	Multiple Sclerosis
NGS	Normal Goat Serum
OPO	Optical Parametric Oscillator
PB	Phosphate Buffer
PBS	Phosphate-Buffered Saline
PC	Principal Component
PCA	Principal Component Analysis
PCR	Polymerase Chain Reaction
PFA	Paraformaldehyde
PI	Propidium iodide
PTX	Pertussis Toxin
qRT-PCR	quantitative Real Time Polymerase Chain Reaction
RFP	Red Fluorescent Protein
RIN	Ribonucleic Acid Integrity Number
RNA	Ribonucleic Acid
RNA-Seq	Ribonucleic Acid Sequencing
RRMS	Relapsing-Remitting Multiple Sclerosis
RT	Room Temperature
s.c.	Subcutaneous
SEM	Standard Error of the Mean
SSC	Sideward Scatter
SSMS	Secondary Progressive Multiple Sclerosis
Th	T helper
TNF	Tumor Necrosis Factor
TPLSM	Two-Photon Laser Scanning Microscopy
TREM2	Triggering receptor expressed on myeloid cells 2
WGA	Wheat Germ Agglutinin
WM	Wash Medium

Index of Illustrations and Tables

Acknowledgements

An dieser Stelle möchte ich mich ganz herzlich bei allen Menschen bedanken, die zu dem Gelingen dieser Arbeit beigetragen haben.

Allen voran gilt mein Dank **Prof. Dr. xxxxxx xxxx**, die es mir nicht nur ermöglicht hat, diese Arbeit in ihrer Gruppe auszuführen. Darüber hinaus verschaffte sie mir die Gelegenheiten, meine Ergebnisse auf zahlreichen internationalen Konferenzen vorzustellen und somit Kontakte mit Wissenschaftlern verschiedenster Forschungsgebiete zu knüpfen. Ich möchte mich für Ihre Betreuung und die konzeptionelle Unterstützung bedanken.

Des Weiteren gilt ein besonderer Dank auch **Prof. Dr. xxxxxxx xxxxxxxxxxx** für die Zweitbetreuung meiner Doktorarbeit. Durch die Übernahme meiner Zweitbetreuung erlaubte sie es mir als einer biomedizinischen Chemikerin, diese interdisziplinäre Doktorarbeit im Fachbereich Chemie vorlegen zu können. Ich möchte mich für ihr durchgehendes Interesse und die positiven Rückmeldungen bezüglich meiner Ergebnisse bedanken.

Für fruchtbare fachliche Diskussionen und die enge Zusammenarbeit in einer sehr angenehmen, motivierenden Atmosphäre gilt ein spezieller Dank auch **Prof. Dr. xxxxxx xxxxxx** und **Dr. xxxx xxxxxxxx**. Ihre Unterstützung und permanente Ansprechbarkeit trug maßgeblich zu dem Gelingen meiner Doktorarbeit bei und ich bin dankbar, dass ich von ihrer wissenschaftlichen und technischen Erfahrung profitieren durfte. **xxxx** möchte ich auch insbesondere für die Einarbeitung und die Zwei-Photonen-Mikroskopie danken. Es hat nicht nur Spaß gemacht, sondern war auch sehr wertvoll für mich, mit ihm zusammenarbeiten zu können. An dieser Stelle möchte ich mich auch bei **Dr. xxxxxx xxxxxx** bedanken, die mich insbesondere im ersten Jahr meiner Doktorarbeit unterstützte und in das Themengebiet einarbeitete. Bei **xxxxxx** möchte ich mich für die Übernahme dieser Betreuung bedanken und zusätzlich auch für die Möglichkeit, selbst Masterstudenten und medizinische Doktoranden mit zu betreuen und somit einen tieferen Einblick in ein erweitertes Forschungsgebiet zu erhalten.

Ich möchte mich bei der gesamten Arbeitsgruppe für die Begleitung durch die Doktorarbeit bedanken. **Dr. xxxxxxxxx xxxxxxx** und **Dr. xxxxxx xxxxxx** danke ich ganz besonders für die

angenehme Atmosphäre während unserer gemeinsamen Doktorandenzeit, in der wir eng zusammengearbeitet haben. Für die positive Stimmung und die erfolgreiche Zusammenarbeit danke ich ebenfalls besonders **xxxxxxx xxxxx**, **xxxx xxxxxxx**, **xxxxxx xxxxxx** und **xxxxx xxxx**. Darüber hinaus möchte ich **xxxxxxxx xxxxxxxxxx**, **xxxxx xxxxxxxxx**, **xxxxxx xxxxxxxxxxx**, **xxxxxx xxxxxxx**, **xxxxxxxxx xxxxxx** und **xxxxxxx xxxxx** für ihre technische Unterstützung danken. **xxxxxxxx** danke ich zusätzlich auch insbesondere für die private gemeinsame Zeit.

Special thanks are also dedicated to **xxxxxx xxxxxx** for proofreading the whole thesis. Thank you for your great support!

Neben der verlässlichen Unterstützung im beruflichen Umfeld, war mir auch insbesondere der private Rückhalt von Freunden und Familie eine große Hilfe. Ein besonderer Dank gilt hierbei **Dr. xxx-xxxxx xxxxxxxxxx**, die schon seit Studienbeginn für viel privaten Ausgleich durch gemeinsame Unternehmungen gesorgt hat. Auch **xxxxxx xxxxx** und allen **„Schrödingers Cat Friends“** danke ich für die schöne gemeinsame Zeit während des Studiums und auch im Anschluss daran. **xxxxx xxxxxx** danke ich für die langjährige Freundschaft. Es ist unbeschreiblich wertvoll, eine Freundin wie sie zu haben, die immer für mich da ist und mich versteht, egal, wie lange wir uns zwischenzeitlich dann mal nicht sehen. Für viel Spaß neben des Studiums danke ich auch **xxxxx xxxxx**.

Ich danke meinem **Papa xxxxxxx xxxxxx** für seine ganze Hilfe nicht nur während des Studiums, sondern in allen Lebenslagen. Papa, ich möchte dir auch dafür danken, dass du immer stolz auf mich bist, egal, ob ich gerade gute oder schlechte Forschungsergebnisse habe. Ich bin froh, dass ich dich habe! **Meinen Schwestern xxxxxxx und xxxxxx** danke ich für immer wieder schöne Ablenkungen vom Studium und auch dafür, dass ihr immer für mich da seid. Ihr seid die besten Schwestern, die ich mir vorstellen kann.

Ein großer Dank gilt auch meinem liebsten Dr. **xxx-Schatz**! Ich glaube, ohne dich hätte ich meine Doktorarbeit niemals mit so viel Freude machen können. Du warst jeden Tag für mich da, wenn ich gerade Aufmunterung oder Ablenkung brauchte. Ich danke dir auch dafür, dass du immer Verständnis dafür hattest, wenn ich einmal wieder länger oder am Wochenende gearbeitet oder die Arbeit einfach zu ernst genommen habe. Ich danke dir für alles. Ich liebe dich!

Abschließend möchte ich noch meiner **Mama** danken, der ich diese Arbeit widme. Ich danke ihr dafür, dass sie mir geholfen hat, der Mensch zu werden, der ich jetzt bin. Mama, ich hab dich lieb!